博士論文

Multifunctional MEMS Devices for *in situ* TEM Liquid-Phase Experimentation

（液相TEMによるその場実験用多機能MEMS素子）

令和２年１１月２日提出

指導教員　年吉　洋　教授

東京大学大学院工学系研究科

電気系工学専攻

37-167090

メノン　ヴィヴェーク　アナンド

Menon, Vivek Anand

Table of Contents

Chapter Summaries

Chapter 1: Introduction

The visual observation of physical samples is a fundamental scientific investigative technique. Biology, chemistry, materials science, and other scientific fields require imaging techniques that are capable of providing resolutions at or beyond the characteristic size of the sample being observed. While optical and light-based microscopy techniques are easily capable of achieving micrometer resolutions but become limited by diffraction when nanometer scale resolutions are necessary. Electron microscopy techniques in general, and Transmission Electron Microscopy (TEM) specifically, are capable of reaching nanometer and sub-nanometer imaging resolutions in ideal conditions.

When the target of observation exists in a gaseous or liquid medium, conventional TEM techniques cannot be applied due to the nature of the probing electron beam. Specialized modified TEM techniques such as gas-phase Environmental Transmission Electron Microscopy (ETEM) and encapsulated liquid cell devices and holders enable the observation of gasses and liquids using TEM. For the investigation of liquids, these techniques offer an attractive combination of resolving power and representative environmental conditions.

While liquid cell TEM technology has been developed previously, it tends to be limited in the ability to manipulate the sample during observation. Liquid cell TEM allows for the real-time observation of sample dynamics, so it is necessary to develop techniques that can induce or alter these dynamics in order to replicate the experimental capabilities of non-TEM-based conventional analyses. Specifically, liquid-phase samples are often manipulated through the use of electrical biasing, heating, and mixing. While

custom liquid cell TEM holders exist to achieve these individual capabilities, they are often prohibitively expensive and represent an investment that is unpalatable to all but the most specialized laboratories.

The primary objective for this study is the development of a liquid cell device that is fully self-contained, does not require a specialized TEM holder, and is capable of electrically biasing, heating, and controlling flow in the loaded fluid sample. A device that is itself fully hermetically sealed independently of any external clamping holders or gaskets is more likely to be allowed for use in high-performance microscopy centers with delicate TEM systems. Furthermore, if no custom TEM holder is required to achieve sample interactivity in addition to sample sealing, the device becomes more accessible to scientific researchers who do not already have access to specialized liquid TEM facilities but could benefit from the technique.

Chapter 2: Basic Design and Device Development

In order to develop the active liquid cell structures called for in Chapter 1, a basic device platform must be developed. Previous endeavors toward complex device functionality have been hampered by poor reliability and repeatability of the basic liquid cell structure and encapsulation properties. To mitigate these problems and facilitate the achievement of higher-order sample interactivity, the fundamental liquid cell structure was first refined and standardized.

In this chapter, the two device strategies pursued in this study are introduced. The first, known as the “two-chip” liquid cell, is based on conventional liquid cell structures and is comprised to two micromachined chips with TEM observation window membranes that sandwich the target fluid and encapsulate it to prevent evaporation and leaking in the

TEM high-vacuum chamber. The design considerations to enable high fabrication yields and reliable liquid cell operation are discussed.

The second device structure is known as the “nanochannel” device and features a suspended hollow channel that is used for TEM imaging. Developed in collaboration with Dr. Edin Sarajlic, the nanochannel offers higher resolving power and more consistent imaging conditions than the two-chip device. This and other comparisons regarding the utility of the two platforms are made after detailing the basic imaging characteristics of each.

Chapter 3: MEMS-Based Sample Interaction

Both of the basic liquid cell structures described in Chapter 2 fulfil the functional requirements that the developed device should be both self-contained and not require a customized TEM holder. In this chapter, the means by which active MEMS components are integrated into the devices to achieve electrical, thermal, and flow control without violating those criteria are described. All sample interactivity is achieved through the electrical interconnects of a generic, non-sealing TEM holder.

Electrical biasing functionality is the most fundamental active capability for liquid cells and serves as the foundation upon which subsequent features are based. Previous works have used onboard electrodes for a variety of purposes, so the focus for this study was to use the electrode pattern to perform testing on the robustness of the membrane in order to assess the feasibility of certain techniques for later achieving heating and flow control. Device heating was also achieved, and the ability for the device to be used for temperature control during TEM observation was demonstrated. Finally, a pressure-driven hydrophobic burst valve design was integrated onto the two-chip device in order to control liquid flow in TEM. Using the electrode patterns previously characterized,

electrolysis of a portion of the sample fluid can be used to generate a pressure gradient and induce fluid motion within the fully-encapsulated liquid cell. This technique is described and demonstrated. A single device incorporating all components is introduced.

Chapter 4: Scientific Demonstrations and Applications

Here, the device structures described in Chapters 3 and 4 are applied for the investigation of various scientifically-relevant samples. In total, three distinct sample systems are included, and the ability for the liquid cell devices to provide information that would be otherwise inaccessible is demonstrated.

The first system described consists of silver nanoparticles coated with synthetic calix[n]arene biomolecules. Calixarenes are being extensively studied for their ability to interact with enzymes and induce and inhibit various biological processes. Here, silver nanoparticles coated with *para*-suphonato-calix[8]arene remained stabilized as a colloid in solution until the introduction of a protein induced the formation of aggregate structures. This protein-driven aggregation was observed directly and in real time.

Zeolites, as complex porous structures, are a unique material structure being investigated for their use in the filtration and transport of various materials including petroleum and potable water. In this experiment, the ability for the type X faujasite zeolite to retain and exchange various aqueous ions was investigated with the ultimate purpose of elucidating the material's functionality for use as a mechanism for the *in vivo* contrast enhancement for the Magnetic Resonance Imaging (MRI) of tissue. The relative contrast of the zeolite structures during liquid cell STEM imaging was indicative of the ion complexed within the material. The flow control capabilities of the two-chip device were also used to investigate the propensity for ion exchange in the presence of a concentration gradient.

The final system to be introduced here involves complexes of DNA-linked gold nanoparticles (DNA/AuNP). The use of controlled DNA sequences for the formation of large aggregates of gold nanoparticles has been explored as a means to generate engineered crystal structures. The specific DNA sequences used in combination with precise control of the hybridization temperature can be used to create novel crystalline AuNP aggregates in a directed manner. Here, the use of the heater-integrated liquid cell is explored as a means to directly observe the DNA-based motion of AuNP complexes is attempted, and subsequent studies incorporating the use of the flow control system to introduce DNA sequences to AuNP in the un-aggregated state are proposed.

Chapter 5: Summary, Perspectives, and Conclusions

The main achievements of this study include the refinement of the existing liquid cell platforms as well as the integration of biasing, heating, and flow capabilities without the use of a specialized TEM holder. While previous devices have been unreliable and were regularly damaged during fabrication, the current fabrication process minimizes device loss and yields more stable and resilient liquid cells. The incorporation of active MEMS components also represents a step forward in terms of the utility of the device as an experimental platform that is compatible with generic TEM holders with electrical interconnects. Preliminary demonstrations of the use of the developed liquid cell devices to investigate various sample systems also indicate that the devices can be used for scientific studies in various fields. While liquid cell electron microscopy suffers from limitations involving the effect of the electron beam and the nature of TEM contrasting, the development of a liquid cell platform capable of multiple avenues of sample interaction opens the door to the wider applicability of the technique as a valid and accessible analytical method.

List of Figures

Chapter 1: Introduction

The direct observation of a material or phenomenon is one of the most fundamental investigative techniques available. Nothing is more basic that learning more about something by looking at it, and that is no different now that so many diverse scientific imaging techniques are available. In this study, the investigation of liquid samples though the use of Transmission Electron Microscopy (TEM) will be explored with a focus on *in situ* interaction with the sample in a variety of ways.

1.1. Background

1.1.1. Biology, Chemistry, and Imaging Techniques

Microscopy serves as an essential scientific technique that reveals the mystery of the world around us. The investigation of small phenomena is critical to many scientific fields because the properties of materials and systems are derived from their smaller components and constituents. A wide variety of microscopy techniques exist, each with its advantages and disadvantages. This report deals with the observation of liquid-phase samples, so discussing microscopy from a biological and chemical perspective makes sense as these fields often involve fluid and other soft matter.

Conventional Microscopy

Optical microscopy is the most ubiquitous technique for the magnification of small objects, and in the case of the analysis of liquid-phase samples can be quite appropriate for imaging aqueous materials. However, optical microscopy suffers from resolution limits arising from the diffraction of light at any given wavelength, so the

development of secondary imaging techniques such as fluorescent microscopy has been successful in mitigating such limitations.

Fluorescent Microscopy

The selective application of fluorescent labels to scientifically relevant targets can allow the subversion of the diffraction limit in some imaging setups. By detecting the light emitted by a fluorophore upon the application of excitation light, the presence and activity of a particle smaller than the diffraction limit can potentially be detected and tracked. This type of "indirect imaging" forms the basis of fluorescence microscopy and has been applied for use in an extremely wide and versatile range of biological assays and analytical techniques. Various techniques exist to increase the effective resolution, such as Stimulated Emission Depletion Microscopy (STED) and Single Molecule Localization Microscopy (SMLM). STED involves the direct excitation of a sample using a laser which rasters over the sample, thereby inducing spontaneous photon emission of the characteristic fluorescent wavelength. A second beam of a usually lower wavelength is applied simultaneously that features an annular phased pattern with zero-intensity at the center. This second beam, known as the STED beam, induces the stimulated emission of photons from the excited fluorophore with the same wavelength of the STED beam. This stimulated emission thereby relaxes the fluorophore from the excited state without spontaneous fluorescent emission. As the STED beam overlaps with the original excitation beam, it effectively quenches or suppresses fluorescent emission in an annulus around the excitation beam. Practically-speaking, this means that photons with the characteristic fluorescent wavelength are only emitted from the small spot within the center of the pattern that is excited by the excitation beam and not the STED beam. Such photons can thereby be selected for with a filtered detector, and yield an effective

fluorescence spot size lower than the conventional diffraction limit [1] [2]. A schematic of the STED concept can be seen below in Figure 1.1.

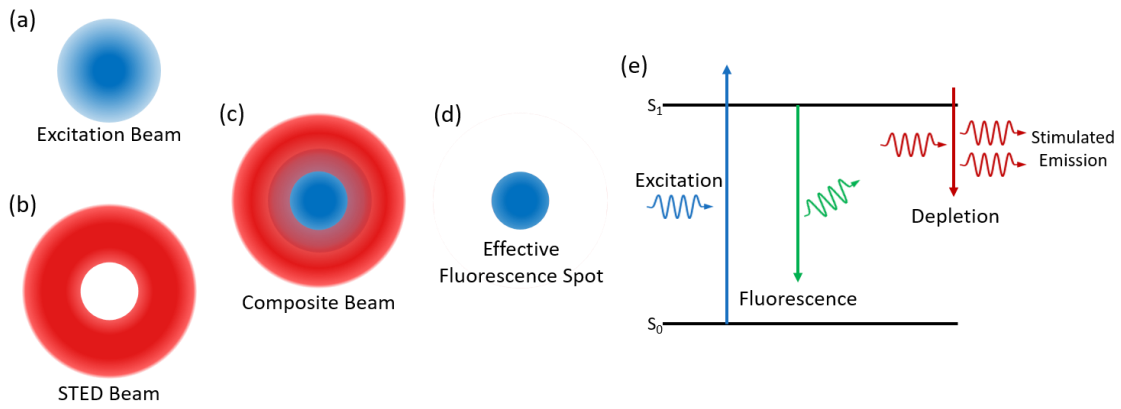

Figure 1.1: STED effective spot size reduction. (a) Diffraction-limited fluorescence excitation beam. (b) Annular depletion beam. (c) Concentric beams to form overall excitation/depletion signal. (d) Resultant smaller effective spot size for fluorescence. (e) Schematic of fluorophore excitation states during excitation, fluorescence, and stimulated emission resulting in depletion.

In SMLM, an array of molecular fluorescent labels with photo-switchable activity is used. The application of an excitation signal near the switching threshold can cause a certain subset of probes within the array to fluoresce at any given time. When the density of the activated probes is low enough such that they are separated by a distance above the diffraction limit, several images can be taken to obtain a statistical set of data to determine the most probable point location of the activated probes. The probes can then be deactivated through photobleaching or another conversion process. Another set of probes can then be activated, imaged, and located via the same process. By repeating this process several times until all probes present in the sample have been imaged, a composite image can be formed where each individual set is superposed, thereby locating each probe, and achieving an effective result that exceeds the limitations of diffraction [3] [4] [5]. A schematic of this process for an individual pair of fluorophores within a larger sample is shown below in Figure 1.2.

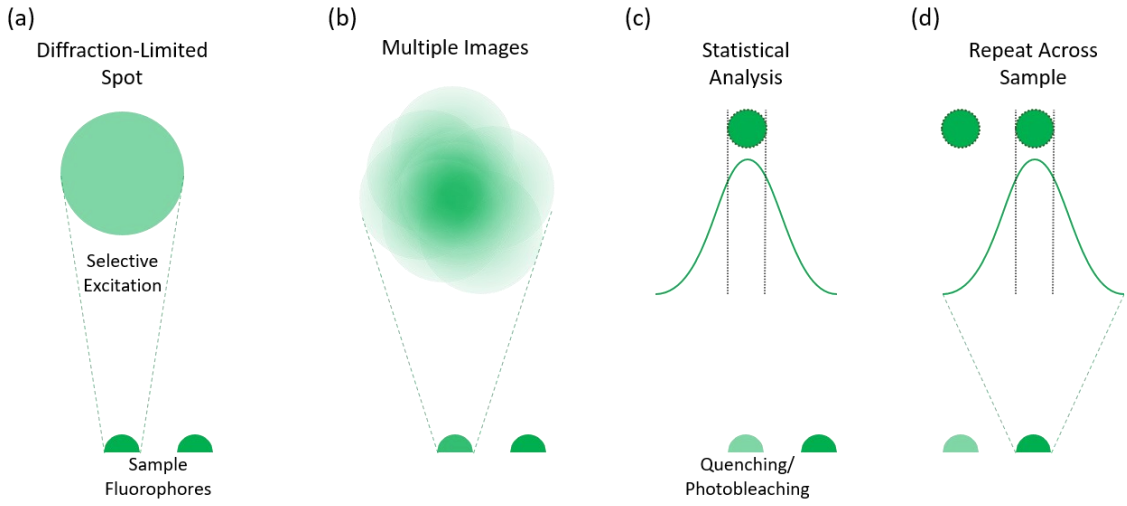

Figure 1.2: Localization process for SMLM. (a) A single excited fluorophore produces a diffraction-limited fluorescence pattern. (b) Multiple rapidly-captured images generate a set of fluorescence patterns. (c) Fluorophore is quenched via photobleaching or other process and image set can be analyzed to approximate the location of the fluorophore. (d) New excitation event triggers nearby fluorophore and process is repeated.

These and other so-called "super-resolution" fluorescence microscopy techniques have been used to achieve effective resolutions of 10-100 nm in precise conditions [6] [7]. While super-resolution is achievable in these ways, STED and related techniques suffer from the need for relatively high fluorescent signals and susceptibility to premature photobleaching. SMLM is an inherently slow process as it requires taking thousands of images and data post-processing to form one composite, and therefore cannot be used to image dynamic or mobile systems. The selection of appropriate fluorophore labels to suit the specific requirements of the technique, sample, and situation can also be a significant limiting factor for sub-diffraction fluorescence microscopy [8].

Electron Microscopy

Another method available to circumvent the diffraction limit for light-based microscopy techniques is the use of electrons for the generation of images instead of photons. By avoiding the use of photons, electrons accelerated at high voltages can be

imparted a much lower effective wavelength than the light used in optical or even ultraviolet microscopy techniques. The accelerated electrons can then be manipulated and focused using magnetic and electrostatic lenses for the purposes of interacting with and imaging a sample. In this way, the normal diffraction limits associated with light-based microscopy can be bypassed, and a variety of techniques exist to take advantage of this phenomenon [9].

1.1.2. Transmission Electron Microscopy

Transmission Electron Microscopy (TEM) functions in a manner quite similar to conventional optical microscopy but using electrons rather than photons to mitigate normal the diffraction limit involved with light-based techniques. The use of a coherent electron beam, however, introduces complications when the desired observational target is in the liquid-phase. A variety of techniques exist to overcome these limitations, some of which are described here.

Principles and Applications

TEM systems use specialized electron emitters and magnetic lenses to generate a highly-ordered collimated electron beam that is allowed to interact with a sample by passing through it and on to an electron detector. The TEM emitter tip accelerates electrons at high voltage, 200 kV for the system used in this report, with higher acceleration voltages corresponding to higher theoretical resolution limits but increased risk of sample damage [9] [10]. A combination of electrostatic and magnetic lenses focuses the electron beam on the sample stage where it can interact with the observation target [11]. A combination of elastic and inelastic scattering events generates a characteristic pattern as the electrons pass through the sample and reach the detectors

below. A combination of spatial electron detectors and scattering angle detectors can be used to generate TEM images and perform various analyses [12] [13].

Sub-nanometer imaging is regularly possible using TEM [14], provided conditions are appropriate, allowing for the direct observation of atomic structures and crystal lattices. Unlike direct physical contact measurements such as Atomic Force or Probe Microscopy, TEM relies on an electron beam and detector. As such, the beam can be refreshed rapidly, and the real-time nanoscale observation of samples is not only common but standard in modern TEM systems with normal systems capable of 30 fps video. Conventional TEM (CTEM) functions most similarly to optical microscopy in which the electron beam is focused down and illuminates the entire sample visual area at once in order to generate an image. Scanning TEM (STEM) functions by sweeping through the sample area pixel-by-pixel with a highly-focused electron beam. STEM systems are also capable of Annular Dark Field (ADF) and High Angle ADF (HAADF) imaging, in which the brightness value for a given pixel is not determined by the simple transmission of the electron through the sample, but is instead determined by the angle at which electrons are elastically scattered when interacting with the atomic nuclei of the sample. This technique allows for the differentiation of materials based on their atomic weight, known as Z-contrasting, and can be useful when dealing with thick samples of disparate materials [15].

Limitations of Conventional TEM Systems for Liquids

In order to generate high-resolution images, the TEM electron beam must be highly coherent and free of aberrations or other interference. This means that TEM chambers are kept in ultra-high-vacuum condition to prevent blurring of the beam in air.

While this is acceptable for many samples, especially solid-phase ones, this restriction can present a significant challenge for the investigation of liquid or gaseous samples.

1.1.3. Electron Microscopy of Non-Solid Targets

When investigating gasses and liquids, care must be taken to avoid damaging either the sample itself or the TEM system in use. This is usually achieved by preventing gasses or liquids from entering the main TEM vacuum chamber, though distinct methods exist for achieving this.

Challenges for Gaseous and Liquid TEM

When imaging gaseous of liquid-based samples, care must be taken to prevent the excessive evaporation of the sample medium that could both contaminate the electron emitter apparatus as well as interfere with the coherence of the imaging electron beam. Furthermore, depending on the setup, the ability to generate a signal contrast between the target of imaging and the gaseous or liquid medium in which it resides can be much more difficult than with conventional dry TEM.

Environmental Electron Microscopy

Environmental Electron Microscopy (ETEM or ESEM for Scanning Electron Microscopy) involves the use of differential pumping systems to preserve the vacuum condition of the main beam chamber. ETEM techniques allow for atmospheric conditions to be maintained directly around the observational target while the electron emitter tip and related systems are maintained at high-vacuum [16] [17] [18]. Doing so has enabled the direct TEM observation of a variety of exotic phenomena, including monitoring of catalytic surfaces during gaseous reactions [19] [20] [21] [22], the chemical vapor deposition growth of carbon nanotubes [23] [24] and gallium-based nanowires [25] [26].

While the differential pumping techniques enable the observation of gas-phase reactions within the TEM chamber, they are generally still unsuitable for the observation of liquids in atmospheric conditions. To observe liquids that exhibit any degree of volatility within TEM, an encapsulated observation cell is usually required.

Encapsulated Electron Microscopy

In contrast with ETEM and ESEM setups in which the volatile sample is exposed within the vacuum chamber, encapsulated electron microscopy involves the physical isolation of the sample from the surrounding vacuum. By surrounding the sample in a barrier material, evaporation and contamination can be prevented, while still allowing for the imaging of the sample within.

1.1.4. Liquid Cells for TEM

The primary TEM technique for the observation of non-solids involves the total encapsulation of the sample in a physical structure that is capable of sealing the liquid or gas inside and preventing it from escaping in to the high-vacuum environment while also allowing the imaging electron beam to interact with the sample within [27]. This can be achieved by sandwiching a liquid layer between two micromachined chips with thin membranes that allow the TEM beam to image the sample [28]. This type of technique, when applied for the imaging of liquids in TEM is commonly referred to as “liquid cell” TEM (LCTEM) as the device forms a sort of capsule or cell for the liquid to occupy.

General Structure

Conventionally, the most standard modern liquid cell devices consist of a pair of chips, usually silicon, with membrane-covered windows, usually silicon nitride [29] though more recently graphene has been pursued [30] [31] [32] , that are assembled

together with a sample liquid in between. The chips can be bonded using glue or epoxy, or fused with anodic or other bonding techniques. Alternatively, and more common recently, is the used of specialized clamping TEM holders that apply pressure to the top and bottom of the chips in order to prevent leakage. By sealing the liquid within the cell in this manner, its contents can be safely viewed using TEM.

As discussed previously, in order to successfully utilize TEM, various conditions must be met. First the sample must be able to survive in the TEM vacuum chamber without disrupting the environment necessary for electron beam emission and cohesion. Furthermore, the sample itself must be thin and transmissive enough to allow the imaging beam to actually pass through the sample and reach the detectors. Finally, the composition of the sample must be such that interactions with the electron beam are sufficient to generate contrast between the desired target and the background medium. In order to meet these requirements, LCTEM techniques follow a common general structure that allows for liquid sample observation in TEM.

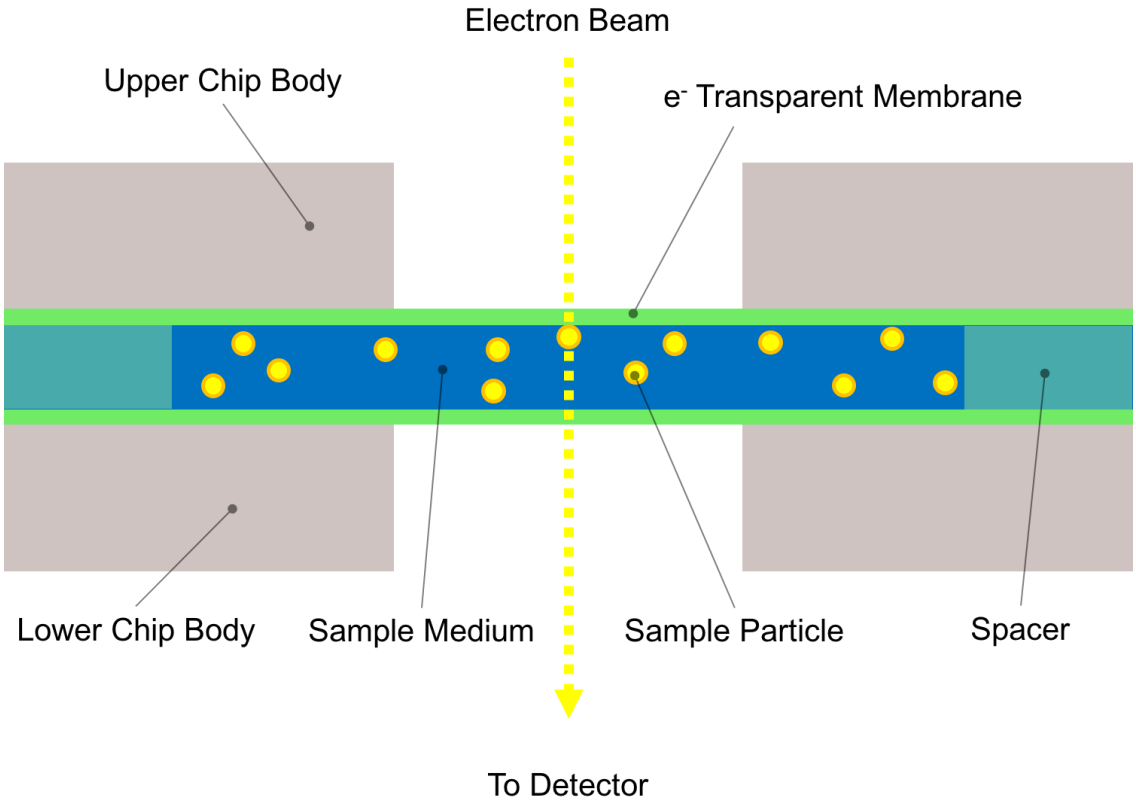

Figure 1.3: Cross-sectional schematic illustration of a common liquid cell structure as inserted into a TEM chamber.

When viewing samples suspended in a liquid that would evaporate in a vacuum environment, LCTEM setups preserve the vacuum by physically isolating the sample. The sample fluid is usually sealed within a sample chamber formed by sandwiching two chips together that can maintain the near-atmospheric pressure of the loaded liquid when the assembly is inserted into the vacuum of the TEM column. Figure 1.3 shows a cross-sectional view of the critical observation area of a liquid cell device within a TEM vacuum chamber. The liquid sample medium is surrounded by two chips which seal the sample and prevent evaporation into the surrounding vacuum environment. In contrast with low-vapor-pressure samples or ETEM techniques where the sample is exposed within the TEM, LCTEM works by physically encapsulating the sample and isolating it from the vacuum chamber.

While the physical encapsulation of the sample prevents sample evaporation and maintains the TEM vacuum environment for the electron beam, the introduction of the liquid cell structure represents an obstacle to the path of the electron beam, potentially preventing electron transmission. In order to maintain the pressurized seal of the liquid chamber while also enabling transmission of the electron beam, thin membranes are used in the sealing chips as "windows" through which electrons can be transmitted while still preventing sample leakage. In Figure 1.3, the membranes can be seen on both chip bodies, forming a capsule that maintains the seal in the area where the thicker chip structure is removed to allow for the transmission of the electron beam through the liquid sample within. These electron-transparent membranes are usually less than 500-nm-thick to allow for transmission, and as such must exhibit sufficient strength in order to prevent failure under atmospheric pressure loads in vacuums up to and beyond 10^{-5} Pa. As mentioned previously, the most common materials used for membranes in LCTEM are silicon nitride and graphene.

Finally, with the liquid sample encapsulated and the electron beam preserved and able to pass through the device, the sample itself must be conducive to the generation of contrast and thereby an interpretable image. As discussed previously, TEM contrast is largely based either on the outright occlusion of imaging beam in the case of CTEM or on electron-nucleus interactions in the case of Z-contrast imaging with STEM. Both of these factors scale with the amount of material in the path of the electron beam. In order to view a sample suspended in a liquid, metallic nanoparticles in a colloidal liquid or cells in a culture suspension for example, the imaging target must create a detectable change in contrast in comparison to the contrast of the background medium. Figure 1.4 illustrates this concept. The figure shows an STEM image taken in Z-contrast mode of a sealed

liquid cell structure filled with a solution of 50 nm gold nanoparticles. The white background represents the signal generated by the solution itself; if no liquid were present the signal would be black in this imaging mode. However, the presence of the aqueous solution generates a signal which registers as a pale grey in this mode. In this situation, the gold nanoparticles do generate a sufficiently different signal such that they can be distinguished from the background signal of the liquid medium.

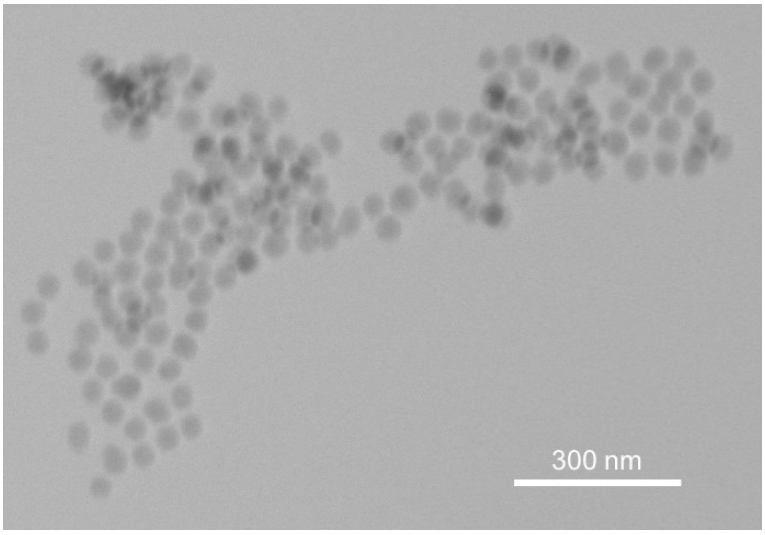

Figure 1.4: LCTEM image of 50 nm gold nanoparticles in an aqueous solution.

In contrast with dry TEM where the only material in the path of the electron beam is the relevant sample, in LCTEM both the sample and the fluid medium contribute to the generated signal. The column of fluid through which the electron beam passes serves to scatter and impede the direct transmission of electrons largely through elastic interactions between the incident electrons and the medium. The mean free path l for scattering of electrons in a material can be given by the expression $l = \frac{W}{\sigma \rho N_A}$ where W is the effective atomic weight of the material, σ is the cross-section for electron scattering in the material, ρ is the material density, and N_A is Avogadro's number [33]. For elastic scattering under typical STEM parameters in water, l_w is approximately 10 μm [34] [35] [36]. To minimize

the signal generated by the background medium, the amount material in the path of the electron beam must be kept as low as possible. Practically speaking, this means that the thickness of the liquid within the liquid cell should be kept well below the mean free path of electrons in that liquid. Liquid cells, therefore, are usually designed to maintain a fluid column on the order of or below 1 μm. In the most common chip-type device structure, as shown in Figure 1.3, the thickness of the fluid is usually defined by a spacer that maintains the gap between the two chips that the liquid occupies. In contrast, envelope-type devices as shown in Figure 1.5 feature sealing membranes, usually made of graphene [30] [31], that are placed directly around sample droplets with the thickness defined by the size of the sample itself and sealing achieved through surface tension and adhesion between the membrane layers. In these ways, the fluid column is kept thin enough both to allow for sufficient electron transmission as well as the generation of contrast between sample particles and the background medium.

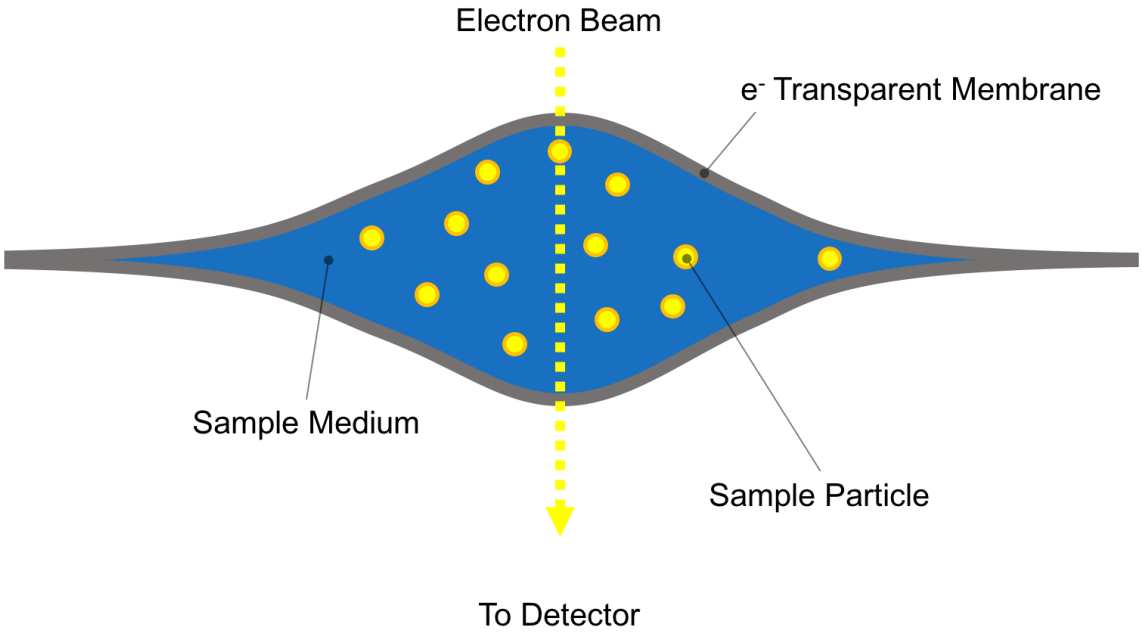

Figure 1.5: Cross-sectional schematic of "envelope-type" liquid cell device. The membrane layers are held together by mutual adhesion between the sample and the membrane material.

TEM Holders and Liquid Cells

Above the general architecture of liquid cell devices themselves was described, but for most existing LCTEM systems, the TEM holder also plays a significant role in achieving the functionality of the device. Standard TEM holders for dry samples serve to hold the sample in position within the TEM chamber while maintaining the vacuum seal of the chamber body and also allow for the exchange of specimens by withdrawing and re-inserting the holder. The tip of the holder where the specimen is affixed is often quite small and thin, usually under 1 cm^2 in area and 1-mm-thick.

In addition, holders designed for use with microchips may also feature electrical interconnects allowing for the application of electrical signals to specimens within the TEM chamber. Figure 1.6 shows the electrical interconnect TEM holder used in this study. The available specimen size for this holder is 4 mm by 5.5 mm by 1.5 mm as illustrated in Figure 1.7. In addition to basic holders with electrical interconnects, holders with heating and cooling capabilities are also available [37] [38] [39] [40], though functions beyond electrical interconnects require more complex holder structures and are more expensive.

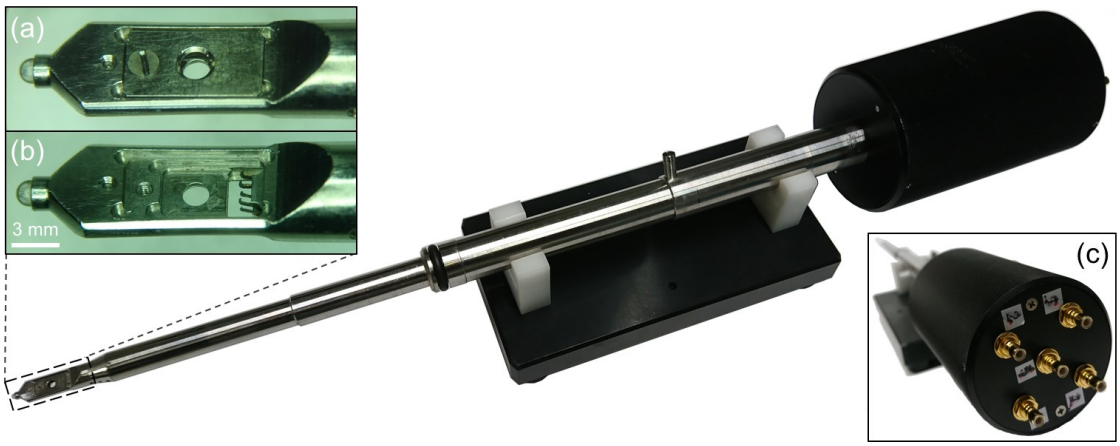

Figure 1.6: Microchip TEM Holder. (a) Holder tip with cover affixed and (b) removed with electrical pins visible. (c) Backside of holder with electrical interconnect plugs.

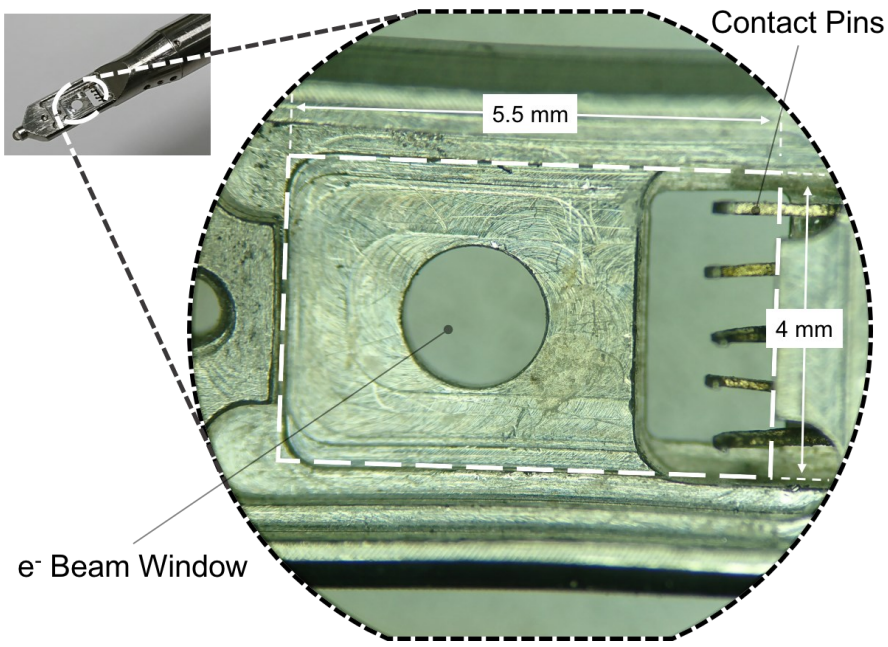

Figure 1.7: TEM holder showing available device area (white dashed box).

In the case of LCTEM, most current solutions rely on specialized holders to enable the sealing of the liquid cell structure. Most commonly, the holder tip will feature clamping apparatus including O-rings to help form a seal between the two device chips and the internal structure of the holder [29] [41] [42] [39]. LCTEM devices with this kind of structure are somewhat limited in that they can only be used with holders equipped with the specialized clamping features that are not found on more general-purpose TEM holders. However, as will be discussed later, this type of device is often capable of more sophisticated sample interaction than other existing designs.

Other "self-contained" devices involve the permanent bonding of the two chips together using epoxy, solder, or direct bonding methods to form a container whose inlets are sealed using similar bonding methods [43] [44] [45]. This kind of fully sealed device is compatible with more generic TEM holders as there is no special clamping or sealing requirement for the holder itself. As such, LCTEM solutions following this design paradigm are potentially more accessible as they require less specialized equipment

beyond the chip itself. However, a significant drawback for these designs is the relative inaccessibility of the loaded sample. Because the chamber is fully sealed, it is difficult to apply stimulus to the sample. Sample interaction for both of these device types will be explored in the following section.

Liquid-Phase Investigations

A wide variety of liquid-phase experiments have been performed by researchers using LCTEM techniques [46] [47] [48] [49]. Many involve the observation of the growth of metallic nanoparticles from a precursor solution [43] [50] [51] [44] [52]. Oftentimes, electrons from the imaging beam itself are used to precipitate the growth of nanoparticles out of solution. This phenomenon is discussed further in Section 5.2.1. Other researchers used liquid cells to study biological cells both of bacteria and eukaryotes [53] [34]. The ability to monitor biological components such as vesicles or labeled proteins within cells has also been demonstrated [54] [55] [56]. With a wide variety of applications even for non-interactive observation of liquid-phase systems, LCTEM techniques can be made more sophisticated through the use of sample-interaction capabilities.

1.2. State of the Art

The ability to image static liquids and distinguish particles within TEM represents a powerful tool in itself, having been applied to observe the synthesis and growth of nanoparticles [44] as well as whole cells and biological mechanisms in solution [53]. However, the capabilities of basic LCTEM techniques can be further augmented in order to enable more sophisticated experiments that take advantage of the dynamic nature of liquid-phase microscopy. The kinetics of reactions within liquid samples are associated with the physical motion of constituent particles within the solution, be they molecular

reactants or larger particles with active surfaces. LCTEM can allow for the direct observation of this motion in response to and as a result of active reactions within the liquid cell. However, the volume of liquid sample contained within a liquid cell is very small, usually on the scale of picoliters, and as such non-continuous reactions can run out of the reactants necessary to continue very quickly: often before TEM observation can be established. In order to properly investigate reaction dynamics using LCTEM techniques it is necessary to control various sample variables in order to initiate or trigger the desired activity as needed rather than allow it to occur spontaneously. By directly interacting with the contained sample, this kind of reaction control can be achieved and used not only to determine the timing of a reaction to ensure optimal TEM observation conditions, but also to enable more in-depth quantitative experimental analysis in conjunction with TEM visualization through the precise control of the sample environment.

1.2.1. TEM Liquid Cells and Sample Interaction

The main requirement for liquid cell technology for TEM is the hermetic sealing of the device. As stated previously, leakage can cause damage to the highly-sensitive TEM equipment. However, the complete sealing of the cell often works to render its contents inaccessible from the outside. In non-TEM investigative techniques involving liquid-phase samples, it is common to apply an electrical signal or manipulate the temperature of the target of study in order to induce some form of action or reaction and observe the results. Liquids are by their nature dynamic, and given that TEM is capable of real-time imaging of the sample liquid, any inherent motion or action within the sample can be observed. While this is appropriate for long-term reactions or other ongoing phenomena, the very small sample sizes involved with liquid-phase TEM systems means that by the time observation is achieved, the action is finished [28]. In order to observe

dynamic phenomena in liquid cells, it is often necessary to trigger it by manipulating the sample in some way.

Liquid-Phase Experimental Variables

The most basic and accessible experimental variables and stimuli that must be controlled during the analysis of liquid-phase systems are applied electrical voltage, temperature, and concentration of the solution and its constituents. All fundamental reactions require some threshold amount of reactants as well as energy, usually in the form of either thermal or electrical excitation, to occur. This is the same for samples under TEM observation, and as such it is beneficial for an LCTEM system to be capable of controlling and manipulating these variables. Sample interaction, in the form of electrical biasing, heating, and mixing, is necessary to properly control the sample environment and enable both the triggering of reactions at will as well as the execution of specific and quantitative scientific analyses of liquid-phase systems.

Existing Solutions

Within LCTEM techniques, the most readily achievable sample interaction method is the application of external voltage. Given that electrical signal can be conducted directly through solid metallic lines built directly into generic, non-LCTEM-specific TEM holders, one of the first modern LCTEM devices was already equipped with electrodes that were used to study electrodeposition [43] [29]. Many subsequent studies of similar systems have been performed, both in self-contained sealed cells [45] [57] [58] as well as specialized holder-based devices [59].

Temperature control for LCTEM systems can be also be achieved using heated TEM holders coupled with self-contained LCTEM devices. Such techniques have been

used to observe the growth of various nanoparticles [60] [61]. Heating with the device can even be achieved through the use of a laser integrated into the TEM system [52]. Additionally, since electrical interconnects are readily available in TEM holders, it is possible to use an externally applied electrical signal to generate heat within the liquid cell. The integration of Joule-heating elements into the liquid cell device itself can be used in conjunction with a TEM holder with electrical interconnects to generate heat directly. This direct integration of a heating element has been used to study the localized evaporation of water within a liquid cell to form nanobubbles [62]. In addition to these various methods for achieving sample heating, at least one group has pursued an LCTEM setup to actively cool the sample liquid within the TEM chamber. By designing a custom TEM holder with an externally cooled copper rod that was held in contact with a liquid cell structure affixed to the tip of the holder, temperatures as low as 220 K were achieved and used to study the formation of crystalline water from the liquid phase [63]. In these ways, various holder-based and chip-based techniques exist to achieve the control of temperature within liquid cell structures.

The ability to control the concentration of samples loaded within LCTEM structures represents arguably the most challenging means of applying stimulus to liquid cell structures. While electrical and thermal biasing involve the conduction of energy through static materials, concentration control for LCTEM systems is only practically achieved through the initiation of liquid flow within the liquid cell. Because this necessitates the movement of material in the form of the sample fluid, existing commercial and custom solutions exclusively involve the use of specialized TEM holders that feature embedded fluidic channels within the holder body to pass through the threshold of the TEM chamber while maintaining a vacuum [64] [42] [41]. Such systems

are by their nature complex and consequently expensive, but they do enable users to initiate flow within the liquid cell. While the TEM holder allows liquid to enter the TEM chamber, it is also necessary to safely transfer the fluid from the holder conduit to the liquid cell device itself without leaking into the surrounding vacuum. This can be achieved using sets of O-rings and clamping pressure provided by the customized holder apparatus that seal the holder conduits to the liquid cell. The holder piping thereby connects either to the space between the liquid cell chips [34] [65] [66] [67], or to inlets for a channel on the device [68] [69]. This type of system is most commonly used to maintain the concentration of a sample solution at a constant level and remove any bubbles that may form within the viewing area [70], but setups do exist to achieve sample mixing by merging two or more inlet pipes just before the liquid enters the liquid cell region [42] [71].

	Self-Contained Device	**Holder-Based Activity**
Biasing	Demonstrated [43] [58]	Demonstrated [59]
Heating	Demonstrated [62] [72]	Demonstrated [61] [73]
Flow	Not previously demonstrated	Demonstrated [65] [68]

Table 1: Selected examples of existing active liquid cell systems

Critically, it should be noted that no LCTEM flow systems could be found that achieved liquid flow within a self-contained liquid cell without relying on fluid flow-through TEM holders beyond those developed in this research [74].

1.2.2. Barriers and Limitations

In order to access and manipulate the hermetically sealed contents of the liquid cell, the specialized TEM holders described above feature electrodes, heating elements,

and even flow tubes to introduce new fluid to the holder during TEM observation. While such devices offer excellent manipulative capabilities, they are quite costly and are often specifically designed for single purposes that limit their accessibility for general users. Someone looking to get involved in the manipulation of liquid-phase samples in TEM is often faced with the paradox of investing into a highly-specialized and non-versatile TEM holder or a generic holder that offers only reduced sample interactivity, usually through electrical interconnects only.

Cell Sealing and Feed-through

As introduced above, there is a very real tradeoff between the "sealability" of a liquid cell structure and the ease with which its contents can be accessed. Standalone self-contained liquid cell devices that are permanently or semi-permanently sealed via wafer-bonding or epoxies are often much more compatible and useable with a wider variety of generic TEM holders not specifically designed for LCTEM. Because these liquid cells are sealed by themselves, more commonly available holders that are either static or equipped with temperature control or electrical biasing features can be used interchangeably. However, thus far achieving fluid flow within such devices has not been possible as there is no way to pass material through the fully sealed device by definition.

Conversely, dedicated LCTEM holders that achieve sealing via clamping features on the TEM holder are much more conducive to the integration of flow features as they can be customized or ordered to be equipped with fluidic feed-throughs in addition to the necessary heating or biasing elements. As mentioned previously, the use of dedicated TEM holders with O-ring seals combined with liquid cell chips can allow the user to apply fluid flow from an external pump, through the holder-integrated conduits, and across the area between the chips. However, a majority of existing commercial and

custom devices rely on introducing fluid throughout the area between the two chips rather than flowing it across a dedicated channel confined to the viewable region of the device. Such systems allow a significant amount of liquid to pass around the membrane area that is visible in TEM due to the arrangement of the external conduits. This can limit the responsiveness of the system to the application of a new liquid as transport to the visible region is dependent on a combination of diffusion and direct flow rather than one or the other [75] [76] [69]. Designs with direct inlet-channel flow require multiple sets of interlocking O-rings to achieve sufficient sealing and can be vulnerable to overpressure induced by the external pumps. Critically both types of design are fully reliant on the use of specialized, dedicated TEM holders and cannot be used with more generic, widely-available holders.

Equipment Availability

As suggested above, the tradeoff between self-contained and holder-sealed liquid cells in terms of compatibility with generic holders translates directly to the relative accessibility of the respective LCTEM technique. Fully sealed liquid cell structures can theoretically be used in any TEM holder as long as it is physically small enough to fit within the specimen stage. This makes such devices somewhat more accessible in a laboratory environment that is limited by the TEM infrastructure available. For holder-based LCTEM systems, the opposite is true, as the design of the liquid cell corresponds specifically to a certain type of holder, and usually cannot be used with generic TEM holders or even other LCTEM holders. This can serve to inhibit the use of liquid-phase TEM techniques for researchers who do not already specialize in TEM or LCTEM as it requires a not-insignificant initial investment in both the advanced holder and associated auxiliary equipment in order to begin experimentation. Even if a researcher has access to

an external electron microscopy center with a variety of general-purpose TEM holders, unless they possess the specialized LCTEM equipment necessary, the technique remains inaccessible. As a result of this effective barrier to entry for the technique, LCTEM remains an investigative method pursued primarily by research groups focused on the technique itself, rather than researchers from the broader range of academic fields that could potentially benefit from its use.

1.3. Research Overview

1.3.1. Functional Objectives

While a wide variety of liquid cell devices have been developed in the past with various functionalities, this study is focused on the development of devices that fulfill certain criteria aimed at increasing both the accessibility of liquid cell technology as well as its efficacy. The overall aim of this research is to achieve the advanced sample interaction capabilities described in Section 1.2.1 without the use of specialized TEM holders or other intricate equipment. Achieving this goal will help elevate active LCTEM methodologies from being a relatively niche specialist technique to more utilitarian and accessible investigative tool. Doing so will allow the nanoscale reaction kinetics previously investigated with complex LCTEM setups to be explored by a wider range of researchers lacking the TEM equipment and expertise previously required for such experiments.

In order to make the devices more applicable to general users and safe to use in a wide variety of TEM systems, the device first must achieve sealing without the use of external clamps or structures. Secondly, the contents of the liquid cell must be accessible without the use of a dedicated TEM holder. Finally, the device must specifically be able

to control the electrical, thermal, and flow-based variables of its contents as directed by the used.

Self-Containment

While many liquid cell devices currently in use rely on O-rings and external clamps to achieve sealing, such designs are inherently limited to use with those specific apparatuses and cannot easily be used in a wide variety of microscopy environments. If liquid cell sealing is achieved through the use of clamps and O-rings present on the TEM holder, it is difficult to move and manipulate the liquid cell in other experimental setups such as probe stations for device calibrations or other non-TEM-based tests. To overcome this issue, any and all functionality of the device both in terms of sample sealing and sample interactivity should be contained to the device itself as much as possible. This way, not only is the use of a specialized TEM holder precluded, but the device can also be easily used in a wider variety of non-TEM experimental setups such as optical microscopy and probe stations.

Holder Compatibility

Related to the first criteria, the liquid cell structure should be compatible with a wider variety of generic TEM holders. One of the major drawbacks of liquid cell technology is the common requirement for a highly specialized TEM holder specifically designed to achieve control of a single experimental variable or condition that limits its applicability outside of that one scenario. For such devices, researchers must invest not only in a specialized liquid cell chip, but also a dedicated TEM holder for liquid cell experimentation. A liquid cell device that can achieve its desired functionality while still being compatible with generic and widely-available TEM holders would be much more

accessible for liquid-phase experimentation. As such, the liquid cell devices developed in this study must achieve all of their functionality using TEM holders that do not provide any mechanical sealing or higher-order features beyond the ability to apply electrical signals to the device through simple wire-based interconnects.

Electrical, Thermal, and Flow Control

Finally, and most critically, in order to initiate sample activity to observe nanoscale reaction kinetics the liquid cell device should allow the user to interact with the sample during TEM observation through the application of electrical biasing, heating, and mixing or flow control. These three variables cover a wide range of experimental conditions that must be controlled in liquid-phase science, so any TEM device designed to investigate liquids should be capable of replicating such environmental controls available at a normal laboratory bench.

In summary, the liquid cell devices proposed in this study aim to replicate and integrate the same experimental capabilities present in existing individual specialized active LCTEM setups while containing all functionality to a single device that is self-contained and compatible with generic and widely-available TEM holders. These overall objectives are summarized below in Table 2.

		Capability	Limitation
Existing Devices	Custom cells	Biasing, heating	No flow control Specialized holder
	Active holders	Biasing, heating, flow	Specialized chip Specialized setup

		Capability	Advantage
Proposed Solution	Standalone cell	Biasing, heating, flow	Self-contained Generic holder Combined function

Table 2: Summary of existing device limitations and proposed device solutions

The principle novelty of this research is first in the achievement of liquid flow within an LCTEM device without the use of external plumbing which has not been otherwise achieved to date. Existing flow-capable LCTEM systems are based on external pumps and complex fluidic interconnects to the TEM vacuum chamber. Sealing a sample liquid within a chamber inside the liquid cell and transferring it to another chamber using only electrical interconnects during TEM observation represents an experimental capability not yet demonstrated elsewhere and helps to make LCTEM flow control more accessible to researchers without specialized LCTEM holders. Furthermore, the integration of biasing, heating, and flow capabilities onto a single standalone device also represents a capability not yet demonstrated elsewhere. While certain commercial devices are capable of these three functionalities, they require highly complex and specialized TEM holders with various plumbing and electrical interconnects. As mentioned above, achieving similar functionality on a standalone device using a generic electrical

interconnect TEM holder makes the technique more accessible and applicable in a wider variety of experimental situations.

1.3.2. Research Outline

In order to achieve the objectives outlined above, two distinct device platforms were pursued. Described in detail in the following chapter, the two-chip devices and nanochannel devices, respectively, were developed and then augmented to achieve active sample interaction capabilities. Finally, these devices were used to demonstrate the possibility of scientific studies using interactive LCTEM experimentation.

Platform Development

Initially, the basic structures of both device platforms were developed in order to function successfully as static liquid cells. The ability to fully seal liquid and generate a TEM image was prioritized and optimized to increase device yields and usability. Specifically, the fabrication processes through which the observation membrane is released, the spacer layer is deposited, and the chips are separated were all improved to increase device yield and facilitate further development. In this phase of the study, rather than developing novel functionality, the reliability and efficacy of the underlying liquid cell structure was developed and refined to serve as a foundation upon which future advanced functionality could be based.

Integration of Active Components

Next, the basic two-chip liquid cell platform was augmented with active sample interaction features that allowed for the application of external stimuli to the samples loaded within. Once the fundamental two-chip structure was established, the ability to apply electrical bias, heating, and initiate flow within the self-contained liquid cell

devices was pursued and achieved using devices both outside of and within the TEM chamber. During this stage of the study, the focus was on the development and characterization of these three distinct MEMS-based functionalities first on an individual basis and subsequently with the aim of total integration of all active features onto a single device. Once the MEMS components could be successfully integrated and characterized, the next stage of research involved the demonstration of their use for *in situ* TEM experimentation.

Demonstration of Scientific Applications

Finally, the device platforms and the active components that were developed were demonstrated with a variety of sample solutions in order to demonstrate both the functionality of the integrated active components as well as the feasibility of applying these devices for proper scientific studies. In addition to the fabrication of a single device featuring all three active MEMS interactive capabilities, the use of the developed devices to investigate and observe several distinct liquid-phase samples in TEM was also demonstrated. The general structure of these three research stages of device development and use is shown below in Figure 1.8.

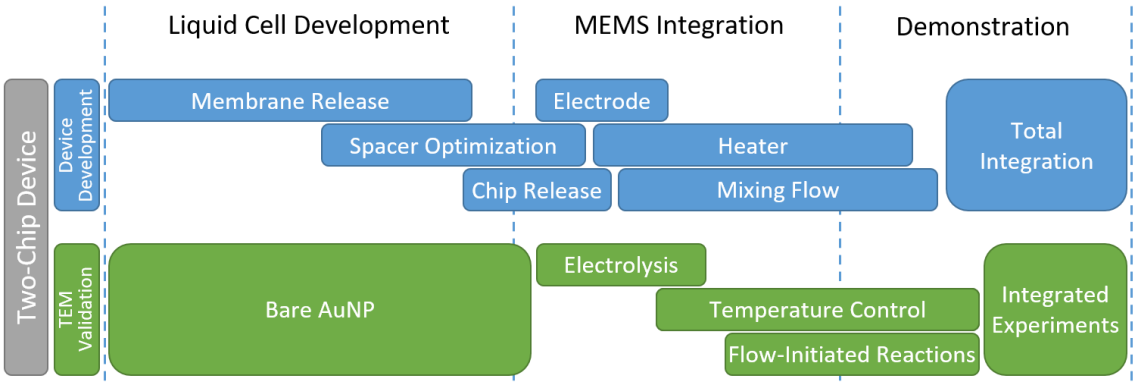

Figure 1.8: General research phases for the development and demonstration of the novel two-chip liquid cell device

Chapter 2: Basic Design and Device Development

In order to develop more complex active liquid cell devices, it is necessary to first establish a reliable static liquid cell platform on which further work can be built. Previous versions of the liquid cell have suffered from low fabrication yield and limited process flexibility. To meet the objectives of self-containment, simple holder compatibility, and the integration of electrical, thermal, and flow control features, standardized liquid cell structures were first developed to avoid compounding issues with the development of each component.

Fundamentally, in order to function as a self-contained liquid cell, the device must be capable of both hermetically sealing the sample from the surrounding vacuum environment while still providing a means for the imaging electron beam to interact with and transmit through the sample. Furthermore, to achieve active sample interactivity using only a simple electrical-interconnect TEM holder, the device must be capable of integrating additional features in addition to its basic liquid cell structure. In this study, two distinct platforms have been used with these goals in mind. The first, called here the "two-chip liquid cell" is based on a classical sandwiching chip design and is most readily augmented with active MEMS components. Most of the device development in this study was performed on this platform. The second, known as the "nanochannel" features a more exotic suspended cylinder structure to achieve sealing and TEM imaging. This device is currently capable of higher imaging resolutions, but is more challenging to supplement with active features and as such was used primarily for sample verification. In this chapter, the fundamental structure of these two platforms will be described in detail, with the following chapter detailing the integration of active features.

2.1. Two-Chip Device

The two-chip liquid cell structure described here is based specifically on a previous design [77] consisting of micromachined silicon chips with nitride viewing membranes which is itself based on one of the more conventionally-pursued liquid cell geometries for TEM as introduced previously [43] [34] [29] [28] [46]. In order to achieve the device objectives of holder compatibility and sample interactivity as discussed in previous chapters, the two-chip device itself is entirely self-contained, relying on epoxy rather than the TEM holder to achieve sealing. Furthermore, sample manipulation capabilities are achieved through the integration of MEMS features directly within the device itself, the details of which will be described in the next chapter. These properties mean that the final device does not require a specialized holder to achieve either liquid sealing, heating, or flow. A general TEM holder with only electrical interconnects can be used, significantly increasing the accessibility of the device for prospective users.

The main advantages of the two-chip liquid cell platform in terms of development and functionality include the accessibility of the liquid chamber and the relative simplicity of the fabrication and assembly process. Because each individual chip makes up only one side of the final sample chamber, the majority of the chip face can be used for the integration of MEMS components. The fabrication process leaves the chip face accessible until the final assembly step, and as such allows for significant process flexibility as compared to other liquid cell techniques. In addition to the accessibility of the chip surface, the two-part structure is finally assembled using a simple epoxy-based bonding process, which allows for further process flexibility as there are no significant restrictions on the state of the chip surface to achieve proper bonding. These qualities make the two-

chip device an ideal platform for integrating diverse MEMS components enabling various sample interaction capabilities that are fully contained within the device itself.

In this section, the fundamental structure of the new two-chip platform will be explained, focusing on the features of the device that allow it to operate as an effective liquid cell for the integration of active MEMS features. The details of those specific components will be discussed in the next chapter.

2.1.1. Overall Structure

As introduced previously, the two-chip device is comprised of a classical liquid cell structure in which the sample is sandwiched between two distinct micromachined chips. The rigid structure of the chips prevents the liquid sample from leaking out into the vacuum chamber when the chips are hermetically sealed together with epoxy. Each chip also features electron-transparent viewing windows which are thin enough to allow for TEM imaging while also sealing the liquid inside of the cell.

Figure 2.1 shows a schematic rendering of the two-chip device features before assembly. The top and bottom chips are fabricated on a single wafer as separate components and are later assembled to form the completed liquid cell. The viewing windows are located centrally on each chip and represent the area that will be visible during TEM observation. This experimental region is defined by the observation membrane, the spacer that forms the sample chamber, and the active components of the device that are included in the region.

The observation windows themselves are made of thin membranes of silicon nitride that are deposited on the silicon chip surface and subsequently exposed via plasma etching of the backside silicon. The nitride membranes maintain the hermetic seal between the atmospheric pressure within the liquid cell and the high-vacuum TEM

chamber while also providing a minimal amount of interference to the TEM electron beam which allows for the imaging of the cell contents. The contents of the cell are only visible in the areas where the observation membranes of the top and bottom chips are aligned, allowing the electron beam to transmit. The path of the electron beam through the assembled cell can be seen schematically in Figure 2.2.

The spacer ensures a degree of separation between the two chips, outlines the shape of the sample chamber, and serves as the nominal bonded surface of the device. When the liquid sample to be imaged is loaded into the device via the loading inlets on the bottom chip, it must occupy the space between the top and bottom chips, and the spacer serves to define that channel in a controllable manner. In addition to maintaining the separation height between the two chips when assembled, the spacer also prevents the membrane from coming into contact with any external surfaces during fabrication and handling prior to assembly. Various membrane and spacer layouts and designs were used in the experimental portion of the study and the design of each are described subsequently in this section and summarized in Table 6.

A summary of the general design parameters for the device and these components as well as typical values used in this research can be seen in Table 3. The generic electrical-contact TEM holder defines a specific specimen size and features five contact probes. With regard to the liquid cell itself, as discussed above, the membrane must be a material strong enough to serve as a pressure-holding thin while also being process compatible. The thickness should be minimized to increase potential resolution while maintaining structural integrity. Similarly, a larger membrane enables a larger potential viewing area, but is more susceptible to damage due to handling and operation. The spacer material in general is not critical beyond its compatibility for the fabrication process, but

as discussed in Section 3.3, a hydrophobic material is more conducive to designing flow control capabilities. The spacer thickness, which determines the channel height, can limit the largest particles or aggregates than can enter the observable region and be imaged, but an overly thick channel significantly reduces TEM resolution.

	Parameter	**Constraint/Tradeoff**	**Nominal Value**
TEM Holder	Device Size	4x5.5x1.5 mm	4x5.5x1.5 mm
	Contacts	5	≤5
Membrane	Material	Compatibility vs. performance	Si_3N_4
	Thickness	Strength vs. resolution	30-80 nm
	Area	Observable region vs. fragility	0.03-0.1 mm^2
Spacer	Material	Compatibility vs performance	Resist, Teflon
	Thickness	Max particle size vs. resolution	200-1000 nm

Table 3: General design parameters for two-chip device components.

The active MEMS features of the device consist of the various platinum electrodes on the bottom chip in addition to the liquid gate structure found on both the top and bottom chips. The electrodes within the experimental region can be used for biasing the experimental sample as shown in Figure 2.1 or for controlling the sample temperature. The pump electrodes flanking the loading inlets can be used in conjunction with the hydrophobic liquid gates to control the flow of liquid within the sample chamber along the length of the channel defined by the spacer. The details of the layout and functionality of these active components will be described in Chapter 3.

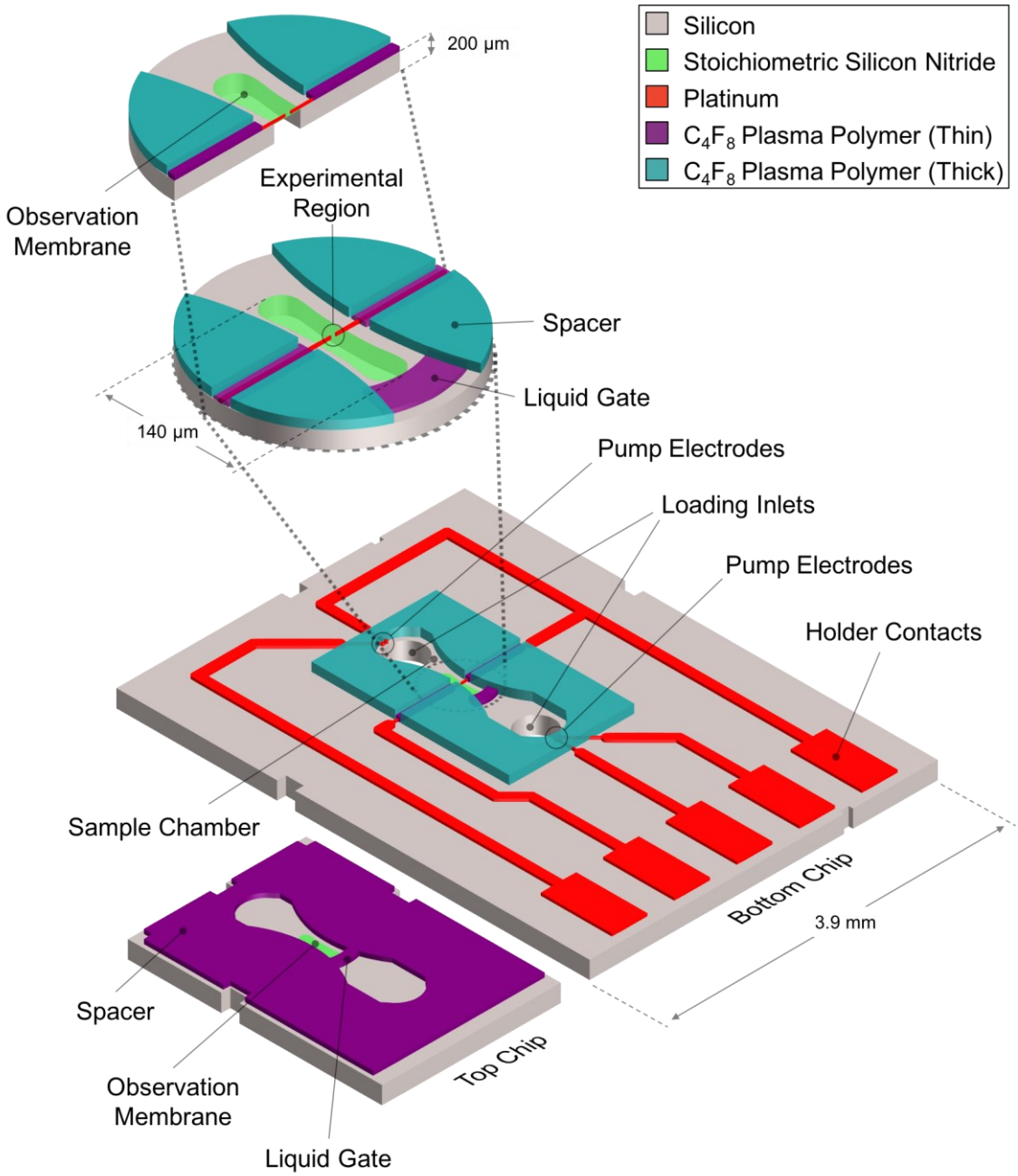

Figure 2.1: Schematic of two-chip liquid cell structure. 1st Inlay: Magnified view of the experimental region of the bottom membrane. 2nd Inlay: Cross-section of magnified area.

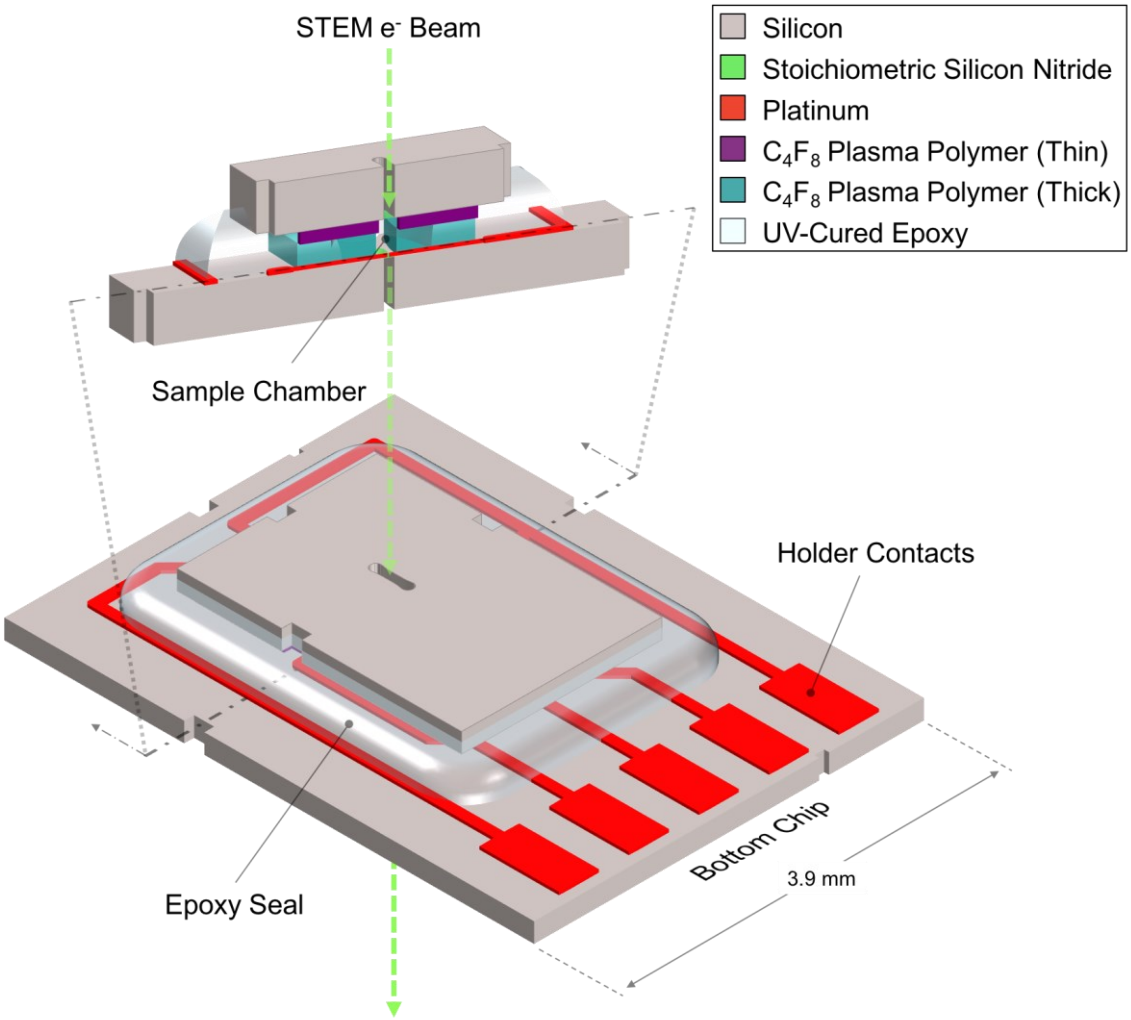

Figure 2.2: Assembled two-chip liquid cell after epoxy sealing. Inlay: Cross-sectional view of experimental region.

Membrane Design

In encapsulated liquid cell structures, the observation membrane is perhaps the most critical features in terms of both device reliability and functionality. The membrane must be able to maintain the liquid inside of the device at or above atmospheric pressure while the surrounding vacuum chamber reaches pressures as low as 10^{-5} Pa. Conversely, the membrane must be thin enough to prevent excessive scattering of the imaging TEM beam. Furthermore, the material used for the membrane can also affect the ultimate imaging capabilities. For a given STEM system used to image a liquid cell in dark field

ADF mode, the normalized number of electrons sufficiently scattered by the encapsulating membranes to create a signal, N/N_0 can be approximated by the following equation where T is the thickness of the membrane, l is the mean free path for elastic scattering, W is the effective atomic weight of the material, ρ is the material density, and N_A is Avogadro's number. Additionally, $\sigma_{el}(\beta)$ is the effective partial cross-section for elastic electron scattering beyond the ADF detector's threshold angle β, which scales with Z or the effective atomic number of the material [28] [33].

$$\frac{N}{N_0} = 1 - e^{-\frac{T}{l}}, l = \frac{W}{\sigma_{el}(\beta)\rho N_{\mathrm{A}}}$$

Equation 1: Electron Detection in STEM [28] [33].

The larger the value of N/N_0, the more incident electrons are scattered by the membrane material: creating noise in the final image and reducing the ability for particles within the liquid sample to be resolved. As can be seen, a higher material thickness T increases the fraction of scattered electrons. Furthermore, a shorter mean free path in the material, usually caused by higher density or atomic number, also serves to scatter more electrons. In general, therefore, a thinner and atomically lighter or less dense membrane will yield a brighter imaging signal and better contrast, with 50-nm-thick silicon nitride being a commonly-used standard material [78].

The ideal material for a liquid cell membrane must feature a balance of high tensile and shear strengths, low elasticity, and low atomic weight and density. Many researchers have and continue to pursue graphene as a particularly strong, thin, and light material for use in TEM in general and liquid cell structures specifically [79] [80] [81] [30] [31]. While graphene has relatively promising mechanical properties, it has proven

to be difficult to integrate into more complex MEMS microstructures due to the fragility of handling when using individual graphene layers and the uneven topology of a micromachined surface [82]. The delicate carbon structure is susceptible to damage if deposited on the wafer surface at the beginning of fabrication, and the unevenness of the final device surface makes a final layer transfer process unreliable. As such, silicon nitride is used in the two-chip design as it features robust mechanical and chemical properties when used as a membrane and is extremely process compatible due to its good selectivity versus many microfabrication etching and cleaning processes.

The initial two-chip device design utilized a combination of Deep Reactive-Ion Etching (DRIE) and vapor-phase HF etching to pattern and release the final silicon nitride membrane window on the chip. Using an 80 nm silicon dioxide stop layer under a 30 nm silicon nitride layer, the backside bulk silicon was etched down to the membrane using DRIE. A timed HF vapor etch was then used to remove the remaining oxide. Variability in the selectivity and etch rate of the DRIE and HF processes prevented the complete etching of the oxide layer without damaging the desired nitride layer. The result was wrinkled membranes with significant out of plane deflections. Figure 2.3 shows a typical membrane with a 150-µm-diameter coupled with a 3D graph of the membrane surface profile as measured with a laser confocal microscope. As can be seen, large deflections of several microns out of plane were present without any loading. This both reduced the overall device yield due to the vulnerability of the membranes to damage during handling and compromised the TEM resolution of the cell due to a thicker fluid column from the bowing of the membrane under pressure. Furthermore, the vapor HF tended to attack both the frontside nitride membrane as well as the other surface features, making this membrane and release system far from ideal.

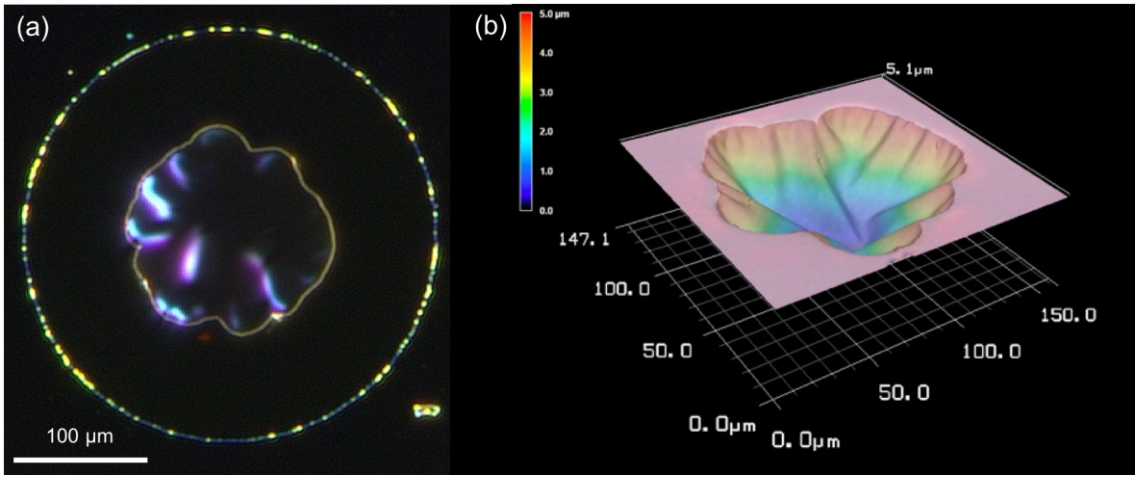

Figure 2.3: (a) Wrinkled nitride/oxide membrane. (b) Laser confocal profilometry of membrane surface.

Over the course of this study, the oxide/nitride bilayer wafer structure was replaced with a process involving only silicon nitride on the original silicon wafer. The backside etching of the nitride membrane is performed using initial DRIE and a final tuned SF_6 plasma etch to selectively etch any remaining silicon while leaving the nitride membrane undamaged and released. 20 Pa of SF_6 flowed at 400 sccm is excited with a 2 kW coil power and accelerated with a 10 W drive-in platen voltage. Since the largest viewing area of the STEM in high-magnification mode is approximately 80x60 µm, the geometry of the membrane was also narrowed to an elongated shape from 80 to 100-µm-wide and 300 to 900-µm-long in order to minimize out-of-plane deflection and reduce the risk of membrane damage during handling. The membrane thickness was also increased to 50-70 nm with no detectable reduction in STEM imaging quality. The results of these changes included higher fabrication yield rates as well as deflections under 20 nm at rest as shown in Figure 2.4.

	Fabrication Yield	Comments
HF Vapor Release	~50%	One-by-one processing
DRIE Only Release	~80%	Wafer-level, poor selectivity
DRIE+Isotropic SF_6 Release	~100%	Wafer-level, good selectivity

Table 4: Approximate device membrane fabrication yields for etching release processes

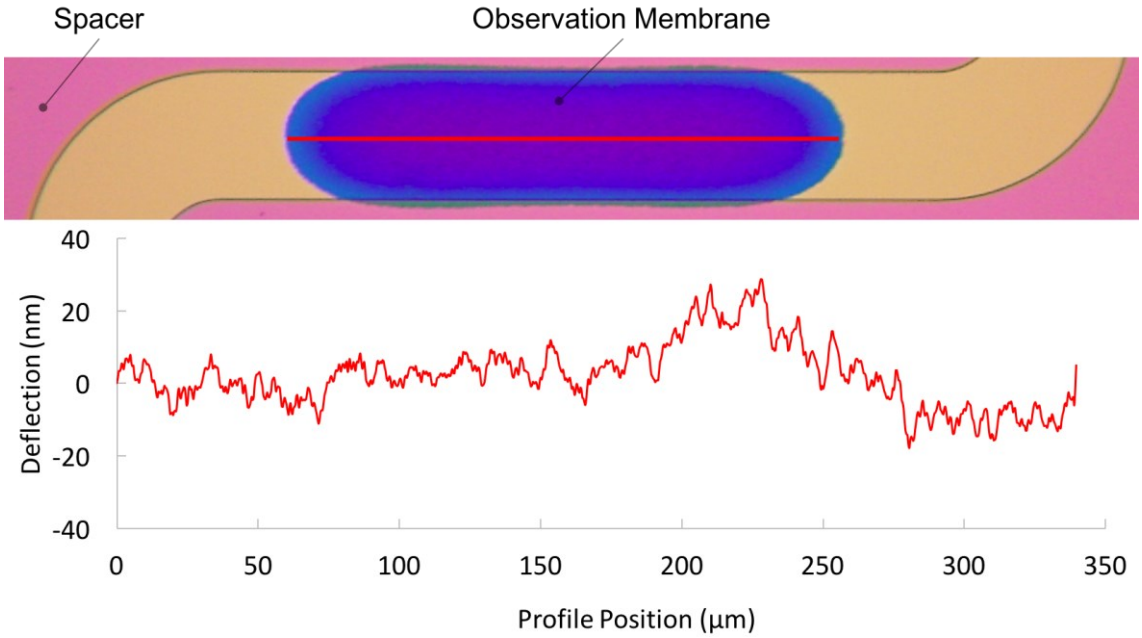

Figure 2.4: Surface profile for final etch release process for a 340 µm x 80 µm x 70 nm membrane

The various membrane sizes and shapes used after refinement of the membrane fabrication process are illustrated in Figure 2.5. The slightly convex shape of the grid and narrow patterns served to compensate for previous etching irregularities that were subsequently eliminated. The 1x3 grid pattern was used to align with an identical pattern on the top chip that is rotated 90º in order to form a grid of nine overlapping observation regions when the chips are assembled together. This served to allow a significant degree of leeway when aligning the chips. Ultimately it was found that manually aligning single 80-µm-wide membranes was reliably achievable, so all membrane designs beside the grid

pattern are aligned and assembled with identical corresponding patterns on their complementary top chips. The long and 2x1 series membrane designs serve to offer a larger potentially observable region along the length of the liquid cell's internal channel. Overall, the shape and size of the membrane has little effect on the active functionality of the liquid cell so long as it enables visualization at the desired location and maintains integrity when loaded with liquid and placed in the high-vacuum STEM chamber.

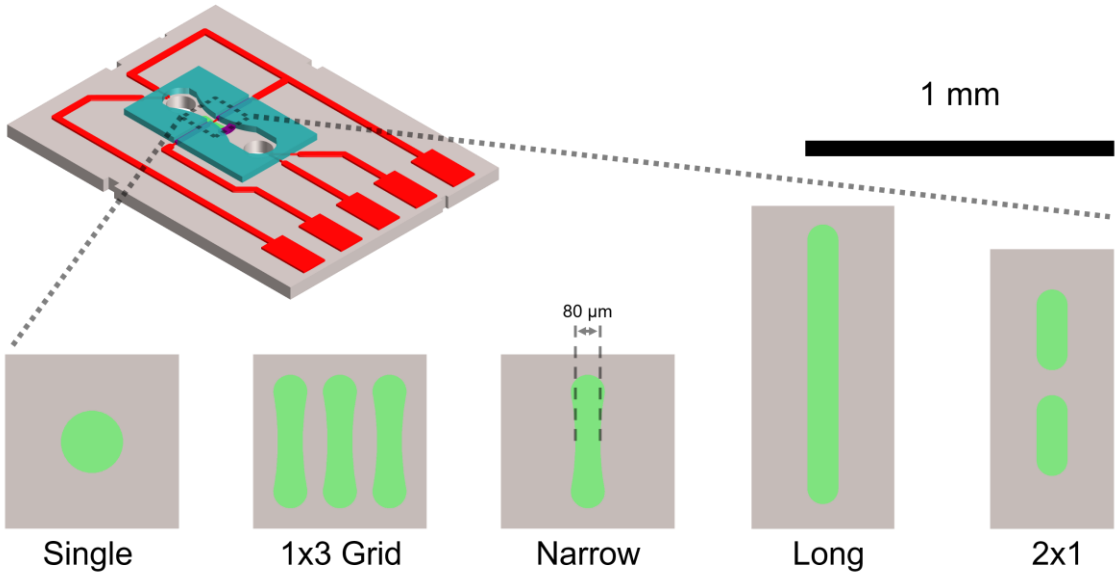

Figure 2.5: Two-chip device membrane shape and size variations

The resilience of the membranes under pressure loading was demonstrated by assembling liquid cell devices, loading sample liquids, subjecting them to high-vacuum environments, and confirming the integrity of the membranes through optical microscopy as well as STEM observation. The primary membrane failure mode during device use was rupture due to handling errors during assembly after chip fabrication and before use in the STEM. During these processes there is no significant pressure gradient across the membrane and failures only occurs due to accidental mechanical contact of the membrane by either probes or other devices. To date, no membranes have broken due to pressure

differentials within testing vacuum chambers or the STEM itself even under additional internal pressurization as demonstrated in Section 3.1.3. The details of the assembly and loading process as well as the most common modes of device failure are described in Section 2.1.2.

Spacer Design

The function of the spacer within the two-chip liquid cell is to provide an area between the two chips for the liquid sample to occupy. By defining the gap distance between the chips, the spacer also determines the thickness of the sample liquid to be observed. The height of the fluid column sandwiched between the two nitride viewing windows will always be greater than or equal to the spacer height due to the slight bowing of the membranes under the pressure differential within the TEM vacuum chamber. Just as the material of the nitride membrane serves to generate noise due to electron scattering, so too does the liquid within the cell. The mean free path for electron scattering in a liquid medium can be found using the same definition introduced in Equation 1; for water under normal STEM conditions, this value is approximately 10 μm [34]. By comparing the background signal generated by a fluid medium of thickness T with the signal generated by a particle suspended in that fluid, the smallest particle size d_{STEM} that can potentially be resolved in an STEM is expressed in Equation 2 where l is the electron mean free path in the given material.

$$d_{\mathrm{STEM}} = 5l_{\mathrm{particle}}\sqrt{\frac{T}{N_0 l_{\mathrm{fluid}}}}$$

Equation 2: Ideal STEM particle resolution in fluid [28].

For any given electron dose N_0, the achievable resolution can be improved by using a thinner fluid column to reduce background scattering. Practically, this is possible through the use of thinner spacer layers that decrease the available gap between the two chips. Conventionally, liquid cells have used spacers as large as 5 μm, which is under the electron mean free path for typical STEM conditions in water which is around 10 μm [34]. In such conditions when viewing gold nanoparticles in water, with a gold mean free path of 73 nm, particles above d_{STEM} = 1.4 nm are potentially resolvable [28] [35].

While the above equation indicates that a thinner fluid column is always better, there are practical considerations that limit the degree to which the spacer layer can be thinned. The first is the preservation of the nitride membrane. One of the most common failure modes for the two-chip device involves stiction occurring between the top and bottom membranes during assembly and filling. If this occurs, the sample fluid can often be forced away from the viewable membrane region and into the rigid silicon-backed surrounding structure, preventing its observation. The use of a thicker spacer prevents the membranes from deflecting excessively under stiction loads, mitigating this issue. Furthermore, if the membranes come into contact during device assembly, any shear forces due to the relative movement of the chips during alignment will easily rupture the membranes. The presence of a spacer layer on each device prevents anything from contacting the membrane even if the device meets another flat surface in the membrane-down orientation. In practice, a combined spacer height of 700-1200 nm with each chip having at least 200 nm of spacer has been shown to be an effective design allowing both membrane preservation and relatively good resolution.

Another consideration for the spacer is its ability to actually confine the sample liquid to a determined channel shape on the device. The spacer layers do not actually

bond to each other, but are rather held together mechanically by the epoxy bonding of the top and bottom chips. This means that even slight roughness of the spacer layers can present vacancies into which the sample fluid can potentially flow. While the liquid would not leak out of the liquid cell as a whole due to the outer epoxy sealing, it can cause vacancies or air bubbles to migrate to the membrane region and prevent viewing of the liquid. Furthermore, for flow control applications, it is necessary to constrain the fluid to the defined channel shape in order to properly manipulate the motion of the fluid in the desired direction. To mitigate these issues, the spacer layer should either be capable of hermetically sealing to the corresponding layer on the opposing chip or be sufficiently hydrophobic to prevent fluid ingress into the layer gap. Ultimately, hydrophobicity was determined as the most appropriate solution.

Initially, S1818 photoresist was used as a spacer material. However, its solubility in organic solvents, weak resistance to plasma etching and other micromachining processes, and mediocre hydrophobicity and stability after processing made it incompatible with the overall fabrication process. Subsequently SU-8 polymer was applied due to its resilience to various microfabrication processes after curing. However, it was found that SU-8 was not sufficiently hydrophobic after final processing to reliably confine the liquid in the experimental region. Finally, the plasma deposition of fluorocarbon polymer films to form stable hydrophobic layers was explored. Both CHF_3 and C_4F_8 plasmas were investigated. The hydrophobicity of bare silicon, silicon nitride, CHF_3-based layers, and C_4F_8-based layers both with and without an oxygen plasma treatment are shown in Table 5. As can be seen, C_4F_8 plasma-based layers were both more hydrophobic compared to the alternatives, but were also more resilient.

	Si	Glass	Si_3N_4	CHF_3	C_4F_8	C_4F_8 (+O_2 Plasma)
Contact Angle (°)	58.2	27.3	44.0	95.6	113.4	105.5

Table 5: Contact angle of various spacer materials

Experimentation with the plasma deposition parameters eventually yielded layers with reasonable deposition rates that also featured good surface adhesion and stability along with hydrophobicity over time. A 2 Pa plasma driven with a coil power of 2 kW with C_4F_8 introduced at a 475 sccm flow rate yielded a stable film deposition rate of approximately 7.2 nm/s. Hydrophobic films of up to 1 µm could be reliably synthesized and patterned using lift-off techniques in conventional organic solvents. Figure 2.6 shows the results of a test deposition and patterning on a silicon shard as well as the contact angles as measured for the data shown in Table 5.

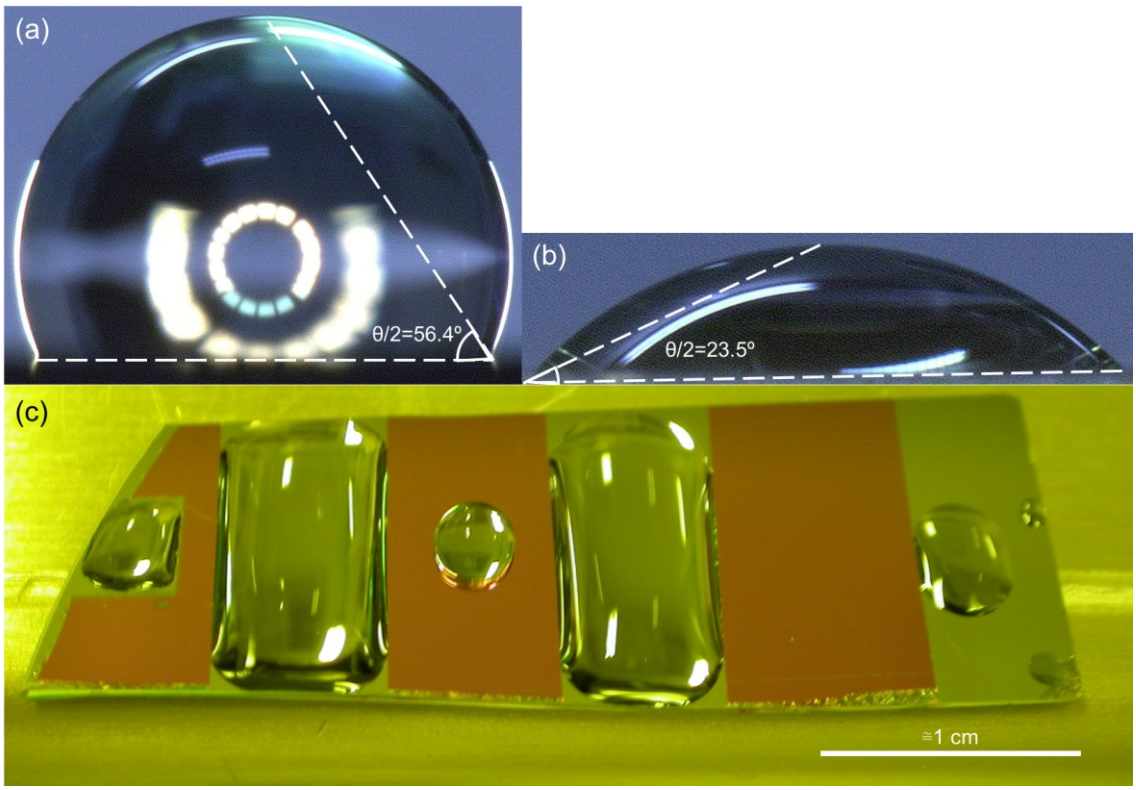

Figure 2.6: (a) Contact angle measurement on bare silicon nitride. (b) Measurement on C4F8 plasma-based layer. (c) Patterned hydrophobic layer on silicon

In order to successfully confine the liquid within the observable region of the channel formed in the liquid cell by the spacer, the layout of the spacer layer must also be considered. In total, three main spacer layouts were utilized to allow liquid to enter the channel through the inlets while not obscuring the suspended nitride membranes. A schematic of the layouts can be seen below in Figure 2.7. The wide and straight designs were developed to accommodate larger membrane designs, specifically the triple grid alignment design discussed above. As such they offer a potentially larger area of view during STEM observation when coupled with a correspondingly large membrane. The narrow design, by contrast, accommodates the single narrow membrane designs. While the potential viewing region is smaller, the narrower channel is more conducive to the development of flow control mechanisms as the liquid is confined to a smaller and more controllable region. The narrower designs are also less susceptible to the introduction of undesired air bubbles in the observation region which can prevent liquid from being successfully viewed. The hybrid design includes a narrow upper channel for use in initiating flow and a wide lower chamber. The lower chamber is designed to be loaded manually with a droplet of sample micropipette before device assembly rather than through an inlet. This potentially allows for the imaging of particles larger than would normally be able to flow through the sub-micron height of the channel to reach the observation membrane. Applying samples directly to the membrane with a micropipette before assembling the device can serve to bypass the so-called “filtration” of larger sample particles as described in Section 2.3.2.

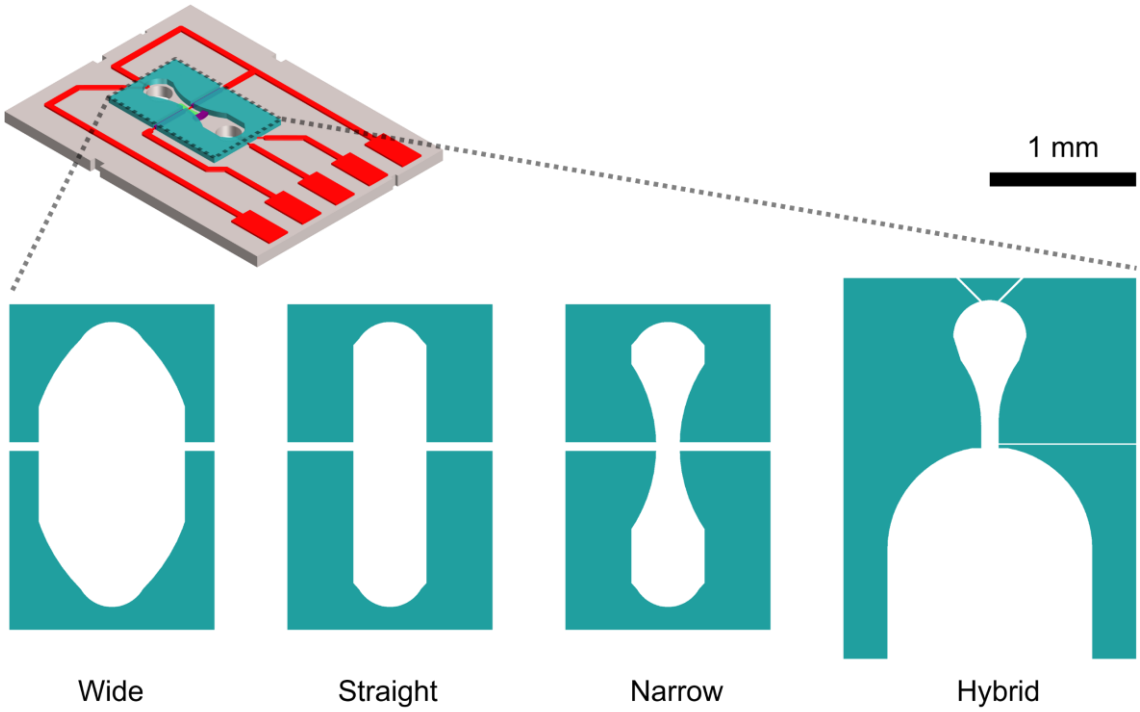

Figure 2.7: Two-chip device spacer layout variations

A summary of the various membrane and spacer configurations used in the devices described in the experiments discussed in this report is shown in Table 6.

Active Components

The basic two-chip structure as described above is capable of both encapsulating the liquid sample without leaking even in high-vacuum environments as well as providing a sufficiently electron-transparent viewing window to enable TEM observation. In this way the device fulfills its function as a basic static liquid cell.

In the next chapter, the integration of MEMS features to achieve electrical biasing, heating, and flow control will be described in detail. Broadly speaking, these capabilities are achieved through the customization of the platinum electrode layer, the secondary hydrophobic spacer/gate layer, and the addition of any necessary insulating layers on the

bottom chip. The combination of these individual components in various configurations enable interaction with the loaded sample fluid using only electrical signals supplied via an electrical-interconnect TEM holder. A schematic illustration of the three main active features to be discussed is shown in Figure 2.8.

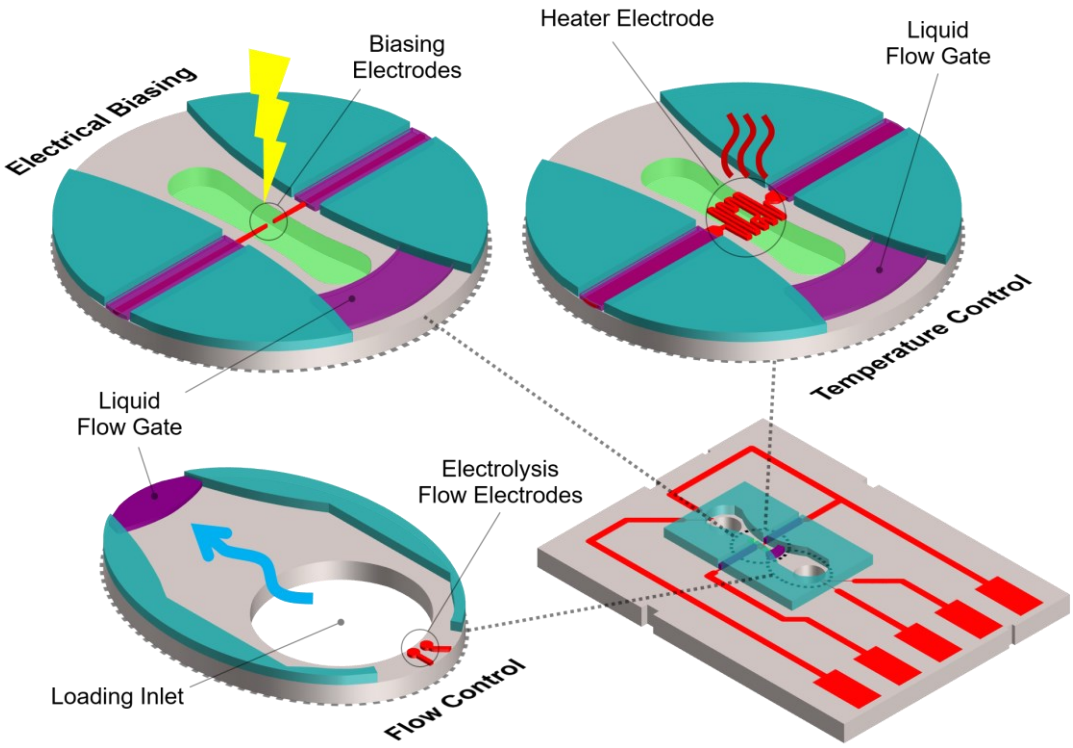

Figure 2.8: Active features of the two-chip liquid cell.

2.1.2. Fabrication, Assembly, and Use

Chip Fabrication

Figure 2.10 shows a full fabrication flow for the two-chip device. The process begins with the LPCVD deposition of 50-70 nm of stoichiometric silicon nitride (Si_3N_4) on a 200-µm-thick double-polished silicon wafer. AZ5214-E reversible photoresist is then applied as a lift-off mask and 100 nm of platinum for electrodes is deposited via sputtering and patterned by immersing in organic solvents with ultrasonic agitation. S1818 photoresist is then deposited as a lift-off mask and approximately 200 nm of silicon

dioxide (SiO_2) is deposited via sputtering and patterned to act as an electrode insulator where necessary. S1818 resist is again used as a lift-off mask for an initial layer of fluorocarbon polymer deposited using C_4F_8 plasma to form the top chip spacer and liquid flow gate patterns that are 200 to 400-nm-thick. This process is then repeated for a longer duration to form the bottom chip spacer which is 500-700 thick. The frontside of the wafer is then coated in an S1818 protection layer and the backside silicon is etched down to approximately 198μm using a standard DRIE recipe. The remaining ≤2 μm of silicon is then removed using a highly-selective low-power SF_6 isotropic plasma etch. SF_6 is flowed at 300 sccm at a chamber pressure of 22 Pa. Plasma is generated with a coil power of 1.8 kW, and a platen drive-in power of 10W. Etching usually lasts only 1-5 seconds. The wafer is then cleaned in a heated mixture of H_2SO_4 and H_2O_2 to remove any resist residue and diced into chips using a Stealth Dicer. The individual chips are completed at this point and are ready for assembly and filling. A summary of the basic device variations used here was shown previously in Table 6.

Cell Assembly and Use

The process of assembling, loading, and sealing the liquid cell device is shown schematically in Figure 2.11. The top chip is inverted and manually aligned with the bottom chip using tweezers so that the observation windows and liquid gate features overlap. The chips are then clamped together lightly so that the gap between them approaches the sum of the heights of the spacers. UV-cured epoxy is then applied around the periphery of the top chip and cured in order to bond the two chips together. The assembled device can then be turned over to reveal the loading inlets on the bottom chip. Depending on the experiment to be performed, one or both of the inlets can be filled with one or two sample solutions and then sealed with the same epoxy. The device is then

loaded into a TEM holder and cleaned in a vacuum plasma cleaner to remove potential contaminants and test for a sufficient epoxy seal. The holder with the cleaned device can then be inserted into the TEM high-vacuum chamber for observation.

STEM Observation

Figure 2.9 shows a typical view of the two-chip device in STEM Z-contrast observation. In this particular experiment colloidal solutions of gold nanoparticles (AuNP) were first dried on the viewing membrane. Another solution of AuNPs was then loaded into one inlet of the device and subsequently flowed into the viewing region using the flow control device. The light background represents the fluid medium, in this case a solution of citrate buffer in water, while the dark circles are AuNPs of both 50 and 100 nm diameters. Here it can be clearly seen that particles under 50 nm can be resolved using the two-chip liquid cell, even when the flow control features are used to fill the membrane. The inlay also shows mobile AuNPs in the liquid as indicated by the streaked particles. As the electron beam scans slowly over the sample during the generation of a still-image, small localized heating effects can cause lighter and smaller particles to move downward in the direction of the beam raster. At lower magnifications, smaller electron accelerating voltages, and faster imaging speeds, this effect can be mitigated.

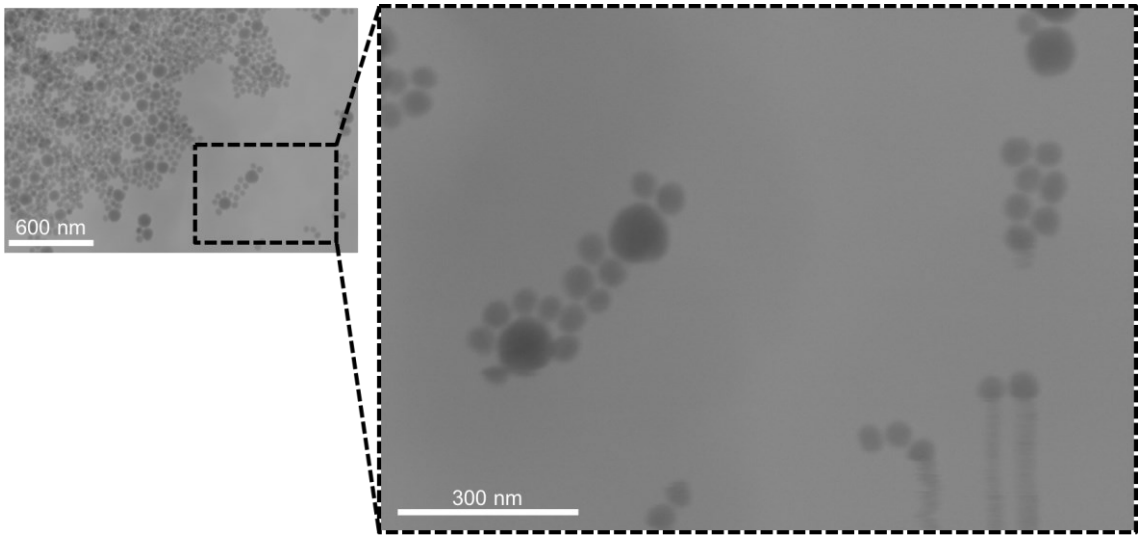

Figure 2.9: Two-chip device STEM observation of 50/100 nm AuNP.

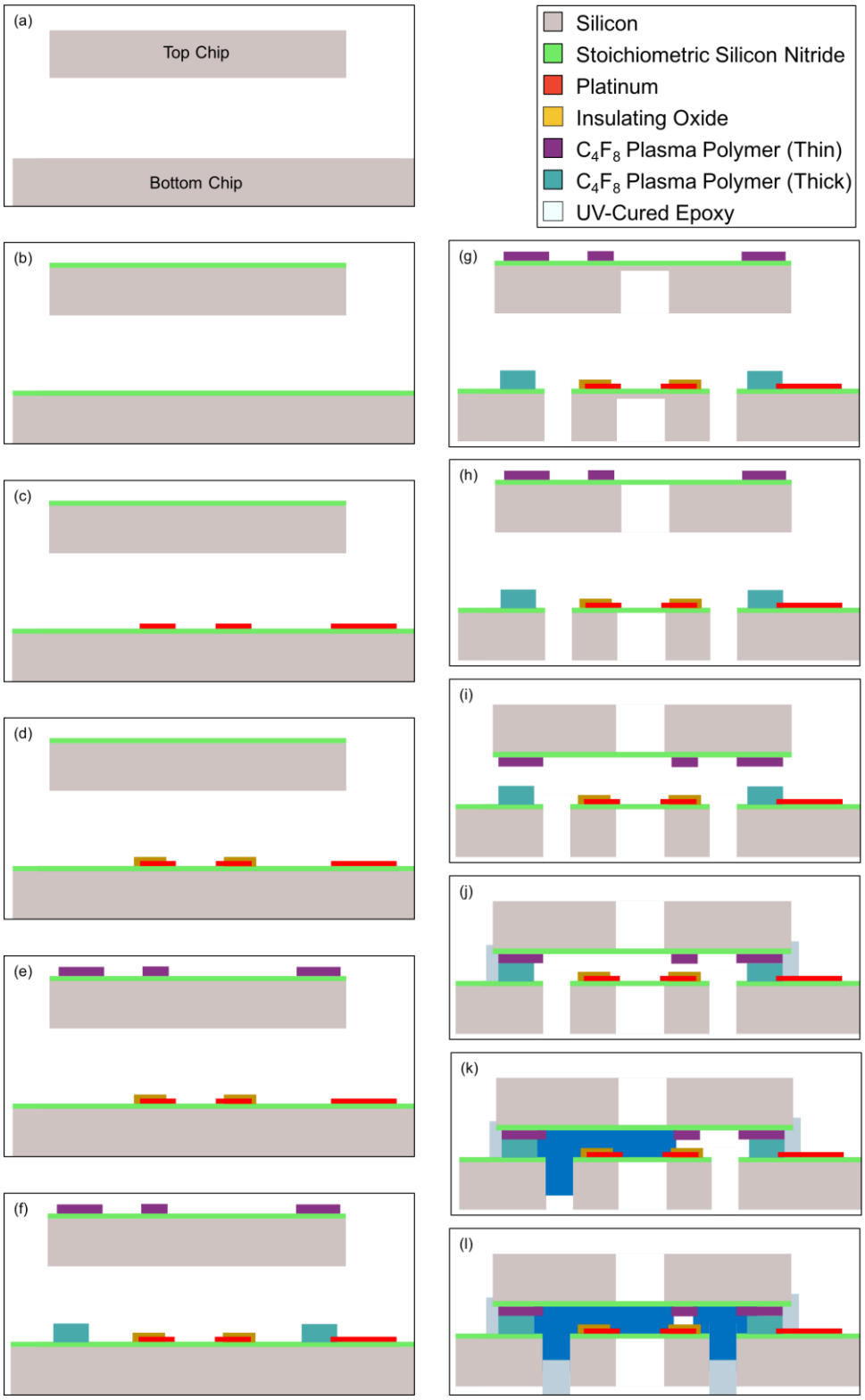

Figure 2.10: Two-chip fabrication flow. (a) Initial wafers. (b) LPCVD nitride. (c) Pt patterning. (d) Oxide patterning. (e) C_4F_8 plasma gate synthesis. (f) C_4F_8 plasma spacer synthesis. (g) Backside DRIE etching. (h) Backside tuned SF_6 plasma membrane release. (i) Chip alignment. (j) Chip clamping and epoxy bonding. (k) First inlet loading. (l) Second inlet loading and epoxy sealing.

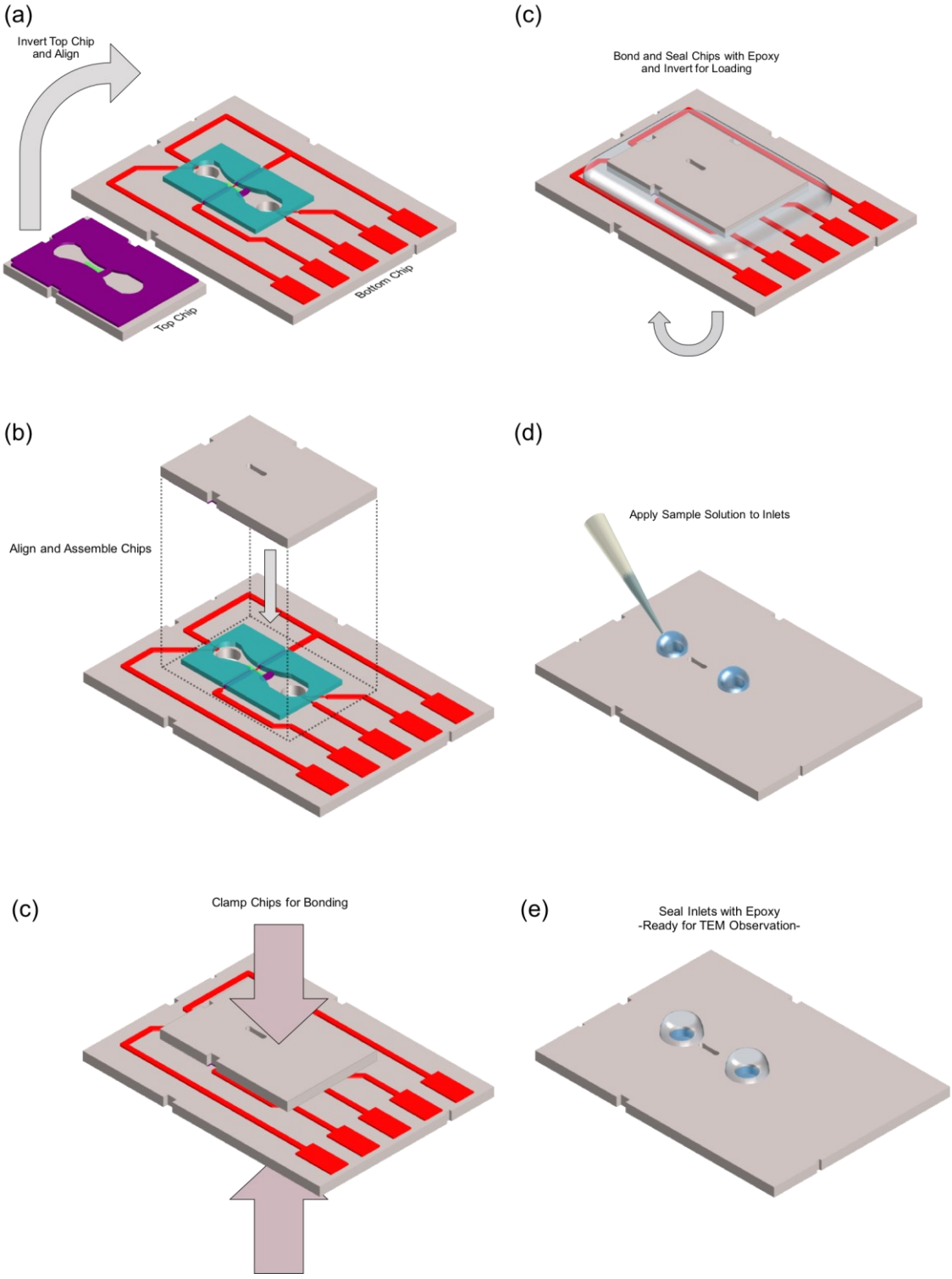

Figure 2.11: Assembly and loading of two-chip device. (a-b) Top chip alignment. (c) Chip clamping. (d) Epoxy bonding. (e) Sample loading. (f) Epoxy sealing

Common Failure Modes

The basic purpose of the two-chip liquid cell platform is essentially twofold: to contain a liquid sample safely within the high-vacuum environment of the STEM chamber and to present that liquid sample in a manner that allows the imaging electron beam to successfully generate an interpretable image. If these criteria are achieved, the liquid sample can be observed not only in its static state, but can also be investigated with the active MEMS components described in Chapter 3. However, failure to contain the liquid sample or maintain it within the appropriate observable region of the STEM will not only inhibit the experiment but can potentially introduce contaminants into the vacuum chamber. Throughout the cycle of fabrication and use of the two-chip device, there are three primary modes of failure for device operation: membrane rupture, failure of the epoxy seal, and the undesired introduction of air bubbles to the observation region.

Counterintuitively, membrane rupture is most likely to occur before atmospheric loading is applied to the liquid cell membrane in the vacuum chamber. As described previously and in Figure 2.11, assembling the liquid cell currently requires the manual alignment and clamping of two chips together. This process, which is performed using a dissection microscope, tweezers, and a clamping chuck, is delicate and requires a certain degree of manual dexterity. The height of the spacer features means that the delicate exposed observation membrane is recessed only approximately 500 nm below the highest surface of chip. When aligned properly with a complementary chip, no material will come into contact with the membrane, but the membrane will be at risk if the chip is dropped on a surface with asperities larger than 500 nm or misaligned to the degree where the corner of one chip comes into contact with the membrane. In these situations, however, the membrane will only break if relative lateral motion is applied to rip the membrane

across its surface; the weight of the chip itself is not enough to puncture the membrane even if it comes into contact with a surface on the complementary chip. The membrane is relatively resilient to distributed surface loading as demonstrated by pressurizing the interior of the assembled two-chip structure and loading the device into high-vacuum. To test the integrity of the membranes, liquid water was loaded into sealed liquid cells and observed in STEM under high-vacuum. As described in Section 3.1.3, electrolysis was used to generate additional gas within liquid cells, thereby increasing the overall pressure gradient between the near atmospheric pressure cell interior and high-vacuum STEM chamber. Even when the pressure gradient was thusly increased by producing gas within the liquid cell, no membrane ruptures have yet been observed. The produced gas displaces all the liquid in the observable membrane region before any leakage or failure of the membrane was observed in all experiments. Any leakage of the two-chip liquid cell device tends to occur in the epoxy seals rather than the nitride membrane.

As described previously, liquid is held within the two-chip device through the use of UV-cured epoxy applied at the inlets of the top chip as seen in stage (e) of Figure 2.11. If the chip surface is insufficiently clean, or if excess sample liquid is present at the inlet, the epoxy applied can potentially fail to seal completely to the chip surface. In this case, upon curing, a vacancy between the epoxy and chip will exist, allowing the liquid within the cell to evaporate when the chip is introduced to the sample chamber. To prevent the introduction of contaminants to the sensitive STEM chamber, the sealed device is first loaded into a plasma cleaner which draws an initial vacuum and then introduces an Ar/O_2 plasma around the liquid cell. This serves to both clean the sample and, in the case of an insufficient epoxy seal, evaporate the liquid within the device and prevent any leakage within the STEM chamber.

The final most common failure mode for the two-chip liquid cell involves air bubbles preventing observation of the liquid sample. When liquid is introduced through one inlet to the internal structure of the cell, the hydrophilic silicon nitride surface of the chip and membrane draws the liquid down the channel while the hydrophobic channel sidewalls formed by the spacer help to confine the liquid within the channel pattern. As mentioned in Section 2.1.1, if the spacer sidewalls are insufficiently hydrophobic, or if the nitride membrane is too hydrophobic, e.g. due to photoresist or other contamination, it is possible for the liquid to adhere excessively to the spacer sidewalls and flow around the membrane, leaving an air bubble covering the entire observation region. During STEM, this would mean that no liquid could be observed, despite it being present in the liquid cell. This was a particular problem in previous versions of the device with wider channels and more hydrophilic spacer materials like SU-8. Upon designing narrower channel structures and switching to highly-hydrophobic spacers made using C_4F_8 plasma deposition, this issue was almost entirely mitigated.

2.2. Nanochannel

The nanochannel device is quite distinct from most existing liquid cell structures. While most liquid cells form a hermetic liquid cavity using O-rings with pressure applied by a specialized TEM holder or by directly sealing two halves of a chamber together [28] [43] [34] [46], one structure that has rarely been pursued for TEM applications is that of a fully encapsulated and suspended membrane channel. the nanochannel device developed by Dr. Edin Sarajlic of the University of Twente and SmartTip B.V. is relatively unique in its design, as the primary means of liquid sealing is a monolithic encapsulated channel structure that is still thin enough to enable high-resolution imaging of loaded samples in both TEM and STEM [83]. As with the two-chip liquid cell, the

nanochannel device is fully self-contained once fabricated. However, unlike the two-chip device, there is no final assembly step required, and samples can simply be loaded directly into the inlets and then sealed using UV-cured epoxy.

The primary advantages of the nanochannel liquid cell as compared to the two-chip device center around its improved resolution and consistent imaging capabilities. Because the imaging region of the device consists of a uniform and fully enclosed membrane channel, the nanochannel device is not as susceptible to damage and contamination as the two-chip structure. The equivalent spacer structure of the nanochannel is fabricated within the device monolithically, so irregularities arising from surface imperfections or impurities introduced during chip bonding are significantly mitigated. This means that the fluid column within the loaded nanochannel can be kept both very thin and regular, which serves to both improve the overall resolution as well as the consistency in observational characteristics from one device to another. Furthermore, the lack of a post-fabrication assembly step reduces the chances of damaging the imaging membrane channel during handling and operation.

While the monolithic composition of the nanochannel device has many advantages in terms of TEM observational power and usability, these benefits come at the at the expense of generally reduced flexibility in terms of the development and integration of active components, as well as the narrowing of potential target samples with increased resolution. In this section, the detailed structure of the nanochannel liquid cell will be discussed in preparation its use in scientific applications as well as the integration of active components.

2.2.1. Overall Structure

As mentioned previously, the primary structure of the nanochannel liquid cell device is the suspended nitride channel. Figure 2.12 shows a schematic representation of the fully-fabricated nanochannel device. The device consists of a micromachined silicon chip bonded to a capping glass chip. The glass chip serves more as a structural and handling support than as a sealing feature as would be the case on more conventional liquid cells. In fact, the cavity to be filled by the sample liquid is contained entirely on the silicon wafer in the form of a silicon nitride channel that runs across the width of the chip. The channel itself is flanked by a layer of polysilicon which serves to support the channel in the suspended region and provide a uniform surface topology to which the glass chip can bond. While the device in Figure 2.12 features a single straight nanochannel, fabricated devices include cross-shaped channels and rectangular islands in the suspended region.

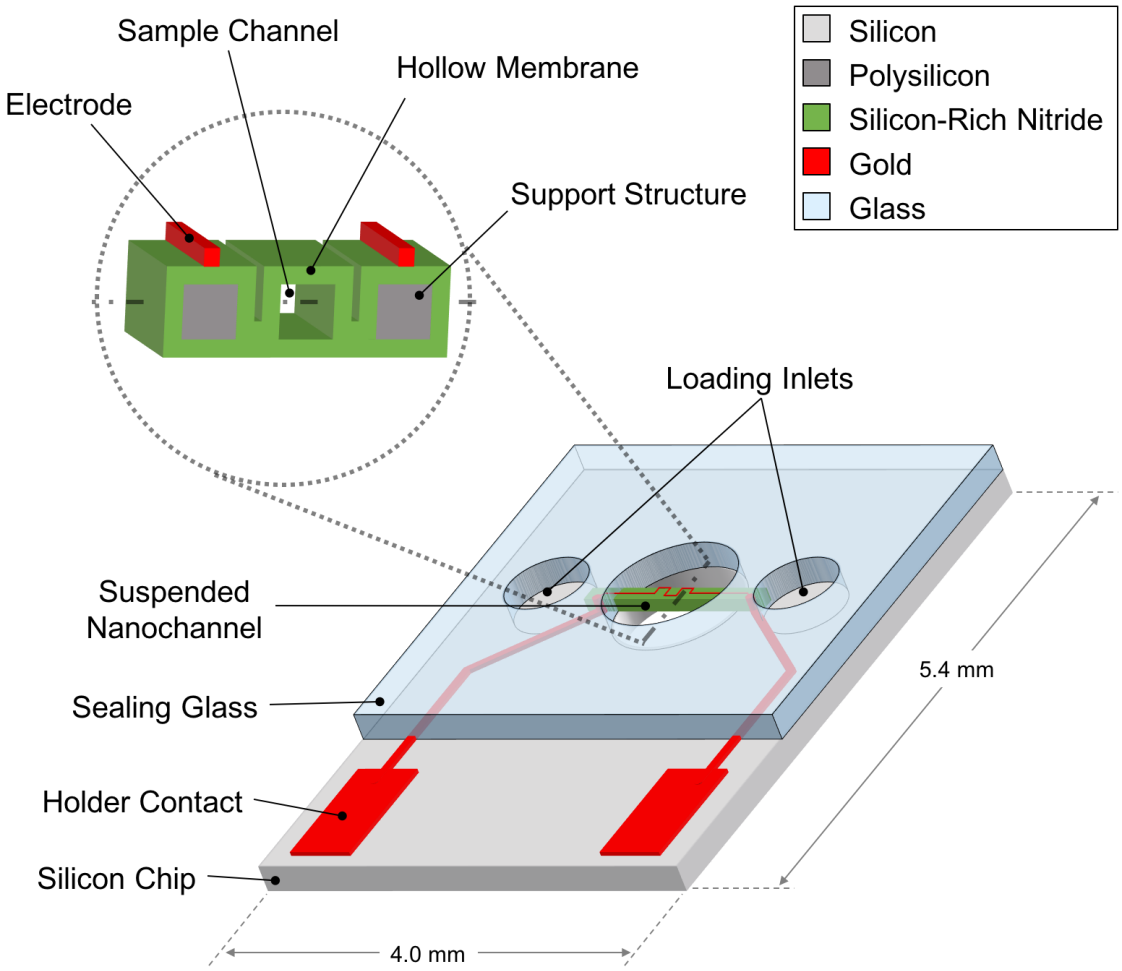

Figure 2.12: Nanochannel device schematic. Inlay: Cross-section of suspended channel.

Suspended Channel

The suspended channel, a cross-section of which is shown in the inlay in Figure 2.12, consists of the hollow membrane channel itself and the surrounding polysilicon support structures, all connected by the same silicon nitride layer. The polysilicon layer serves a similar purpose as the spacer layer in the two-chip device: it defines the height of the fluid column that will be present between the observation membranes. However, in the case of the nanochannel device, the channel membranes are not directly held apart by the spacer as with the two-chip device. Instead, a layer of polysilicon within the nitride membranes is etched away sacrificially to form the central channel with the same height

as the original polysilicon layer. The non-etched regions of the polysilicon layer form supports that provide mechanical stability to the suspended structure after the channel is hollowed out.

As mentioned previously, the channel separation being defined by the monolithic sacrificial etching of the polysilicon layer yields devices much more regularly formed than with the two-chip device with thinner possible fluid columns. In practice, suspended channels up to 400-µm-long, 5 to 10-µm-wide and anywhere from 180 to 500-nm-tall have been fabricated with silicon-rich silicon nitride membranes ranging from 50 to 80-nm-thick. The suspended structure exists on the surface of the silicon wafer and is protected by the frontside bonded glass chip and the backside etched silicon, both of which provide a recessed well that prevents the damaging of the nanochannel during handling from either side without actually interfering with the electron beam path during TEM observation.

In addition to being mechanically resistant to handling damage, the suspended observation membrane provides another benefit. In addition to conventional TEM and Z-contrast imaging techniques, the nanochannel is highly suited to the use of energy spectroscopic analysis. Electron Energy Loss Spectroscopy (EELS) and Energy-Dispersive X-ray spectroscopy (EDX) are both analytical techniques that can be performed in the STEM that utilize the interaction of the electron beam with the sample in order to characterize the material properties of the observation target. The suspended channel structure provides a convenient means to calibrate these measurements by focusing the beam first on an area of vacuum before analyzing the sample itself. The presence of regions of vacancy on the nanochannel device make it well suited for the application of such techniques [83].

2.2.2. Fabrication and Use

The critical process steps for the fabrication of the nanochannel device with an integrated electrode are shown in Figure 2.13. Beginning with a 380-µm-thick silicon wafer, a 50-80 nm silicon-rich nitride (Si_RN) is deposited via LPCVD. A polysilicon layer of 180-500 nm is then deposited via LPCVD and patterned with lithography and plasma etching. This polysilicon structure will define both the height and shape of the final channel structure. A second Si_RN LPCVD deposition is performed and the nitride is RIE-patterned. This patterning will separate the sacrificial polysilicon areas from the protected ones. A gold layer can then be patterned to include an electrode on the outer surface of the channel. A pre-diced glass wafer with both holes for inlets and the suspended channel region is then anodically bonded to the silicon wafer. The sacrificial polysilicon as well as the backside bulk silicon is then etched with TMAH to hollow out and define the nanochannel. Due to the narrow cross-section of the nanochannel, this etching step can take up to 9 hours. After device cleaning and dicing, the nanochannel fabrication is complete and the device is ready to load with sample via the inlets. The hydrophilic nature of the glass wafer and nitride suspended channel enables liquid droplets placed at the inlet via a micropipette to readily enter and fill the channel. The inlets can then be sealed with the same UV-cured epoxy used with the two-chip device. The nanochannel can then be loaded into the TEM holder and observed.

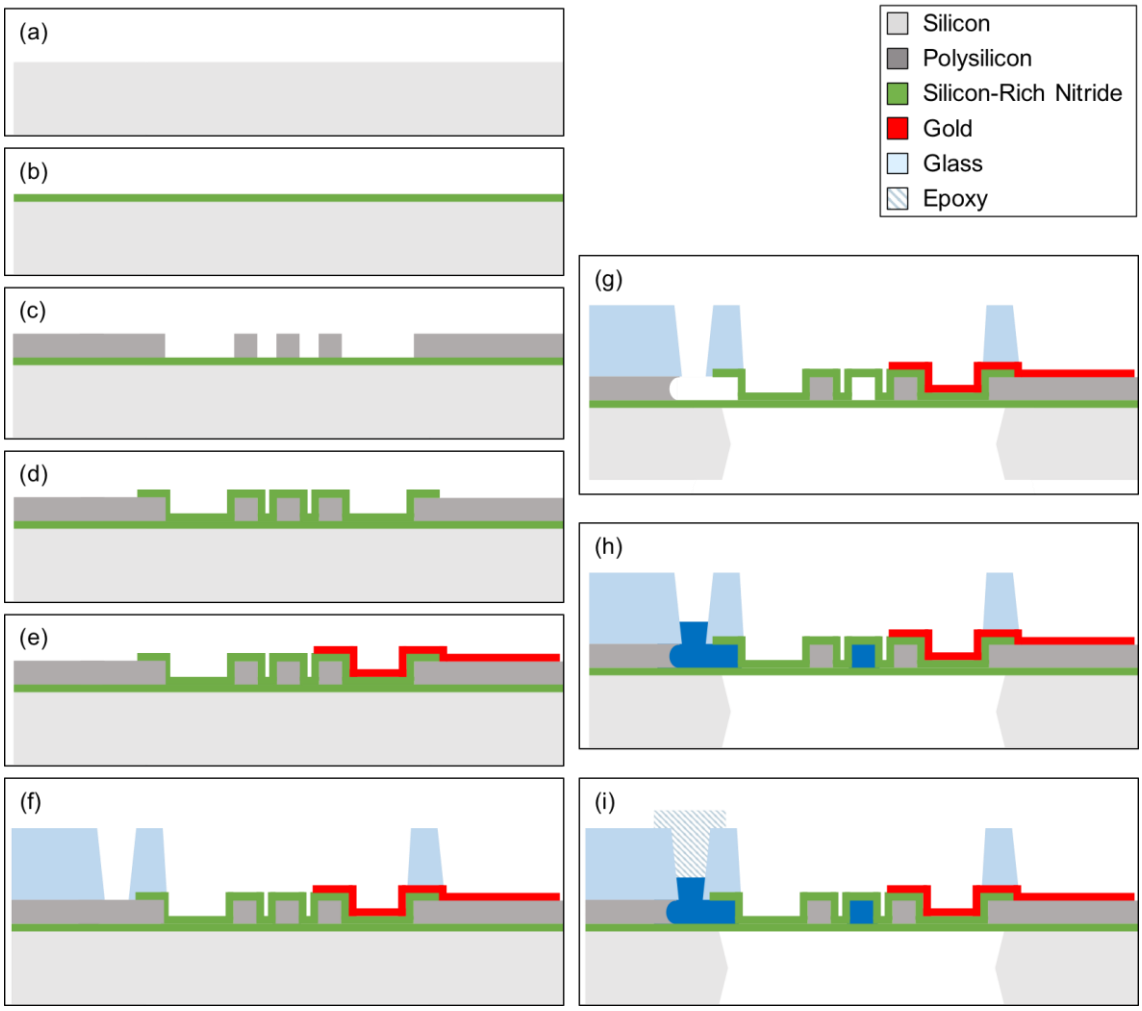

Figure 2.13: Nanochannel fabrication. (a-b) LPCVD nitride deposition. (c) Polysilicon patterning. (d) Second LPCVD nitride deposition and patterning. (e) Gold patterning. (f) Pre-diced glass chip anodic bonding. (g) TMAH etching of sacrificial polysilicon and backside silicon. (h) Sample loading into channel. (i) Epoxy sealing of inlet.

Figure 2.14 shows two characteristic STEM Z-contrast images of various samples as observed using a nanochannel device without any active components. The left image represents a broad-field view of a suspension of approximately 5 nm diameter gold nanoparticles in an aqueous solution. The individual bright dots are discretely resolvable AuNP while the pale doughnut shapes are the background of the nanochannel that is suspected to be characteristic of the sacrificial polysilicon slow TMAH etching process. The right image is of a single gold “nanotriangle” that has come to rest on the channel

surface allowing for high-resolution imaging and the verification of the particle geometry in solution. These two images are typical results when successfully observing liquid-phase samples.

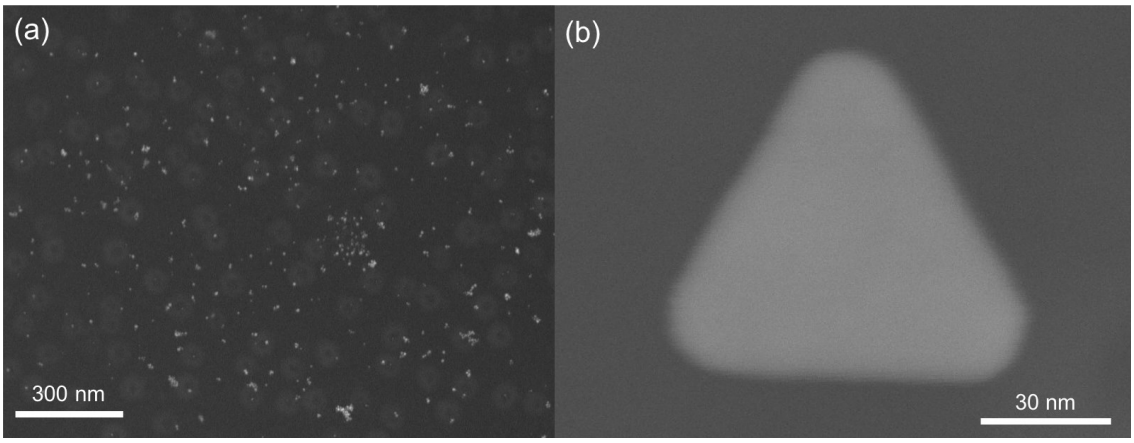

Figure 2.14: (a) 5 nm AuNP suspension. (b) Gold nanotriangle

2.3. Device Comparison

As has been discussed briefly above, the two-chip device and nanochannel represent significantly divergent means to achieving liquid-phase TEM observation. As such, each has advantages and disadvantages compared with the other and are suitable for different application nuances. In this section, the capabilities and affinities of each platform will be compared.

2.3.1. Resolution

As discussed in Equation 2, the smallest resolvable particle by a liquid cell system in STEM scales with the square root of the thickness of the fluid medium in which those particles are suspended [28].

$$d_{\mathrm{STEM}} \propto \sqrt{T_{\mathrm{fluid}}}$$

Equation 3: Proportionality of STEM resolution to fluid column thickness.

As such, in order to maximize the resolving power of liquid cell structure, one must strive to create the thinnest sample possible. Intuitively this makes sense, as the liquid medium serves to scatter the imaging electron beam and generate an ADF signal regardless of whether a target particle is in the imaging path or not. Essentially, the fluid acts to increase the noise threshold in the imaging signal, below which target particles can be lost.

In this regard, from a design perspective, the nanochannel has the clear advantage. While the spacer layer of the two-chip device can theoretically be fabricated to be 100 nm or so despite the increased danger of membrane damage during device handling and assembly, the relatively uneven surface that results from the open-air epoxy bonding process means that the actual fluid thickness is necessarily larger than the combined thickness of the spacer layers. Conversely, the fluid column within the nanochannel is rigidly set based on the height of the nitride channel sidewall that gets deposited during the LPCVD nitride deposition onto the sacrificial polysilicon layer.

This theoretical advantage is more or less borne out empirically when observing various samples in TEM. One sample that makes the difference abundantly clear is a solution of the zeolite faujasite impregnated with Na^+ ions. Unlike dense metallic nanoparticles, this zeolite does not provide a very strong signal in Z-contrast STEM imaging due to its relatively low atomic weight and disperse geometry. As such, while the two-chip device is able to enable the imaging of the structure in the dry state, when the same device is filled with liquid, the signal is washed out. This is most likely due to the relatively large total spacer height of approximately 1 μm combined with the inherently weak in-liquid signal of the faujasite structure. This particular nanochannel, on the other hand, is capable of identifying the same structures at higher magnifications even

in the liquid medium with a fluid column thickness of only 180 nm. This comparison can be seen in Figure 2.15.

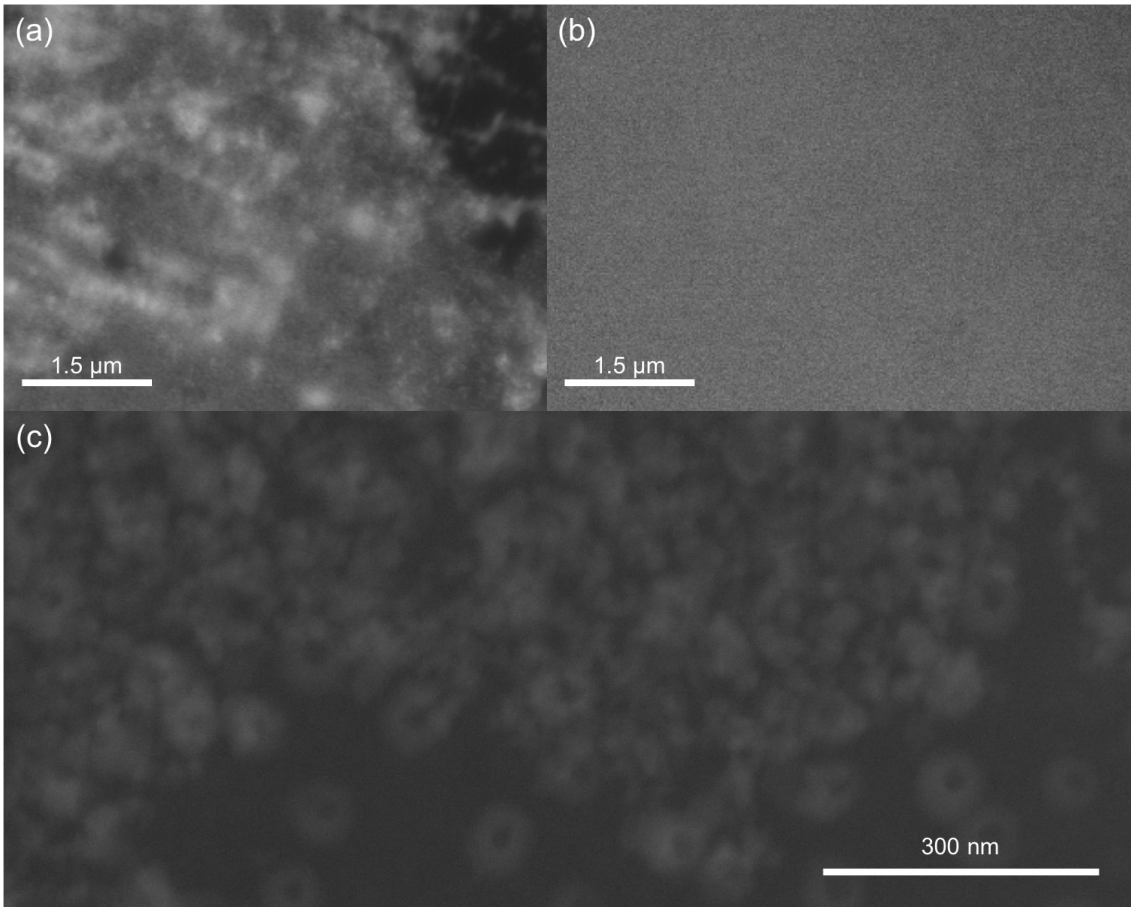

Figure 2.15: (a) Dry faujasite in two-chip cell. (b) Immersed faujasite in two-chip cell. (c) Immersed faujasite in nanochannel

For most liquid cell TEM applications, however, the observational target will involve some sort of metallic nanoparticle. As has been shown above, both the two-chip device and the nanochannel are easily capable of resolving <50 nm AuNP, with the nanochannel showing the ability to distinguish <5 nm particles as well.

2.3.2. Sample Compatibility

While having a narrower fluid column is helpful in increasing the resolution of the liquid cell, there is a significant drawback of such a structure, especially when used

in a channel-based device. In both the nanochannel and two-chip device, the sample solution is supposed to be introduced via the inlets. If the device spacing is excessively narrow, samples that are aggregated or even individually too large will actually be filtered out of the viewing region and will not be visible. Figure 2.16 schematically illustrates this situation. While the concentration of particles in and around the inlets remain high, and some individual particles are able to reach the viewing membrane, most of the larger aggregate structures remain trapped outside of the channel structure, and prevent other particles from entering as well.

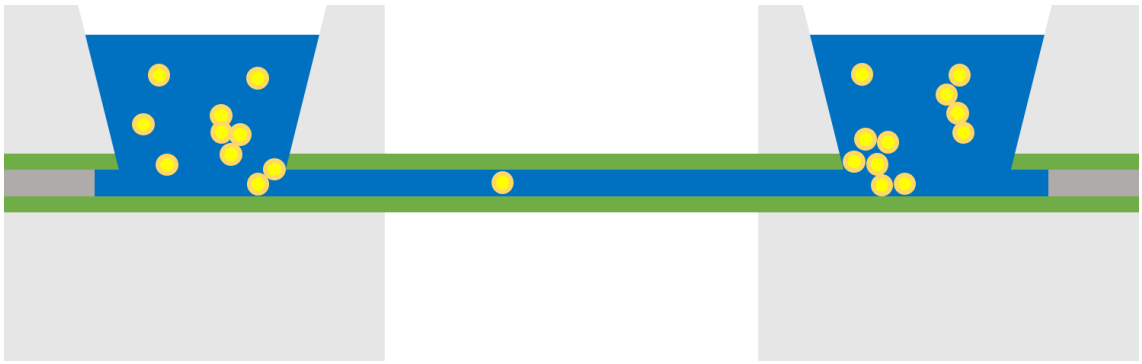

Figure 2.16: Schematic of narrow channel filtration effect

Even if the nominal particle diameter is smaller than the channel height, filtration can occur in samples that tend to cluster or aggregate or are electrostatically repelled by the nitride walls of the chamber. This particle inhibition is perhaps the most significant limitation of the nanochannel device as it can often preclude the observation of interesting samples simply because they are unable to enter the channel structure.

To mitigate the filtration effect in the nanochannel device, a higher particle concentration can be used if the sample is a stable colloid and will not aggregate and further clog the inlets. Often, though, the sample to be observed is either in short supply or otherwise cannot be effectively concentrated beyond its current state. The alternative

is to use a thicker channel height, but due to fabrication limitations, it is difficult to increase past several hundreds of nanometers.

On the other hand, because of the open nature of the two-chip device, sample liquids that are susceptible to filtration, such as aggregates, viscous materials, or large particles, can be placed directly on the imaging membrane, bypassing any filtration that might have occurred. In this regard the two-chip device has the clear advantage over the liquid cell due the flexibility that is afforded by the two-part structure. The filtration effect and the efficacy of direct sample loading can be easily seen when investigating aggregated clusters of DNA-linked gold nanoparticles (DNA/AuNP). Figure 2.17 shows the results of directly depositing the sample solution on the observation membrane before assembling the liquid cell on the left, while the right is the same sample loaded through the inlets of a nanochannel device with a channel height of 500 nm.

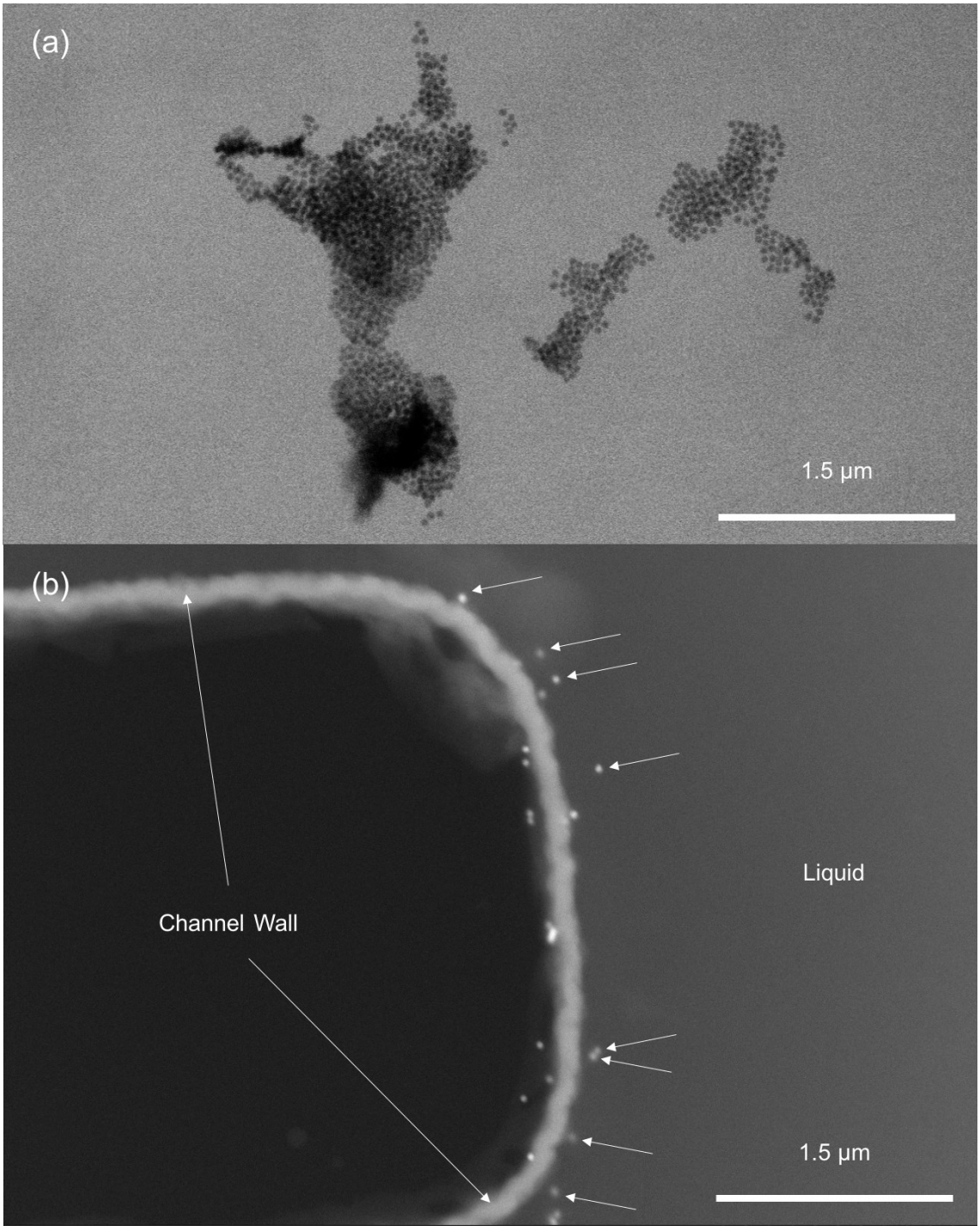

Figure 2.17: (a) Direct deposition of DNA/AuNP solution on two-chip device. (b) Filtration of same AuNP solution through nanochannel. Arrows indicate the only individual nanoparticles than reached the channel

2.3.3. Spectroscopic Capability

As introduced briefly above, certain STEM systems are capable of spectroscopic analyses using the imaging electron beam as an excitation source. In EELS analysis, the electron beam is focused on a particular region, and the interaction of the electron beam with the sample leads to inelastic scattering which causes the electrons to lose a specific amount of energy depending on the material present in the beam path [84]. Analyzing the energy spectrum of the transmitted electrons can allow the operator to identify and quantify the materials being studied. EDX operates on a similar principle, instead using the electron beam to excite the target sample and induce the emission of characteristic X-rays which are then detected and quantified.

Both of these techniques allow for detailed materials analysis to be performed on a sample in addition to and in conjunction with STEM observation. However, in order to make these analyses, the energy and X-ray detectors, respectively, must be calibrated. This is usually achieved by allowing the electron beam to pass unimpeded to the detector, measuring the output produced, and using that to normalize subsequently measured values. For conventional liquid cell structures, such as the two-chip device, there is no area on the chip where the beam can pass through without interacting with the device itself. The nanochannel, on the other hand, features regions of void around the suspended channel. As such, the nanochannel is capable of being used for EELS and EDX spectroscopic analysis of the materials contained within while doing so with the two-chip device is not optimal.

2.3.4. Function Integration and Flexibility

For the purposes of this study, the basic two-chip and nanochannel liquid cell structures are being pursued for the purposes of integrating further sample interactivity

that has previously required more specialized equipment. Specifically, achieving electrical biasing, heating, and flow control are the objectives of this work. As such, one of the criteria by which these basic platforms must be measured is the ease and efficiency with which such capabilities can be incorporated.

While this was touched upon previously, the enhanced TEM performance exhibited by the nanochannel liquid cell come at the cost of both a relatively inaccessible device surface, and an involved and inflexible fabrication process. The channel geometry of the cell itself can be easily customized, but accessing the inside of the channel itself, to integrate a hydrophobic region for example, is quite difficult. This problem arises not only because of the enclosed nature of the channel structure, but also due to specific fabrication steps involved in its creation. The three sequential LPCVD steps necessary for the formation of the channel structure preclude the integration of many materials onto the bottom interior surface of the channel. The high temperatures and volatile gasses involved in the process mean that most polymer or metallic materials would be inappropriate to introduce into the process chamber and would not survive the step anyway. This means that any additional structures or features must be added to the device after the formation of the channel structure.

On the other hand, the two-chip device is quite open both in terms of its device geometry as well as process flexibility. Because the interior of the sample chamber is not closed off until the final assembly of the device, it is available to be machined and processed at liberty. The main restrictions involved in the fabrication flow for the two-chip device are the delicate nature of the released membrane, and the spacer. However, since the membrane is not released until the final fabrication step, and silicon nitride is quite chemically inert, there is little consideration that must be made besides the initial

LPCVD deposition of the nitride itself. Furthermore, the incorporation of the C_4F_8 plasma-based fluorocarbon polymer has yielded a much more stable and robust spacer than was previously available. Coupled with its hydrophobicity, it is resistant to most organic and chemical solvents, and features relatively good adhesion to the substrate. As such the two-chip device is much more amenable to the simple integration of active MEMS components into its structure as compared to the nanochannel. In the next chapter, this distinction will become paramount as some features that can be readily included in the two-chip device represent significant challenges for the nanochannel platform.

2.3.5. Ease of Use

Finally, and perhaps most simply, the practical usability of the two liquid cell platforms can also play a significant role in its successful application for scientific use. What the nanochannel lacks in terms of fabrication accessibility and design flexibility it makes up for in its simplicity when used for TEM observation. The fully packaged and prepared structure only requires the user to pipette the sample liquid onto the inlet and coax it down into the channel surface. Doing so requires a minimal amount of expertise or training, and would be quite accessible to those unfamiliar with the manipulation of MEMS devices. Furthermore, acquiring proper TEM focus is made significantly easier due to the high contrast between the suspended channel structure and the vacancy surrounding it.

The two-chip device requires a higher level of finesse both when assembling and during TEM observation. Because the two chips must be assembled individually, they must be manually aligned and clamped together. Careless assembly can result in broken membranes during the alignment process if the initial chip placement is significantly misaligned or upon the application of excessive clamping pressure. A degree of

experience is necessary to perform the assembly quickly, and large-scale application would benefit from the development of a simple mechanical bonding chuck to align and clamp the chips together. Once the chips are securely clamped, the application of UV-cured epoxy is relatively simple, and upon solidifying, the major risk to the membrane is over. At this point the device is as easy to load and use as the nanochannel. Acquiring TEM focus is somewhat more challenging compared to the nanochannel device due to the somewhat poorer achievable resolution and the lack of any voids in the structure to orient the initial image. An experienced user can achieve a good image in as little as five minutes, however. Overall, in these ways the nanochannel device is more accessible and simpler to operate as an end user, but both are viable for use by a researcher inexperienced with liquid cell technology.

2.4. Summary

In order to meet the design criteria outlined in Chapter 1, the basic and static liquid cell structure had to be refined and optimized. The components that comprise a functional liquid cell were examined and developed, yielding a significantly more reliable and robust device platform. By removing the fundamental structural issues that have plagued previous versions of the device, more ambitious device designs can be pursued. The two-chip device, with its conventional geometry and accessible fabrication process is an ideal prototyping test bed for the integration of various MEMS-based capabilities. The variations in basic structure of the two-chip device used in this study is shown below in Table 6. The nanochannel, while exhibiting better performance as a basic liquid cell, represents a more significant challenge owing to its complex fabrication requirements and closed-off structure.

	Property	Variations
Membrane	Material	Stoichiometric Si_3N_4
	Thickness (nm)	50, 70
	Size (µm)	Ø200-400, 430x80, 900x100, 260x100
	Count	Single, 2x1, 1x3 for grid
Spacer	Total thickness (nm)	700-1200
	Material	SU-8, Teflon-like layer
	Channel shape	Wide, straight, narrow, hybrid

Table 6: Two-chip device structure variations

	Property	Variations
Membrane	Material	Silicon rich nitride: Si(R)N
	Thickness (nm)	50, 80
Channel	Height (nm)	180, 500
	Arrangement	Single channel, crossed channel

Table 7: Nanochannel device structure variations

Chapter 3: MEMS-Based Sample Interaction

With the basic liquid cell structures established in Chapter 2, the integration of more advanced MEMS structures and features is made possible. While liquid cell structures on their own are capable of enabling high-resolution TEM imaging of liquid-phase samples, they do not inherently provide an experimentally significant means of interaction with the sample during observation beyond the imaging beam itself [30] [31] [79] [80] [81].

In non-TEM-based liquid-phase experimentation, some of the most common experimental variables that are controlled and manipulated include electrical biasing of the sample, the alteration of the temperature of the sample, and the induction of a chemical gradient within the sample. Each of these techniques provide energy to the sample, be it electrical, thermal, or chemical, for the purposes of triggering some sort of response to be observed and monitored. In the case of liquid-phase TEM, while it is possible to prepare some of these variables before loading the sample into TEM, more often than not any activity or reactivity induced in a sample via an electrical, thermal, or chemical trigger will not be observable after the fact. This is usually due to the extremely small sample volumes that are involved with liquid cell TEM techniques, which can often involve only several picoliters of fluid. For sample volumes that small, induced reactions or activity are often fully completed in the time it takes to prepare the liquid cell for TEM observation [28]. For liquid-phase TEM analysis to be a successful analytical technique, it therefore is necessary to develop means by which these sample variables can be controlled and activity can be initiated only after TEM observation have begun.

In order to perform interactive experiments, that is, to apply stimuli to the sample under observation, the liquid cell must provide some avenue by which those stimuli can enter into the high-vacuum TEM chamber, the liquid cell, and finally reach the sample contained within. For the most part, previous researchers have achieved this sample access through the use of specialized TEM holder systems. While electrical stimuli can be applied directly through the use of a holder featuring only electrical interconnects [43] [29] [58], temperature control requires the use of either a dedicated TEM holder with a heating element [61] [73] [60], or through the integration of joule heating elements into the liquid cell itself [62]. Control of sample concentration and gradients, most commonly in the form of the mixing of reagents, represents one of the more challenging elements for achievement in liquid-phase TEM. Currently, the primary method for inducing mixing or otherwise controlling gradients within the liquid cell involves the use of highly-specialized TEM holders that contain tubing that passes from external flow controllers to the holder tip [34] [35] [68] [86]. The liquid introduced to the holder tip is then encapsulated by chips with TEM observation membranes which are mechanically sealed with clamping features present on the holder itself. This type of flow-capable TEM holder must either be custom-built or purchased commercially [42] [41], and represents a significant investment that often precludes its use for laboratories not dedicated exclusively to liquid cell microscopy.

As discussed in Chapter 1, the primary objective of this study is to develop liquid cell technology that can be used with a simple electrical interconnect-equipped TEM holder. As such, in addition to electrical biasing, both heating and flow control must be initiated using electrical signals provided through the holder. Figure 3.1 shows the TEM holder tip with the interconnect pins contacting a nanochannel device in the holder.

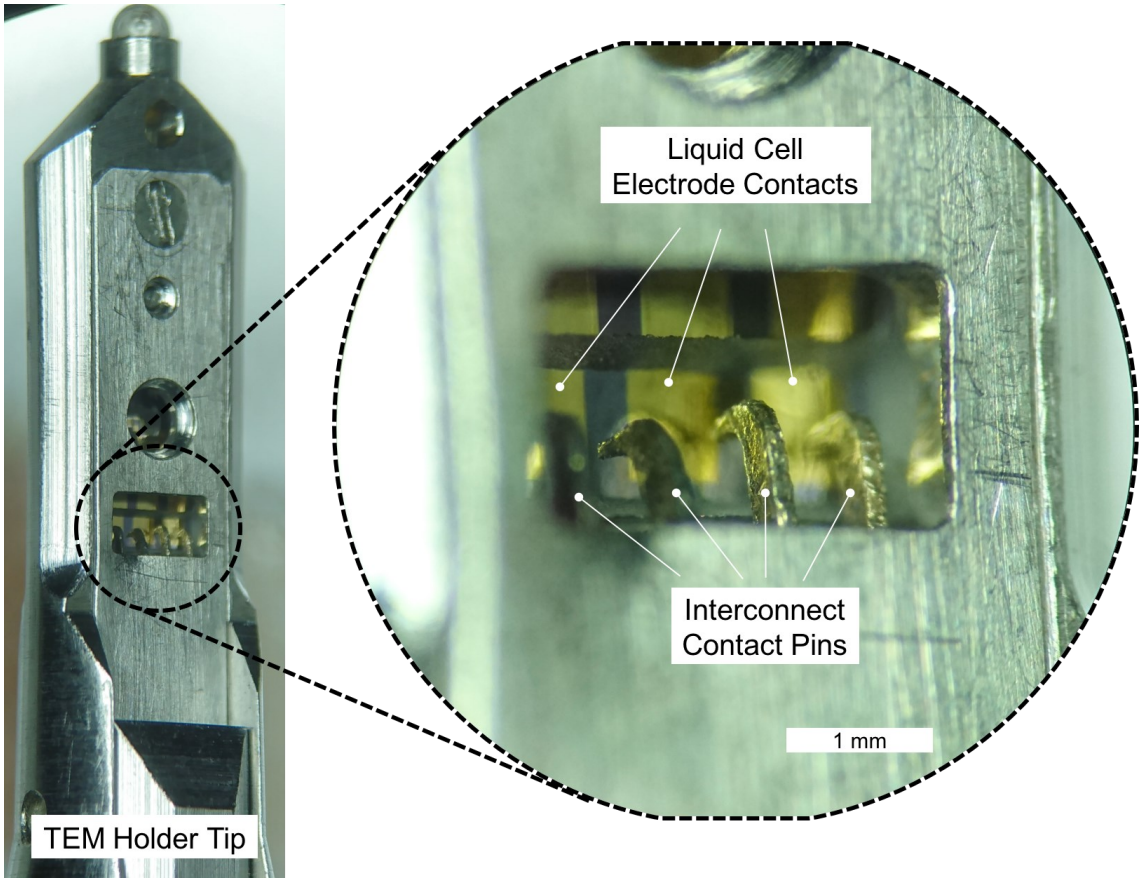

Figure 3.1: TEM holder tip. Inlay: Holder interconnects and cell contact pads.

In this chapter, the design and characterization of active MEMS components to achieve the desired sample interactivity will be detailed. The integration of electrical, thermal, and flow control into the liquid cell devices is described beginning with the two-chip device as outlined in Figure 3.2. The design parameters are discussed in more detail in the following sections, but the general targeted objectives for active MEMS liquid cell components are summarized in Table 8. For electrical control, the ability to verify the presence of liquid in the chamber can be achieved with individual electrodes placed around the channel, while local biasing and electrolysis experiments require electrode pairs. For temperature control, the targeted chemical and biological samples to be used with the device generally exhibit activity from 20ºC to 80ºC, so the device must be capable of reaching such a temperature range, and generally detecting whether a

minimum threshold temperature for a reaction has been achieved. For flow control, the ability to introduce a sample liquid to an initially dry chamber within STEM would be useful for studying the rehydration or reaction of particles when exposed to a given reactant liquid. Similarly, the ability to mix two discrete liquids would enable the direct observation of a much wider variety of chemical reactions.

	Objective	**Parameter/Value**
Electrical Control	Resistance sensing	Single electrodes
	Biasing/electrolysis	Electrode pair
Temperature Control	Heating	20-80ºC
	Sensing	Within 10ºC
Flow Control	Unidirectional flow	Filling of dry chamber
	Mixing	Merging of filled chambers

Table 8: Summary of objectives for liquid cell active MEMS components.

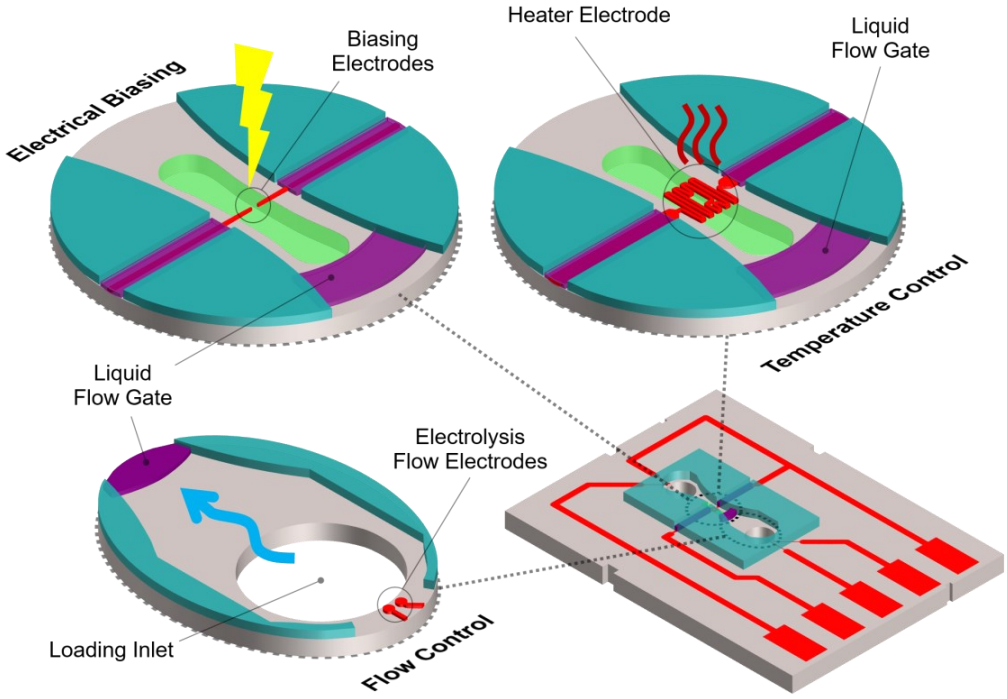

Figure 3.2: Active liquid cell components integrated onto the two-chip device.

3.1. Electrical Control

The simplest and most accessible MEMS device that can be integrated into the liquid cell device is a basic pair of electrodes. The integration of conductive layers that can connect to the contact pins on the TEM holder can allow the user to interact with the sample electrically: applying any arbitrary biasing signal as desired. Many existing liquid cell devices incorporate electrodes for a variety of applications, but in this context the primary use for the integrated electrode features was to both verify the presence of the loaded sample liquid by monitoring the resistance and to induce the electrolysis of the loaded liquid sample itself. Using a pair of opposing electrodes within the liquid cell sample chamber, the conductance of liquid samples can be detected when they come into contact with the electrode pair. In this way the electrodes can be used quite simply to verify the presence of moisture in a given region of the device. Additionally, the opposing-tip electrodes can be used to induce electrolytic splitting of aqueous solutions to generate gaseous hydrogen and oxygen.

The electrolysis of water and the generation of nanoscale bubbles have been investigated due to the role nanoscale gas bubbles can play in a variety of electrochemical reactions such as electrodeposition [87] and surface etching [88]. Conventional techniques usually involve the AFM monitoring of an electrode surface while a current is passed through a liquid electrolyte, usually water, above it [89] [90]. Such techniques have shown that the generated bubbles are around 10-50 nm in size and can be stable over time. However, AFM techniques still struggle with observing the first moments of the nucleation of such bubbles [91]. The real-time nature of TEM imaging coupled with the nominally high imaging resolution can allow for the observation of nanobubble nucleation events [62] [92] [72].

In addition to the scientific study of nanobubble nucleation, the generation of gas bubbles within the liquid cell device can also serve to test the results of the structural refinements discussed in Chapter 2. By generating a gas within a sealed liquid medium, the pressure within the liquid cell is increased. Coupled with the existing pressure differential when the liquid cell is placed in a high-vacuum TEM chamber, membrane rupture is a very real potential failure mode for the liquid cells. By testing electrolytic gas generation in the liquid cell structure first, the ability of the membrane to resist rupture in the event of bubbles reaching the observation window can be verified before attempting more ambitious feature integration such as heating and flow control.

3.1.1. Previous Devices

Previous versions of the liquid cell device have incorporated metallic layers for use as an electroplating target and were able to observe the dendritic growth of the electrode from dissolved ions in the sample solution when an appropriate voltage was applied [58]. Subsequent devices have used various metallic layers to attempt to achieve cell heating [77] as well as flow control [93] with limited success. The specific layout of the liquid cell can vary depending on the desired application, but here the main purpose of the electrodes is inducing electrolysis in the sample liquid. As such, the electrode geometry will be most similar to the electroplating version of the old device in the form of a pair of opposing electrodes.

3.1.2. Electrode Design

In order to achieve the successful electrolysis of liquid within the liquid cell, the electrodes themselves must be designed properly. The material, thickness, and geometry

of the electrode patterns are designed as a compromise between reasonable fabrication limitations and optimal electrolytic capabilities.

While previous versions of the liquid cell involved gold and aluminum electrodes, ultimately it was decided that platinum would serve as the most effective and process-compatible conductive layer. Gold layers tended to be somewhat mechanically fragile and sometimes exhibited less-than-ideal surface adhesion, and aluminum layers were often scratched off by contact probes. Furthermore, aluminum layers would be attacked during the final H_2SO_4:H_2O_2 cleaning process. Ultimately, platinum was selected due to its compatibility with the wafer cleaning process and resistance to corrosion during electrolysis of most solutions. A 50-100 nm thick layer of platinum was used for the electrode patterns and for all subsequent two-chip conductive layers. Thicker metallic layers would be more mechanically robust, but would introduce more surface unevenness which would reduce the effectiveness of the spacer layer. Additionally, the thinner the metallic layer, the less of a signal it generates during TEM observation, and the greater the chance of a target nanoparticle located above or below it has to be resolved over the background noise. Approximately 100 nm of platinum was found to maintain conductivity even when scratched by contact probes while only minimally increasing the spacer height and occluding the TEM resolution.

In order to have the best chance of observing bubble nucleation when it occurs, various electrode geometries were designed and fabricated. Sharp and thin electrodes should serve to concentrate the effective electrostatic potential and cause nanobubble nucleation preferentially as opposed surrounding flat or round shapes [88]. However, because the electrode layer is fabricated using a relatively low-resolution photolithography technique, the smallest tip radius actually achieved was approximately

700 nm. In addition to narrow electrode tips, larger rounded structures as well as T-shaped electrodes were also fabricated. The design of each electrode type is shown in Figure 3.3. Ultimately, no significant performance difference was observed between the sharp, round, and wide patterns, likely due to the lack of pattern resolution in the sharp design. Furthermore, the 100 nm layer thickness limits the effects of any particular electrode shape as the aspect ratio of the layer is significantly smaller than the features of the 2-D electrode pattern overall which helps explain the similarity in performance between the patterns. All three designs could be successfully applied to generate bubbles within the liquid cell as described in Section 3.1.3, however the location of bubble nucleation was not consistent for either design.

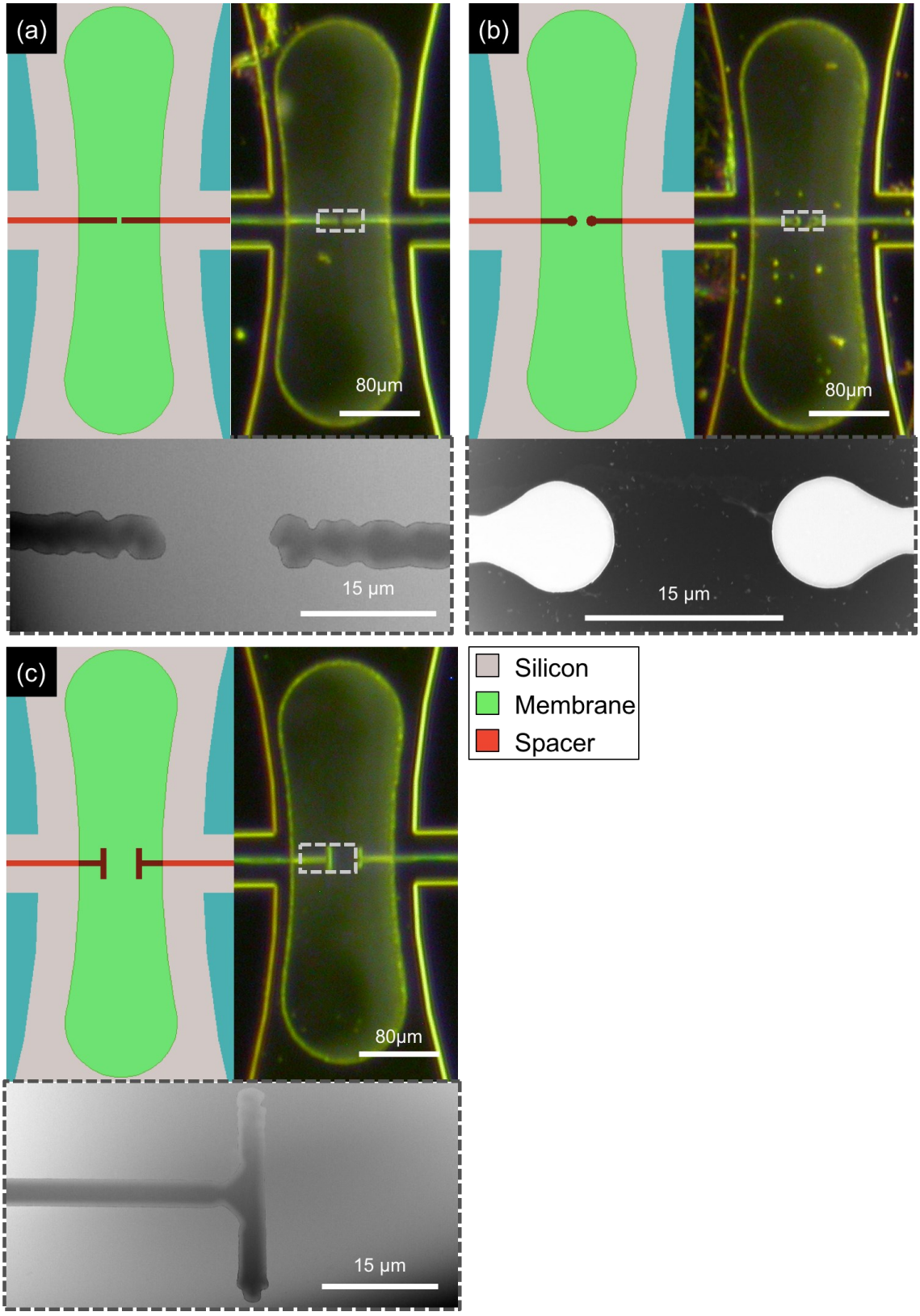

Figure 3.3: Electrode layouts. Design (left), micrograph (right), and TEM image (bottom). (a) Sharp pattern. (b) Round pattern. (c) Wide pattern.

3.1.3. Characterization

In order to demonstrate the ability for the devices to induce electrolysis, they were loaded with deionized liquid water, sealed, and imaged in STEM. Upon acquisition of an image, a DC voltage was applied across the electrodes. The minimum possible electrolysis voltage for liquid water at room temperature is 1.23 V, and the voltage applied across the electrodes was incrementally increased until activity was observed. Figure 3.4 shows the evolution of one such experiment using a 4-μm-wide electrode pair with a 5 μm gap between where the bottom electrode is below the frame. The first observable bubble appeared once the applied voltage reached 3 V_{DC} across the electrode. The bubble was already approximately 15-μm-wide, and grew to above 80 μm in diameter within one second after initial formation. Due to the continuing DC voltage signal, additional bubbles begin to form within 60 ms of the original one they subsequently merge. The continuous application of voltage caused the bubble to grow at a regular rate, stopping when voltage was suspended. In this way, after initial nucleation of the generated gas, the bubble size could be increased controllably. With a more precise electrical setup, the monitoring of the total charge passing through the solution could be compared to the stoichiometry of the electrolytic reaction and potentially be used to control the volume of the generated bubble with a higher level of accuracy. Subsequent experiments failed to identify any pattern to accurately predict the location of the initial bubble nucleation with respect to the driving electrodes.

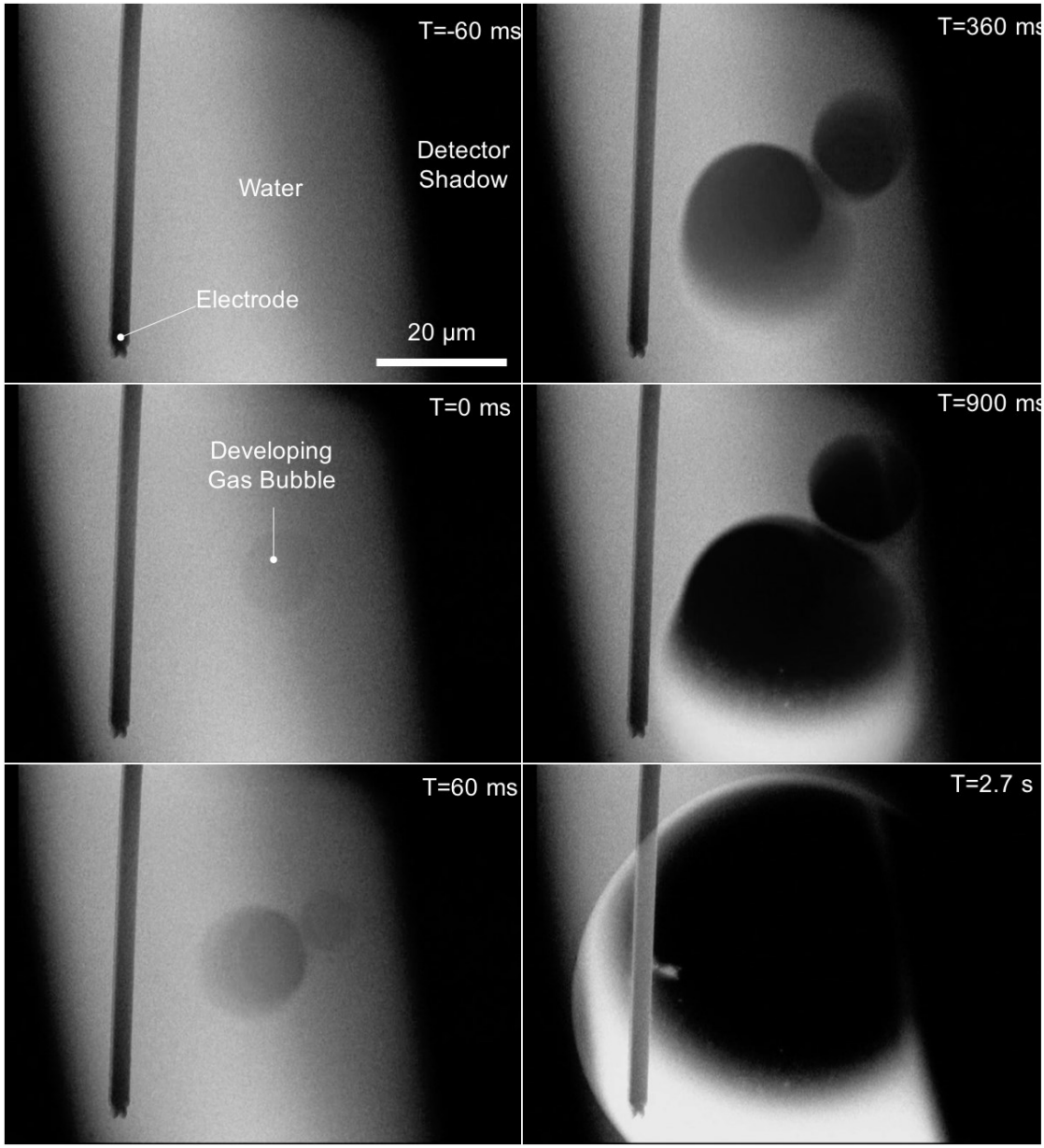

Figure 3.4: Nucleation of electrolytically produced gas. Voltage applied at T=0 was 3.0 V_{DC}.

Bubbles often formed outside of the area being observed in TEM and not directly within the electrode gap as expected. For the *in situ* TEM experiments performed, the average voltage at which observable bubble formation began was found to be 4.65 V, but interestingly the polarity of the signal did not seem to correlate with the nearest electrode to the first bubble formed. It is possible that the 10-50 nm nanobubbles predicted by the literature were in fact forming at lower voltages, but even long-term observation of the

electrode periphery at voltages below the threshold for micron-scale bubble formation did not reveal any bubbles formed even when voltage was applied for up to 20 min. This result indicates that either nanobubble formation was not occurring or, more likely, that the formation could not be observed. It is possible that initially formed nanobubbles would dissolve into the liquid solution before they could be observed and bubbles could only be visualized when gas precipitated out of solution *en masse* or that the initial growth of the bubbles occurred on a timescale unobservable by the 30 frames per second STEM setup. It is also possible that the contrast difference generated by a stable 10 nm diameter gas bubble in a 1-μm-thick fluid column was not sufficient to resolve within this liquid cell structure. It was concluded that the use of uninsulated electrodes, while reliably capable of producing bubbles, was insufficient if the observation of bubble nucleation itself is the experimental target due to the unpredictability of nucleation location. In subsequent designs, the use of electrically insulated electrodes exposed only at the closest point between them would be more appropriate for nucleation studies as well as the use of more precise electrical pulse generators.

Despite the failure to observe the smallest predicted bubble structures, the electrode-equipped liquid cell was indeed able to generate gas within the sample chamber. Critically, after dozens of experiments, no silicon nitride membranes have ruptured upon the generation of bubbles within the observation window. The devices, initially loaded at atmospheric pressure, undergo an increase of internal pressure when electrolysis occurs within as liquid water is converted to a compressible gas. Despite this, even when generated gas fully occupied the observable membrane region, occupying a volume of over 100 picoliters which represents up to 17% of the sample chamber volume, no silicon nitride membranes ruptured and no devices leaked even with the device inside the 10^{-5} Pa

high-vacuum TEM chamber. These experiments served to verify the integrity of the silicon nitride membranes and the two-chip liquid cell structure as a whole. With this confirmation, the more complex challenges of heating and flow control within the liquid cell could be pursued without the risk of device leakage within the TEM chamber.

3.1.4. Nanochannel Electrode Integration

While the fabrication process described in Chapter 2 includes a metallic layer, it is currently unfeasible to incorporate that layer directly within the channel at the observable region of the device. The thermal budget required due to the successive LPCVD steps mean that the metallic layer can only be deposited after the second silicon nitride layer is formed. Because the second nitride layer serves to seal the suspended channel structure, there is no way for the metallic layer to penetrate the nitride and reach the interior of the channel. However, outside of the suspended region, a secondary seal can be formed through the anodic bonding of the glass chip, so through-holes could potentially be patterned in the upper layer of nitride to allow the subsequently-deposited metal to reach into the channel.

3.2. Temperature Control

The control of sample temperature is a critical means by which dynamic events can be initiated within liquid cell structures. Many chemical and biological liquid-phase reactions and interactions require a certain threshold temperature to be met before any activity can occur. In the case of biological systems, this threshold temperature is often around 37º C which corresponds with the temperature of the human body, and rarely exceeds 80-90º C, above which most normal biological materials and organisms will be damaged. As such, a good temperature range for a liquid cell to strive to achieve would

span from room temperature up to 80ºC. Currently, custom TEM holders that feature onboard heating elements capable of achieving such temperatures by heating the holder tip are the most common method pursued for heated liquid cell studies. Such holders have been used in order to investigate the melting of metals [85], and in conjunction with liquid cells to observe the formation of precipitates from a solution [60] [61] [73], and other scientific phenomena.

In order to develop a liquid cell device capable of temperature control without the use of an advanced TEM holder, the liquid cell must be augmented to be capable of both generating heat as well as assessing the internal temperature of the sample chamber. This can be achieved through the use of the electrode layer described previously. The same metal layer used to induce electrolysis in the liquid cell device can be patterned to instead feature a closed electrode loop. If electrical current is passed through this loop, Joule heating will occur, raising the temperature of the electrode as well as its surroundings. The change in temperature of the electrode loop will also result in a proportional change in resistance of that same loop, so the monitoring of the loop resistance can be used to actively measure the temperature of the electrode. If the electrode is placed sufficiently close to the observational window, the temperature of the electrode will serve as a good approximation of the temperature of the membrane and the surrounding liquid during observation.

3.2.1. Previous Devices

Prior versions of the two-chip liquid cell device have included single-loop electrode structures intended for the heating of the entire device. The electrode was placed on the frontside silicon of the chip and ran peripherally around the viewing membrane [77]. While this design was demonstrated to be capable of achieving temperatures

exceeding 100ºC, it required significant power input and voltages exceeding levels that would introduce undesired electrolysis of the sample fluid. This occurred mainly due to the placement of the heater structure on the bulk silicon region of the device. The conductive heat losses through the device and whatever substrate it rests upon, in this case the TEM holder, serve to drive up the required input power and voltage to the detriment of the performance of the device.

3.2.2. Heater and Sensor Loop

In order to reduce the effective thermal mass of the liquid cell heater, subsequent designs pursued in this study have all featured Joule heating electrode loops that are centered on the observational membrane rather than surrounding it. The suspended membrane serves as a heat island, and heat loss to the thermally conductive surrounding bulk silicon is limited by the relatively slow conduction of heat radially outward through the 50 to 70-nm-thick membrane and convective effects from the heated liquid within the chamber. The approximate thermal loss to the surrounding silicon structure was estimated to be below 100 μW/K and demonstrated empirically to be on the order of 30 μW/K [94]. As mentioned previously, devices were designed with a temperature range of 20-80ºC. The heating electrodes were arranged in meandering loops on the suspended observation membrane, and featured a range of resistances from 40-1000 Ω. Figure 3.5 shows a typical design featuring a 633 Ω heater structure on a membrane.

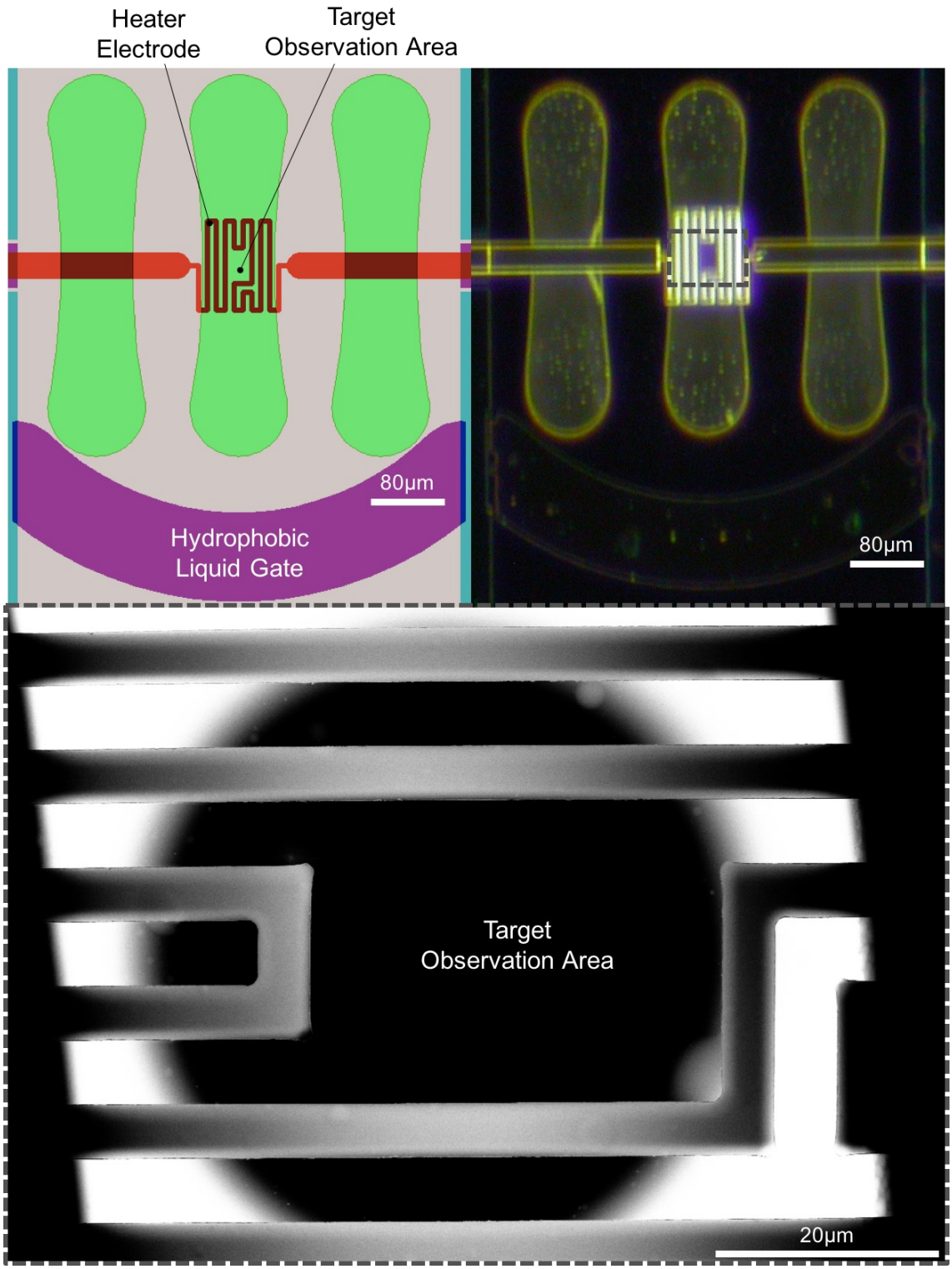

Figure 3.5: Heater-integrated two-chip liquid cell design (left), micrograph (right), and dry TEM image (bottom).

3.2.3. Characterization

The first batch of heater-integrated two-chip liquid cells did not include any insulating layer between the sample chamber and the heating electrode. Initial testing and characterization of the heater was performed with DI water and solutions with relatively low levels of conductivity. By situating the device on the suspended membrane, only the electrode, membrane, and fluid column above the electrode will undergo significant heating. Doing so significantly reduces the required power input and thereby also decreases the voltage that must be applied to achieve that heat flow. Electrodes with resistances varying from 40-1000 Ω were fabricated with the intention of using the relatively low-resistance loops to further reduce the driving voltage and potential conduction through the sample layer. The application AC driving voltages was also implemented to further reduce the effects of conductance through the liquid layer.

In order to characterize the devices, the Temperature Coefficients of Resistance (TCRs) of individual devices were first obtained using external Peltier heating in a probe station. The devices onboard heating capabilities were then verified by placing the device in a TEM holder within a vacuum chamber and cycling the temperature using the onboard heater and sensor. The device was then ready to be loaded with a sample liquid and placed in TEM for observation and experimentation. This experimental flow can be seen in Figure 3.6 in the central line. Proof-of-concept verifications, represented by the offshoots in the flowchart, were also performed to verify the performance of the device, but are not performed during a normal experimental flow. In order to confirm the accuracy of temperature measurement for liquid on or in the device, thermochromic ink was used to externally monitor the temperature of a sample on the device during onboard heating [94]. Furthermore, probe station heating experiments were also performed after devices were

assembled and loaded with liquid. In these ways, the performance of the liquid cell heater device was characterized and is confirmed during a normal experimental process flow.

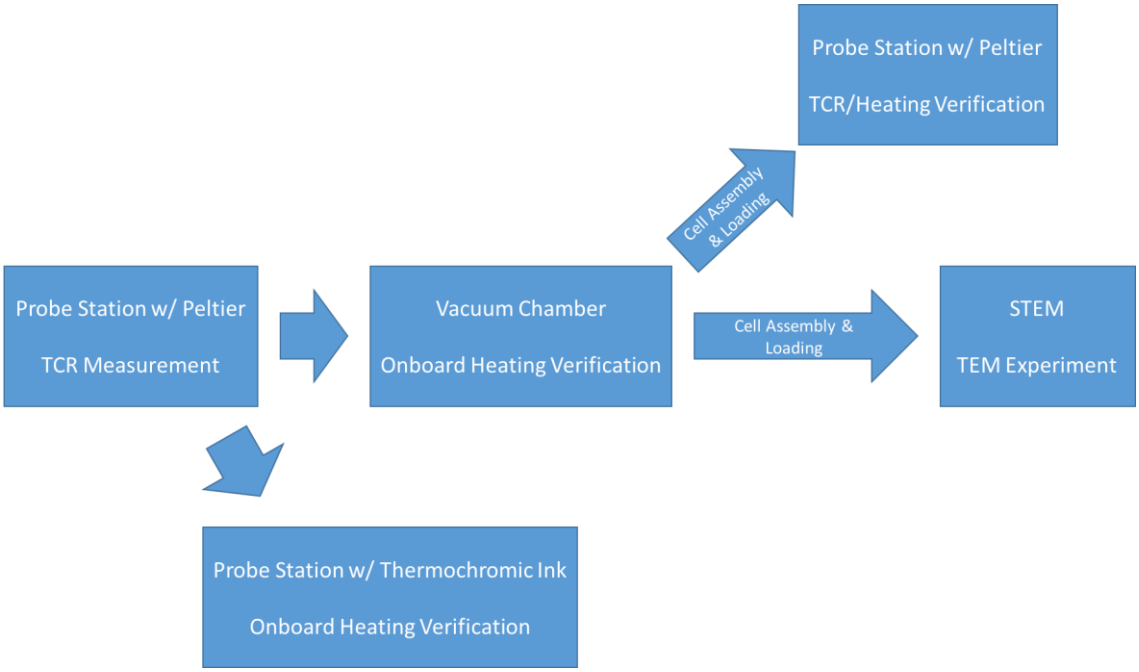

Figure 3.6: Experimental flowchart for temperature control devices

Individual device TCRs were measured by monitoring the resistance of the heater with a SMU while cycling the device temperature from 20º–100º C using a Peltier-based temperature control baseplate and temperature probe. After calibration of the device TCR using external controlled heating, devices were ready for experiments involving onboard heating.

Various proof-of-concept experiments were performed to verify the heating capabilities of the device using thermochromic ink. The temperature-sensitive ink placed on top of an electrode loop was monitored while the electrode was powered to sweep the temperature of the device. The color change of the ink correlated with the onboard measured temperature of the device and exhibited temperature stability in under 5 s for

liquid volumes well in excess of what would be used during STEM liquid cell operation [94].

Figure 3.7 shows a set of characteristic heating curves for a liquid cell heater with a nominal resistance of 80 Ω. The device was loaded into the TEM holder and placed in a plasma cleaner vacuum chamber. A 1000 Hz AC voltage was then applied across the heater loop through the TEM holder. The resulting current and voltage drop across the heating element were monitored with digital multimeters in order to monitor the changing resistance of the device. In this way, the ability for all devices to generate onboard heat and monitor local temperature was demonstrated by monitoring the electrode resistance while current was applied through the loop. With the calibrated TCR value previously acquired for the device, the temperature of the electrode could be calculated in real time based on the measured resistance.

Figure 3.8 shows the result of the same device being used for an *in situ* heating test performed on a liquid sample. A suspension of DNA-linked gold nanoparticles stabilized in a phosphate buffer solution was deposited on the device which was then sealed and loaded the STEM for observation.

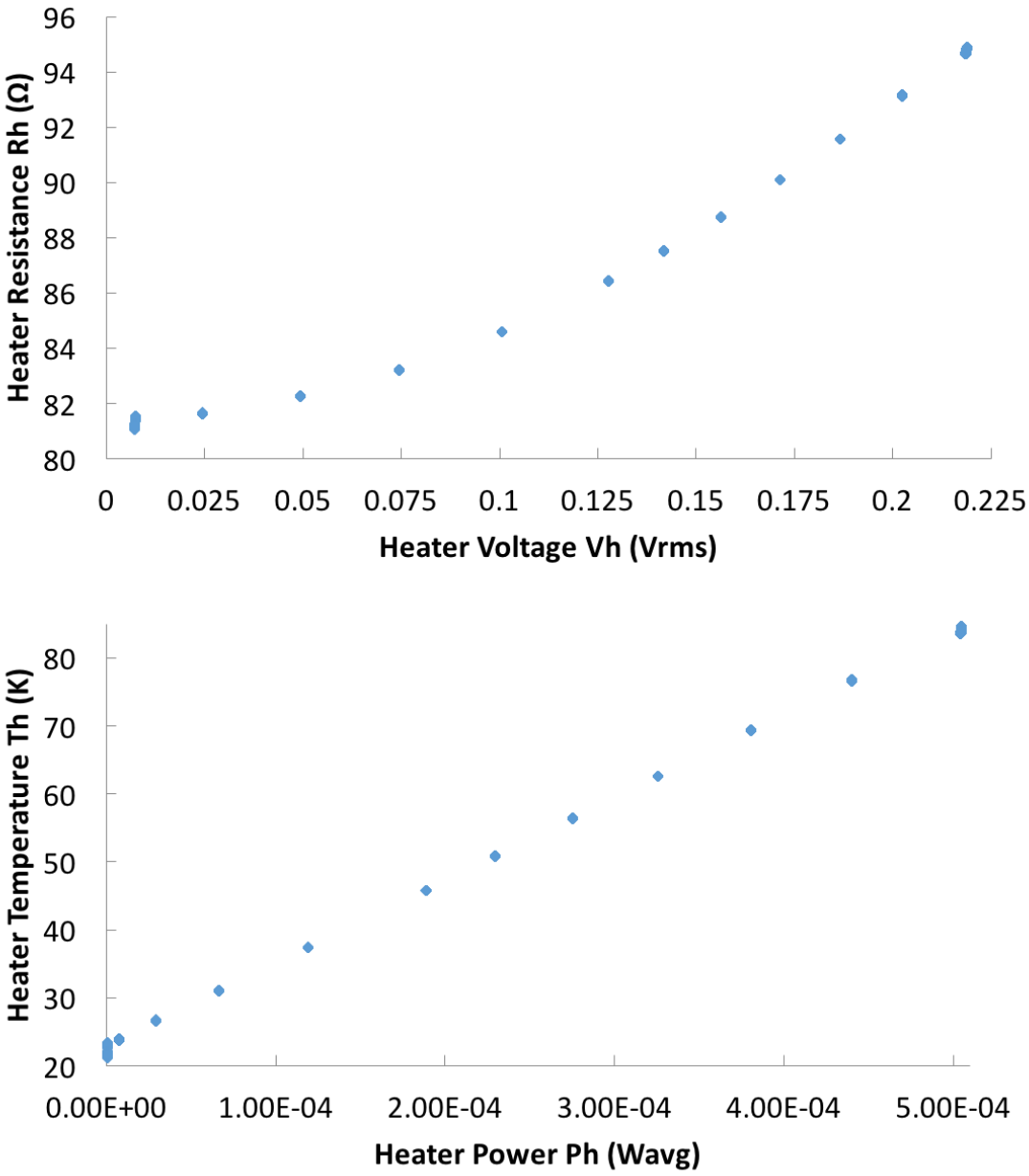

Figure 3.7: Characterization of liquid cell heater chip properties prior to sample loading for device with R_0=80 Ω. Variation of heater resistance with applied AC voltage (above). Derived heater temperature with input power (below)

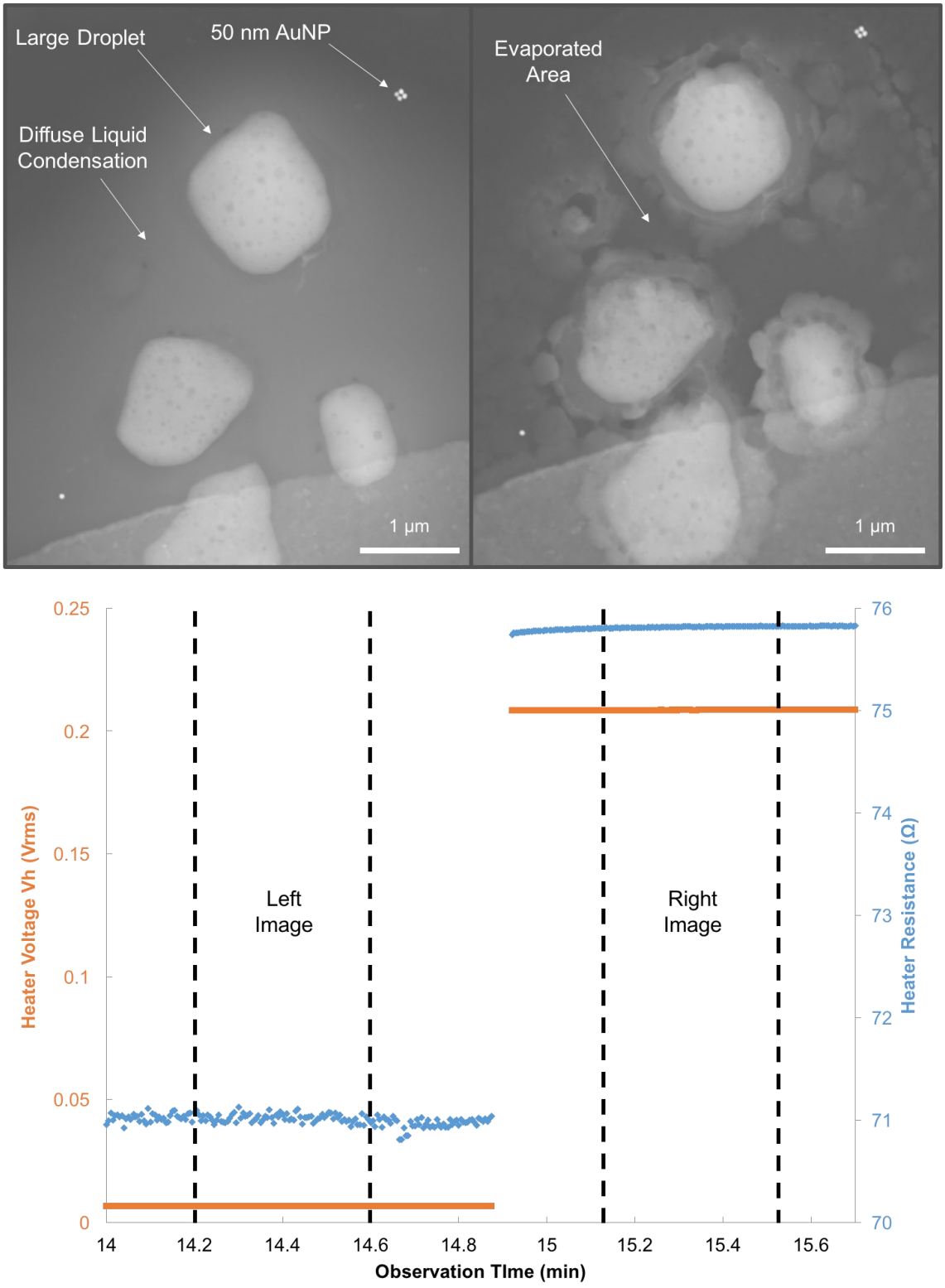

Figure 3.8: STEM imaging of liquid droplets. (Left) Room temperature droplets with condensation. (Right) Elevated temperature reduces liquid-induced brightness. (Bottom) Heating AC voltage and monitored resistance shift.

Discrete droplets of sample solution sandwiched between the observation membranes were observed. In this situation, the device spacers were insufficient to prevent membrane stiction, but the loaded liquid serves to create its own localized gaps between the membranes. In addition, regions with diffuse liquid-phase condensation were found to surround the droplets themselves, generating a pale bright region. The same signal and measurement setup used for the heater characterization was used to heat and monitor the device in TEM. Upon increasing the heater voltage to achieve an apparent temperature of as little as 50º C as occurred in the scenario described by Figure 3.8, an abrupt change in the condensation zones was observed. The signal level decreased, yielding a darker contrast in the areas where condensation existed at low temperature. This process was both reversible and repeatable.

One likely explanation is that elevated temperatures drive off a liquid layer of condensation that wets the hydrophilic silicon nitride membrane in the space between the larger droplets and the stuck membranes surrounding them. The thin liquid layer is more susceptible to evaporation and is vaporized, thereby reducing the signal and generating a darker image in that region. When the temperature is reduced again, the vapor is able to condense back to form the wetting film again. Figure 3.9 is a schematic representation of this reversible wetting phenomenon that gives rise to the changing brightness in areas outside the larger liquid droplets. The observation of this repeatable and reversible liquid motion serves to confirm that the temperature is indeed being elevated within the liquid cell upon the application of a heating voltage.

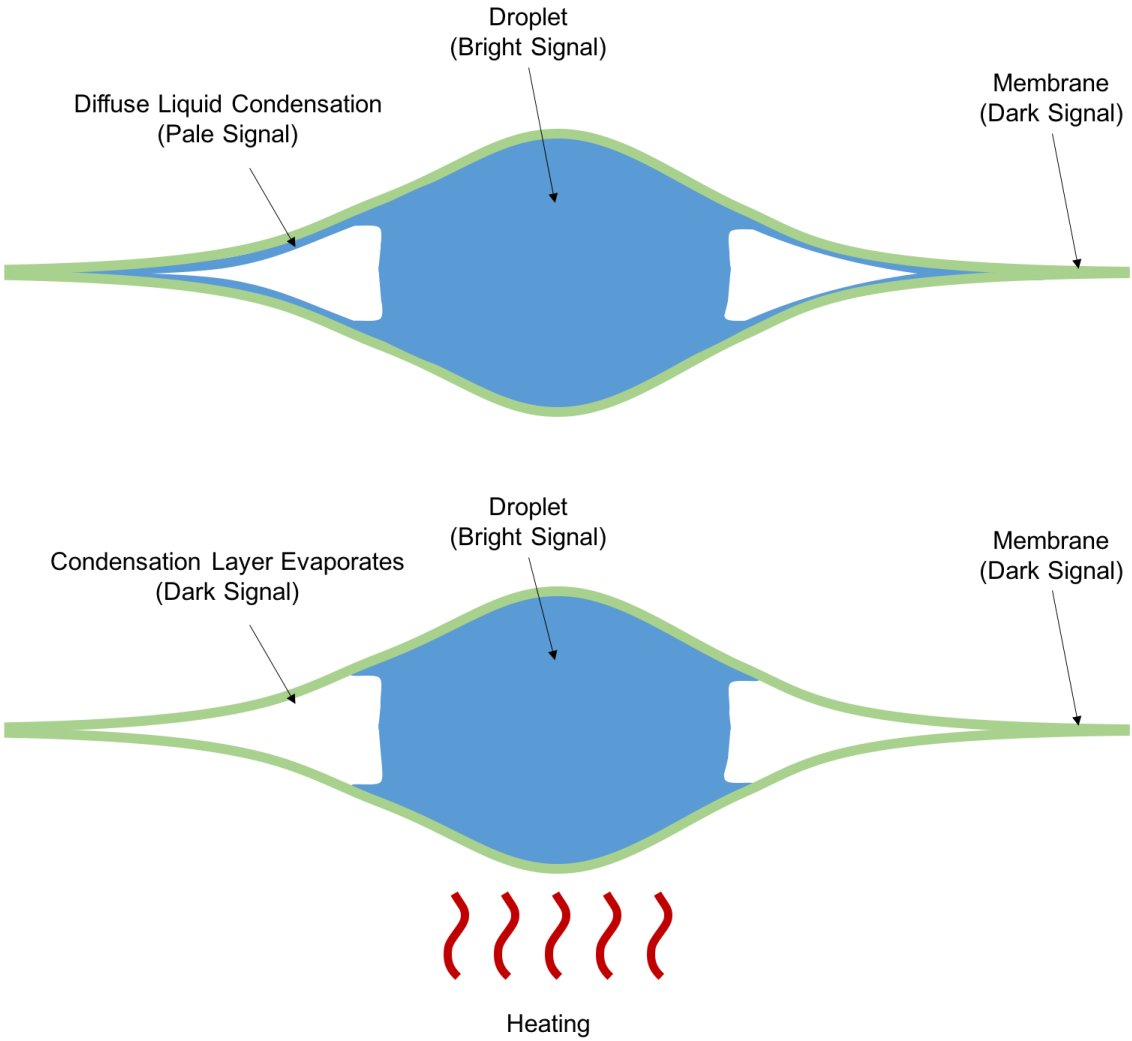

Figure 3.9: Schematic of trapped droplets at room temperature (above) and at elevated temperatures (below).

Figure 3.10 shows data from the same experiment as the temperature of the filled liquid cell was cycled from 56.6ºC to 64.0ºC. As can be seen, the measured temperature is fully stabilized in under 4 s. The data gap occurs due to the recording setup changing input parameters. A more advanced and responsive setup could be used to fully characterize the thermal response of the device, but this was deemed sufficient due to the minute-long time scales of STEM observations.

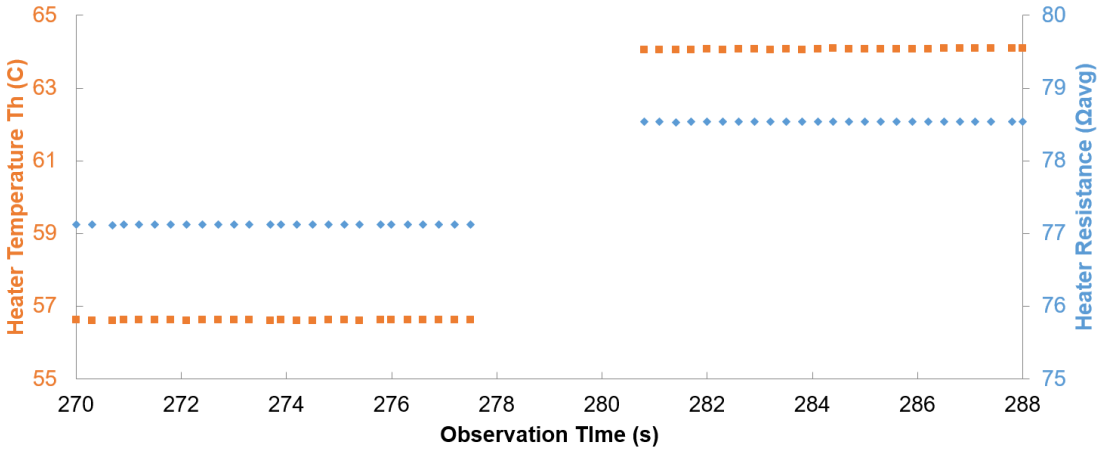

Figure 3.10: Typical thermal response to change in input current. The gap represents data not captured by the measurement setup during input parameter change.

As can be seen from the resistance values in Figure 3.8, the introduction of the liquid-phase sample reduced the overall resistance and change in resistance in the heater for a given input voltage. This can be explained by the increased thermal mass of the sample liquid cooling the electrode, as the liquid provides an additional path for heat to flow convectively from the electrode to the liquid and out to the bulk silicon substrate, and reflects results achieved with DI water and non-conductive samples. Figure 3.11 shows the derived temperature of the resistor, which scales with the total resistance between the contact pads, as a function of the total input power applied for the whole experiment.

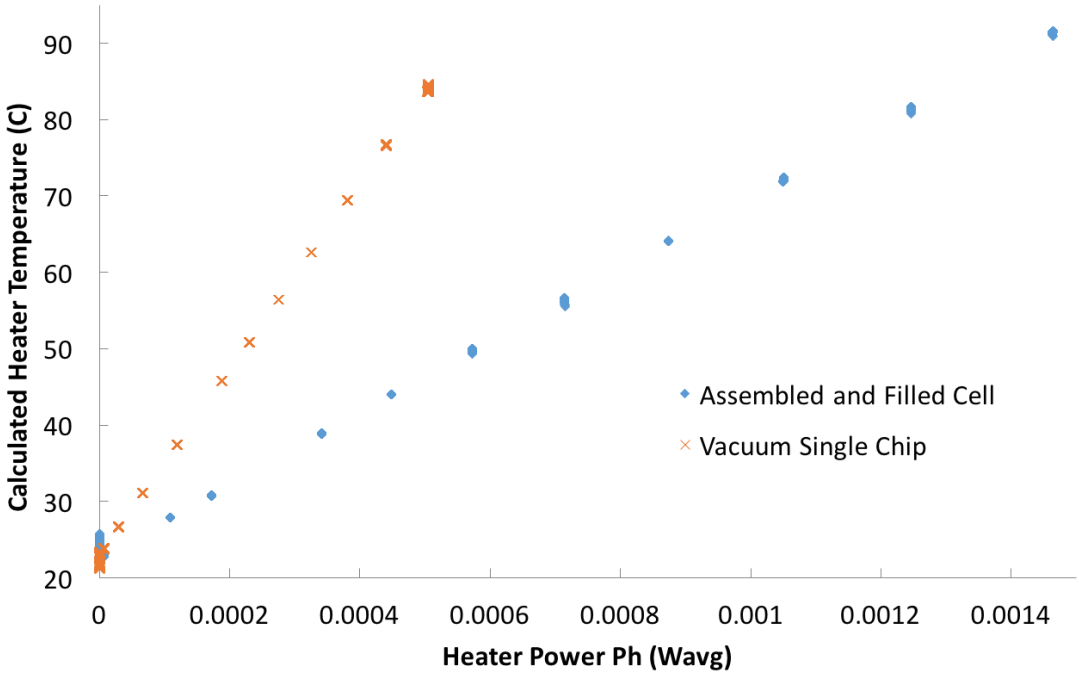

Figure 3.11: Derived cell temperature as a function of input power through all conductive paths for the filled cell and individual chip.

Comparing the total power provides a means of comparing the functionality of device in the dry and wet state. While there is a possibility that the high salinity of the buffer solution used to stabilize the DNA present in the solution caused leakage current through the liquid, joule heating would still occur and the power input would still be applied to the device. The uniformity of the graph suggests that the nonlinearities involved in electrical conduction through ionic solutions were not introduced to the system and that the combination of low heater resistances and AC excitation signals are sufficient to isolate the current path from solutions rich in ions such as phosphate buffer solutions. Sweeping the AC frequency and incorporating an insulating layer on the electrode may be performed in the future to further confirm this capability.

3.2.4. Nanochannel Heating

The nanochannel device as described in Chapter 2 is capable of sporting an active electrode layer, but as discussed earlier in this chapter, it cannot readily be incorporated to the inside of the channel. In the case of heating experiments, though, this does not represent a significant drawback, as heat can be conducted through the nitride layers. While they are separated by a thin silicon nitride membrane, the polysilicon supports of the nanochannel device with electrodes on top can be machined a thermal island that is partially isolated from the silicon bulk via thin suspending struts. A heater placed in this structure should be capable of heating the entire island without requiring an exorbitant amount of energy input. Figure 3.12 shows a micrograph of the fabricated nanochannel heater structure. The separation between the green hollow channel and the blue polysilicon support can clearly be seen, and is only filled by a double-layer of silicon nitride that limits the heat flow from the heater to the observation region of the channel.

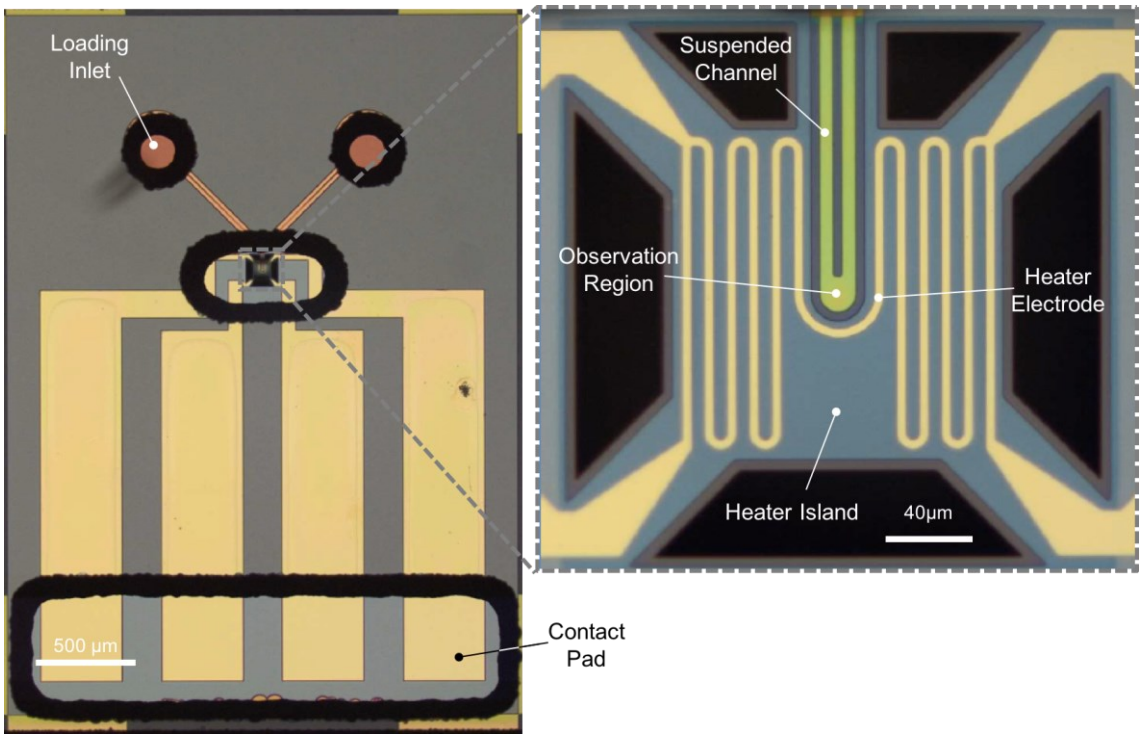

Figure 3.12: Nanochannel with heating electrode and thermal isolation island.

As with the two-chip device, the nanochannel TCR was characterized using an SMU to monitor the electrode resistance while the device temperature was swept by a Peltier temperature control system. Once this calibration was complete, the onboard heating properties of the device were tested. Figure 3.13shows the same characterization that was performed on the two-chip device.

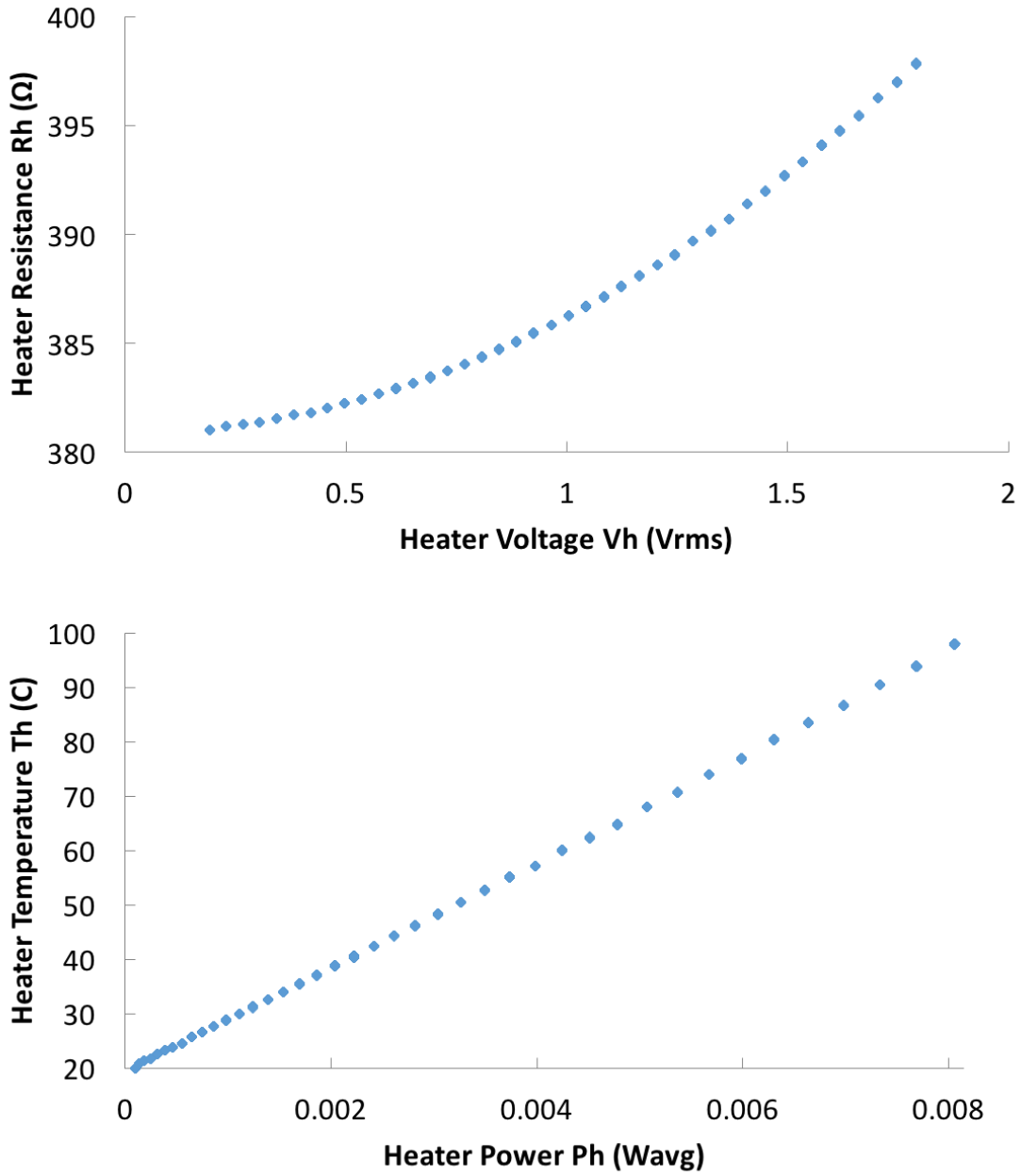

Figure 3.13: Heating properties of the nanochannel liquid cell. Resistance variability with input voltage (above) and temperature dependence on power (below).

The nanochannel heater exhibited similar heating capabilities as the two-chip liquid cell, but required a larger input power to achieve the same temperature values. Given that the heater structure is placed atop a polysilicon layer that is directly in contact with the bulk silicon of the device, the increased power consumption of the nanochannel heater is to be expected. Testing with loaded samples has been attempted, but the filtration effect described in Section 2.3.2 has thus far prevented the observation of particles in the heated nanochannel device.

3.3. Flow Control

Biasing electrodes and heaters in liquid cells are generally static structures, and do not necessarily involve or induce any large-scale motion of the fluid medium within the liquid cell. In both cases, extreme situations such as the prolonged electrolysis or boiling of the liquid can at best interfere with the stable observation of the targeted sample and at worst cause leakage or outright bursting of the cell. Despite these risks, the ability to move fluids around within a TEM liquid cell can enable the observation of previously inaccessible systems through either the triggering of a reaction that would have otherwise reached completion before observation could occur [28] or by replenishing a given reactant to maintain an ongoing process over time [34]. For investigation of such systems in TEM, researchers almost exclusively rely on liquid cell structures equipped with inlet and outlets that connect to small external flow tubes housed in a specialized TEM holder designed for use with that specific structure [35] [68] [86]. While such systems may be appropriate for researchers whose main focus is on liquid-phase microscopy as a technique, for more general users who use TEM as an analytical tool rather than as a research focus, customized TEM holders can be viewed as an overly-niche tool not worth the investment despite the novel information that could potentially be revealed about a

given sample. As such, one of the primary goals of this study is to develop a self-contained TEM liquid cell that is capable of inducing fluid flow for the purposes of sample mixing or rehydration without the need for anything more than a generic TEM holder with electrical interconnects.

3.3.1. Previous Devices

Previous researchers have attempted to induce fluid mixing within the liquid cell structure through the application of an Electro-Wetting-On-Dielectric (EWOD) structure [93]. In addition to the fundamental liquid cell encapsulation structure, an attempt was made to integrate fluidic chambers separated by a CHF_3-treated hydrophobic insulator with a pair of electrodes buried underneath. The application of an electrical signal across the electrodes would, in theory, alter the wettability of the hydrophobic separator and allow the samples within the two chambers to mix. However, progress on this technique was inhibited due to both the limitations of the reliability of the basic liquid cell structure at the time as well as the durability and hydrophobicity of the insulating layer. The high-voltages required for EWOD actuation often caused electrical breakdown in the insulating layer, and the hydrophobicity of the chamber separator was relatively unstable.

3.3.2. Hydrophobic Gate Design

As described in Chapter 2, in addition to the formation of a more reliable and robust basic liquid cell structure, the use of C_4F_8 plasma to deposit stable and consistently hydrophobic fluorocarbon polymer layers, also referred to as a Teflon-like coating, has been developed for use in the two-chip device spacer structure. In addition to confining the sample liquid to the geometry defined by the spacer layout, the same material can be used to form a distinct so-called “hydrophobic gate” feature that inhibits fluid flow down

the channel structure. This kind of liquid pinning is sometimes referred to as a “passive valve” in the context of microfluidics as selectively hydrophobic regions within a channel can stop the flow of a liquid without requiring any external stimulus. Conversely, external stimulus can then be applied to initiate fluid flow as desired, and relatively complex microfluidic systems have been designed based on this concept [95] [96].

In the context of the two-chip liquid cell, the development of the electrode structure provides a simple and direct means for the generation of a pressure gradient along the sample channel. Electrolysis experiments indicated that the liquid cell structure can withstand the pressures involved with the formation of large, membrane-filling gas bubbles, so the hydrophobicity of a passive valve structure can potentially be overcome using pressure from upstream electrolysis of the sample itself.

In order to achieve this liquid gating capability, a hydrophobic patch consisting of a layer of C_4F_8 plasma-based polymer 200 to 400-nm-thick is patterned in the path of the channel formed by the 500 to 700-nm-thick spacer, thereby separating it into two chambers. Figure 3.14 shows the design and layout of a bottom chip of the liquid gating device. The lower chamber defined by the spacer and hydrophobic patch, referred to as the flow chamber, can be loaded with an aqueous sample that is capable of undergoing electrolysis. The hydrophilic exposed surface of the chamber will draw the liquid in, where it will stop proceeding vertically when it encounters the hydrophobic patch. At this point, the liquid is surrounded in all directions by the mating of the top and bottom chip spacer structures, where the liquid faces a cross-section with the top chip spacer and the bottom chip hydrophobic patch. Because the patch is thinner than the spacer, this area represents a gap in the quasi-sealed chamber. However, since the patch is hydrophobic, the liquid will not proceed to enter the gap naturally.

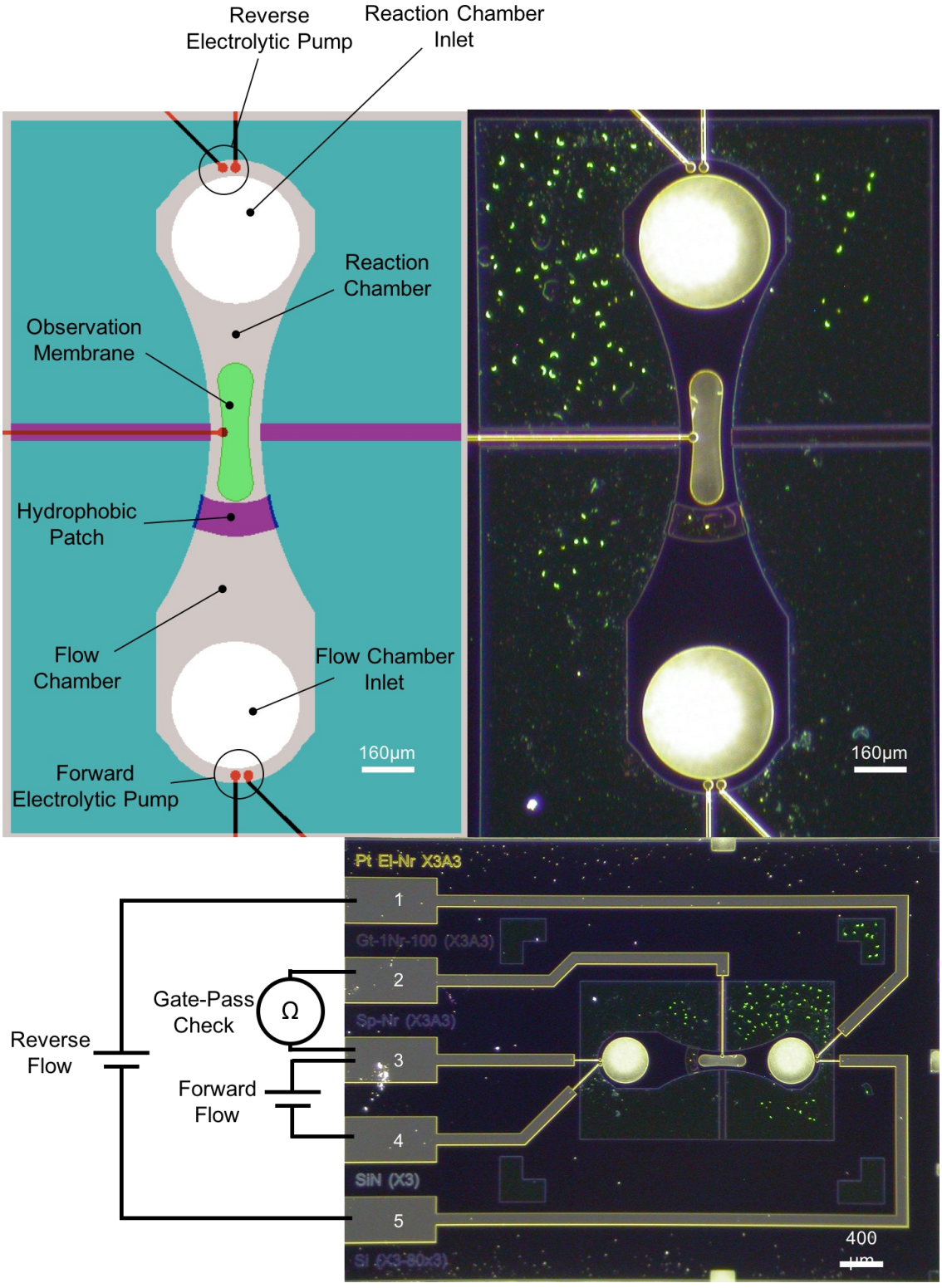

Figure 3.14: Design of the liquid gate device for flow control in TEM (left). Micrograph of fabricated sample chamber with gating features (right). Micrograph of whole chip with schematic of electrode functionalities (bottom).

If a sufficient voltage is applied upstream behind the inlet of the flow chamber between electrodes 3 and 4, the electrolytic splitting of the liquid medium will occur, releasing gaseous bubbles at the back of the flow chamber. The buildup of these bubbles will eventually produce enough pressure to force the liquid through the thin gap made by the hydrophobic patch rather than into the surrounding spacer regions with no ostensible gap. After slowly passing through the hydrophobic gap, the liquid front reaches the hydrophilic silicon nitride surface on the other side and the flow rate suddenly jumps as the reaction chamber is filled. A schematic illustration of this flow process in a cross-section of the device is shown in Figure 3.15. The direction of the flow is determined purely by which chamber is initially filled with sample liquid through its respective inlet. If the upper chamber is filled with sample liquid, for example, applying a voltage to the lower electrode pair will do nothing as there is no liquid present in the lower chamber to initiate electrolysis. Therefore, in this scenario, liquid can only flow from the upper chamber to the lower chamber by applying voltage to the electrode pair in the upper chamber where liquid is present. In the schematic shown in Figure 3.15, because the right-side chamber is initially filled with liquid, applying voltage across the right-side electrodes will initiate electrolysis and cause flow to occur into the left-side chamber.

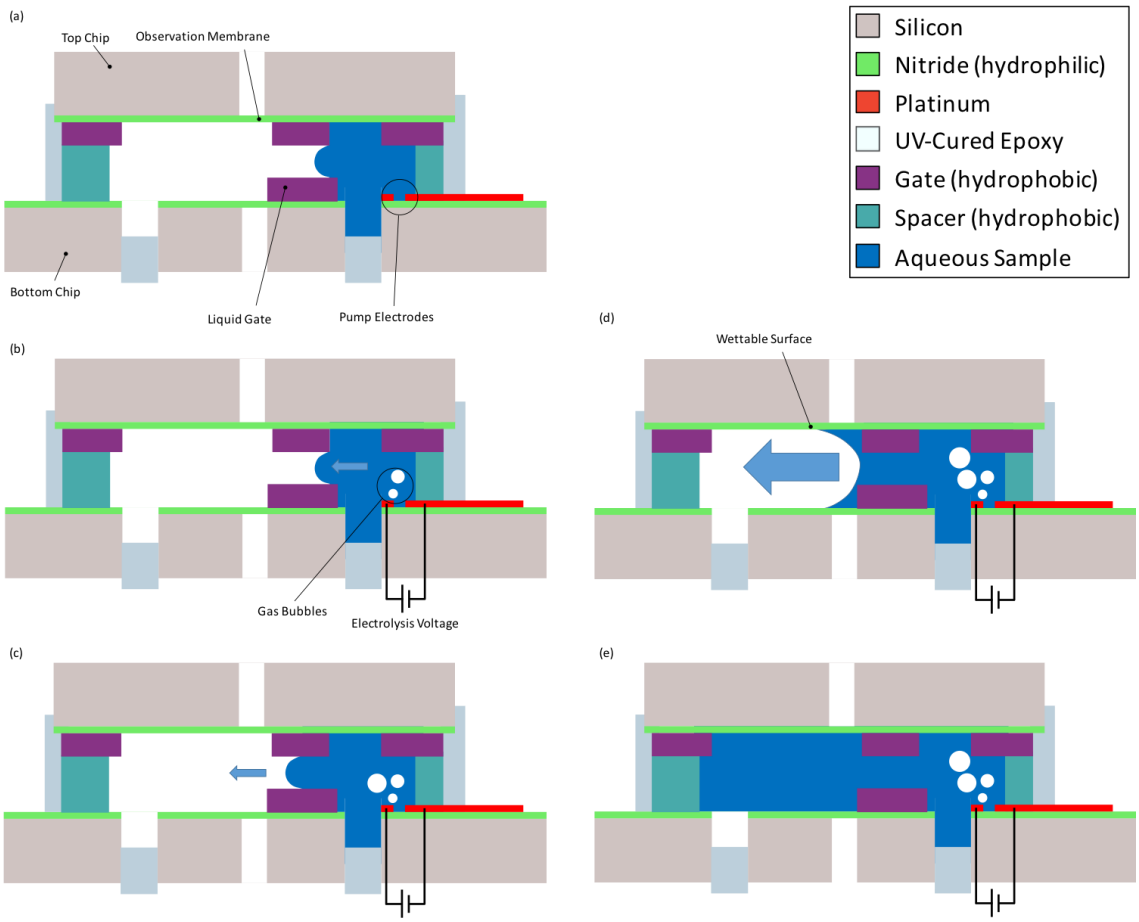

Figure 3.15: Liquid gate operation. (a) Sealed device with liquid in the flow chamber. (b) Electrolysis causes increased chamber pressure. (c) Pressure-driven flow through the hydrophobic gate. (d) Surface-driven flow into the reaction chamber. (e) Fully filled reaction chamber.

3.3.3. Characterization

In order to verify the feasibility of this technique for liquid pinning and gating, initial tests outside of TEM were performed. The top chip of the device was replaced with a hydrophobic glass slide to enable the optical observation of liquid motion within the sample chamber. Using an inverted microscope for surface monitoring, DI water was loaded into the flow chamber of the liquid cell to assess the liquid gate's ability to prevent fluid flow down the channel. Frames from one such experiment are shown in Figure 3.16.

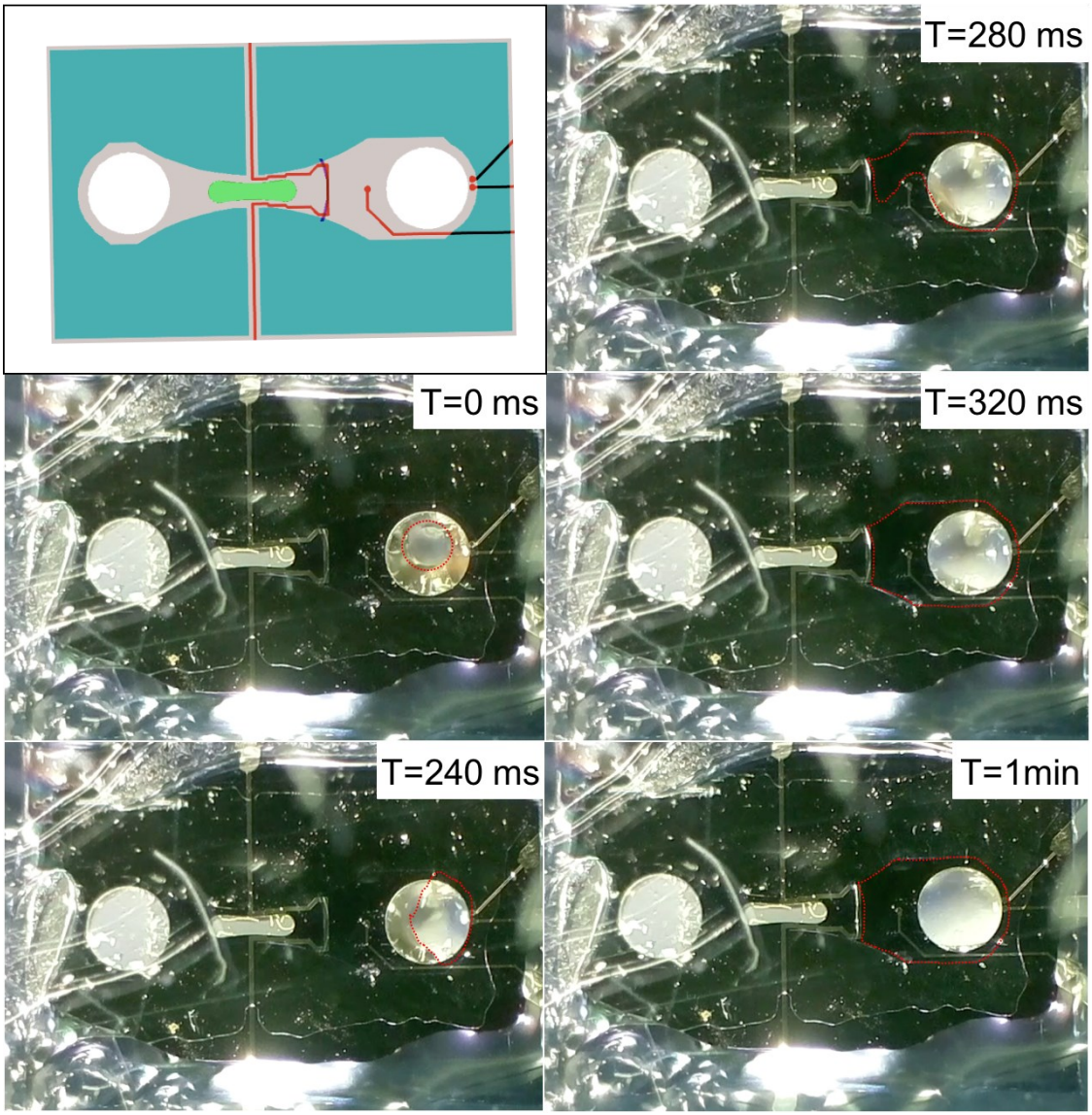

Figure 3.16: Frame-by-frame imaging of liquid entrance and immobilization at the gate structure. The outline of the liquid front is shown in red.

The hydrophobic patch was shown to be effective at preventing the progression of liquid down the channel, so the ability to overcome that hydrophobicity was tested next. The inlets of the cell were sealed with the liquid inside the flow chamber and a constant DC voltage of 5 V was applied at the forward electrolytic pump electrodes in order to generate gas bubbles at the bottom of the channel. As can be seen in Figure 3.17, the electrolytically-produced gas was indeed capable of displacing the liquid in the

channel. Furthermore, rather than spreading across the chip surface haphazardly, the liquid advanced through the gate pattern and into the upper chamber without excessive leaking into the spacer regions. With these successful demonstrations of flow control achieved, the next step was to characterize the operation of the device during TEM observation.

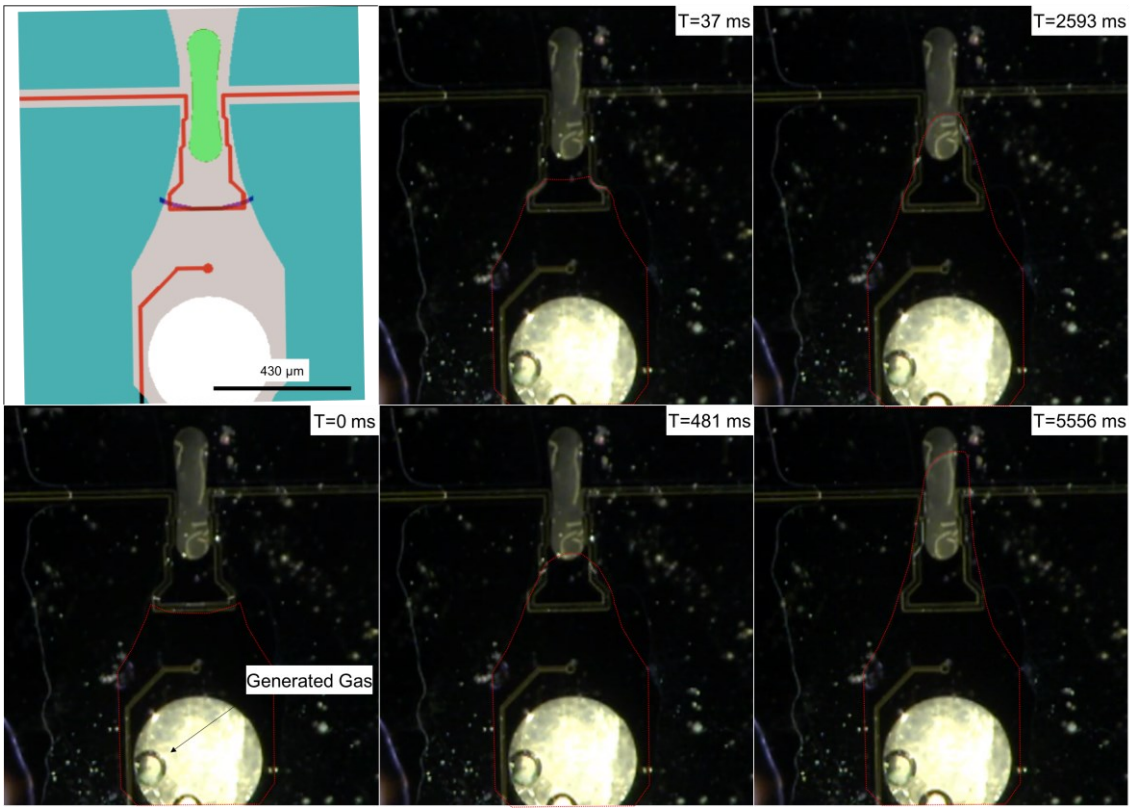

Figure 3.17: Proof-of-concept experiment for liquid gating. 5 V_{DC} applied at the bottom of the channel generated gas until the internal pressure exceeded the hydrophobicity of the gate layer. The advancing liquid front is outlined in red.

While tests using glass chips in place of the proper liquid cell top chips enabled the visualization of the whole bottom chip surface, this is not possible in TEM. Only the observation window can be seen inside of TEM, so the advancing liquid front cannot be monitored unless the gate structure is placed directly on the membrane itself. Tests were performed using gates both on and off of the membrane with a similar methodology as

the glass chip testing. Devices were assembled and liquid was loaded into the flow chamber and pinned. The liquid cell was placed into the STEM chamber, and once vacuum was drawn and an image was achieved, voltage could be applied to the forward pump electrodes to induce the flow of liquids. Figure 3.18 shows the STEM observation of a flow event in which liquid water was flowed past a gate located to the right of the viewing membrane seen in the figure. As the off-screen liquid draws near, condensation occurs in the membrane, droplets form, and the liquid finally bursts past the gate and fills the screen.

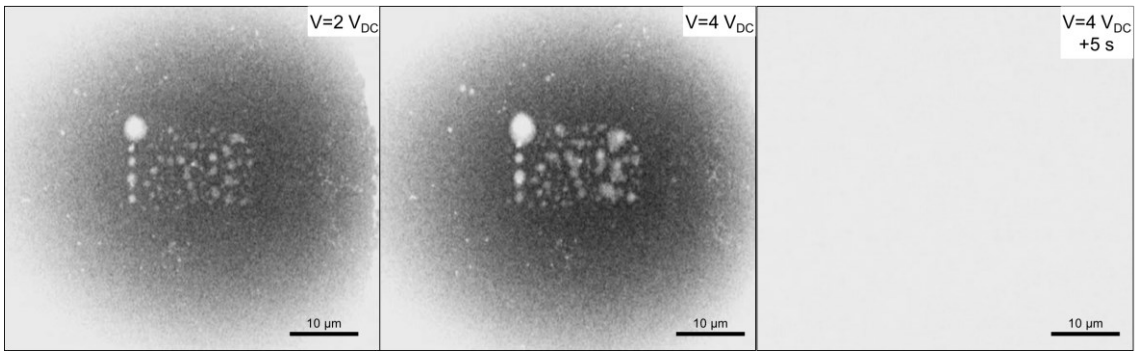

Figure 3.18: On-chip demonstration of fluid flow in STEM. Voltage is applied to an electrolytic pump off-frame to the right. As the liquid front approaches the membrane, moisture condenses in the center of the viewing window (growing white patterns). Finally, the liquid front reaches the observation window and fills it, yielding a bright field image.

In Figure 3.19, the liquid front of a solution of gold nanoparticles, outlined in red, can be seen advancing incrementally across a hydrophobic gate patch, outlined in purple, present on the observation membrane as 5 V_{DC} are applied to the pump electrodes off screen to the right. The white clusters on the right are due to condensation from the very proximal liquid front. As voltage is continually applied, the liquid moves slowly downstream. Once the front reaches the end of the gate structure, the liquid springs forward as it comes into contact with the hydrophilic nitride membrane underneath. Note that no nanoparticles are visible.

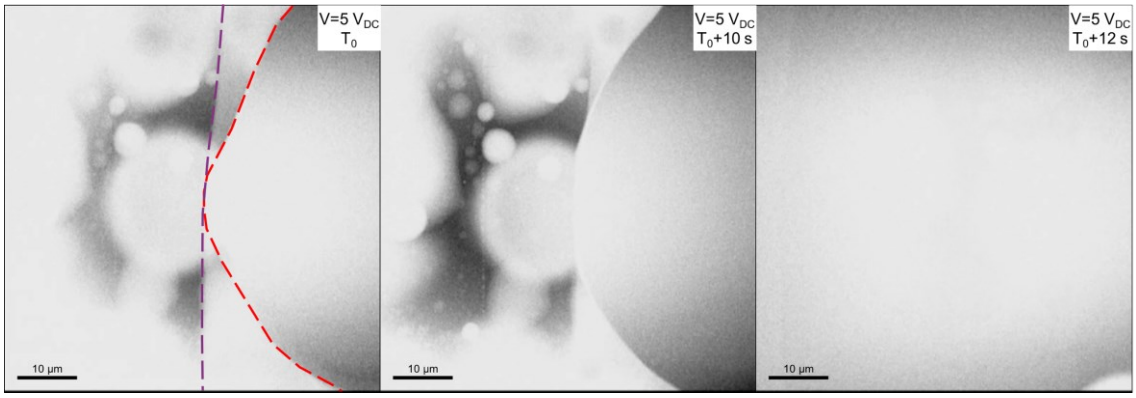

Figure 3.19: Liquid front (red outline) advancing across a hydrophobic gate patch (purple outline) as condensation accumulates on the left. After 12 s, the liquid passes the gate and fills the rest of the channel on the left.

One drawback of this liquid gating technique is that it is very susceptible to the filtration effect described in Chapter 2 due to the narrow gap generated by the gate/spacer structure. While the gap should nominally be above 300 nm, particles as small as 50 nm in diameter were completely filtered during flow experiments. Currently, this device is most suited to experiments in which a target analyte is first deposited on the observation membrane and then rehydrated with some relevant sample solution containing molecular-scale reactants. A demonstration of this kind of technique can be seen in Figure 3.20, in which 50-100 nm diameter gold nanoparticles have been previously dried on the observation membrane and then rehydrated *in situ* with water.

Using this electrolysis-driven pressure generation system, the ability to induce and control fluid motion in a fully encapsulated liquid cell has been achieved and demonstrated. The use of hydrophilic chambers separated by a hydrophobic gate enables "digital" functionality where the downstream chamber can be rapidly filled upon activation of the mechanism. A more "analog" functionality can reasonably be envisioned where a fully hydrophobic downstream chamber can be filled incrementally through the continuous application of increasing electrolytic pressure from the upstream pump. This

type of flow control could potentially be invaluable in the study of reactions at a liquid-gas or even solid-liquid-gas interface where the position of the liquid front must be maintained within a given region. While filtration effects represent a significant limitation in the ability to move nanoparticles and other structures suspended in the mobile liquids, pure liquid-phase flow capabilities can introduce a wide range of sample activities and reactions that can now be investigated directly in TEM.

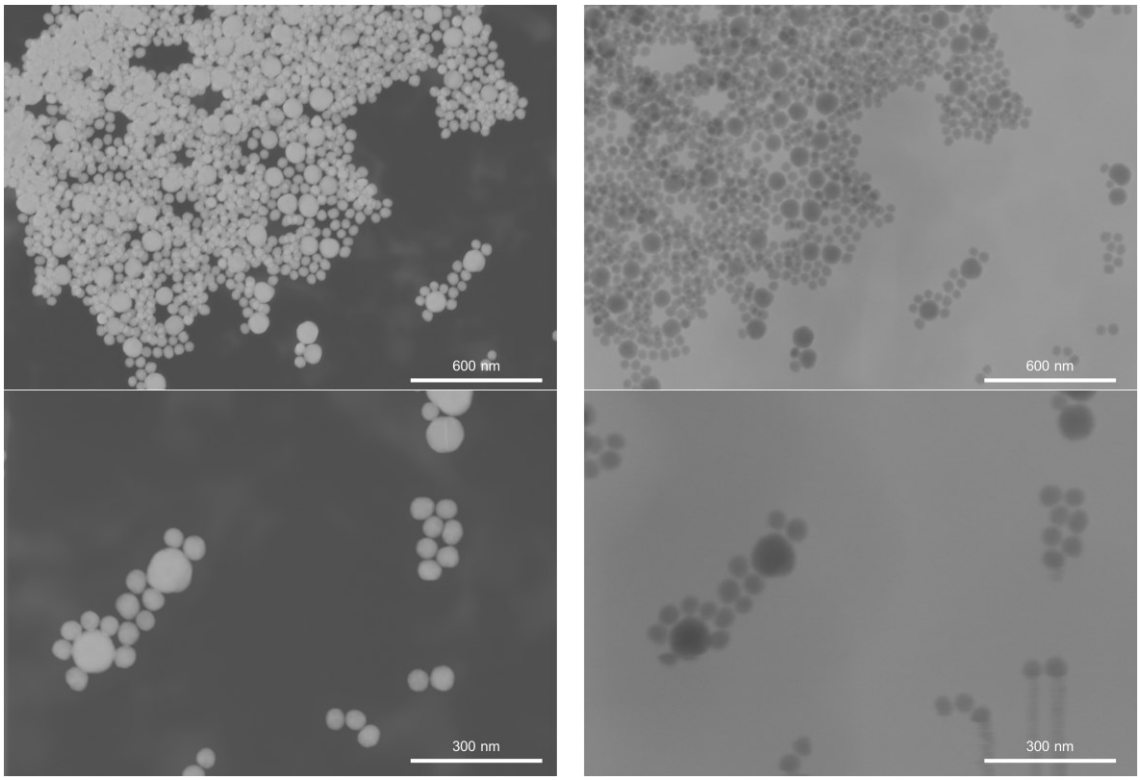

Figure 3.20: Dried 50-100 nm gold nanoparticles (left) rehydrated (right) with water using the onboard pumping electrode.

3.3.4. Flow Control in the Nanochannel

The use of post-fabrication treatment of the nanochannel device to render the interior of the channel hydrophobic has been proposed as a means to incorporate the flow-control technique used in the two-chip device for the nanochannel. If the channel is made hydrophobic, placing electrodes at the inlet structures to generate pressure could allow

for flow to be induced within the channel. One limitation of this proposed technique would be the limited ability to selectively pattern specific regions of the channel only. The narrow dimensions of the nanochannel could cause unacceptable buildup of pressure if the entire structure is made hydrophobic and filled using a pressure gradient. Further testing is necessary to assess the feasibility of this technique.

3.4. Combined Functionality

While each of the MEMS features discussed in this chapter were developed individually, there is nothing preventing the integration of all three components onto a single device. By sharing the electrode contact pads between components that will not be used simultaneously, devices equipped with biasing electrodes, a heater, and electrolytic pumps have already been designed and fabricated as seen in Figure 3.23. The device also features a larger membrane with a region dedicated for loading samples via droplets rather than via an inlet in order to mitigate particle filtration effects.

3.4.1. "Hybrid" Device Design

One of the ultimate objectives for this study is the development of a single liquid cell device that is capable of electrical interaction, temperature control, and flow initiation. The devices and experiments discussed previously were performed using devices incorporated with MEMS components used to achieve each of these capabilities individually for the purposes of device development. Fundamentally, there is no reason that each of the individual MEMS components could not be incorporated on a single device. The primary limiting factor in this regard is the availability of only five probe interconnects available on the TEM holder used in this study. In fact, this is sufficient to achieve the three desired experimental capabilities as certain electrical contacts can be

shared between functions through the use of a shared ground signal. Thus, the newest version of the device described as follows incorporates electrical biasing, heating, and flow initiation capabilities on a single chip.

One major issue that limits the applicability of the device for certain experiments is the "filtration" issue discussed in Section 2.3.2. When the channel formed by the liquid cell is loaded via the inlets on the chip, the narrow channel height formed by the spacer of approximately 1 μm or below can tend to limit the ability for certain particles or aggregates to travel through the channel into the region that can be observed via STEM. One way to mitigate this issue would be to apply a droplet of solution to the surface of the membrane before the sealing chip is assembled, thereby ensuring that the desired sample particles are in the observable region. However, doing so with the conventional two-chip designs discussed thus far limits the ability to subsequently perform flow-initiation experiments as liquid has already been manually placed throughout the chip surface. Therefore, the new "hybrid" device described here features two flow chambers separated by a hydrophobic patch, just like the normal flow control device, but one chamber is much larger and designed to accommodate manual droplet loading prior to assembly of the sealing chip without impeding the performance of the normal flow chamber. A schematic illustration of this device can be seen in Figure 3.21. With this device, droplet samples can be placed directly on the observation membrane prior to bonding with the sealing top chip. The sample can be allowed to dry to deposit sample particles for observation on the membrane, or maintained as liquid and sealed in the chip using the bonding of the top chip. The hydrophobic patch in the experimental region prevents the droplet from spilling up into the flow chamber in this case. After bonding, a second sample liquid can be loaded into the flow chamber through the backside inlet.

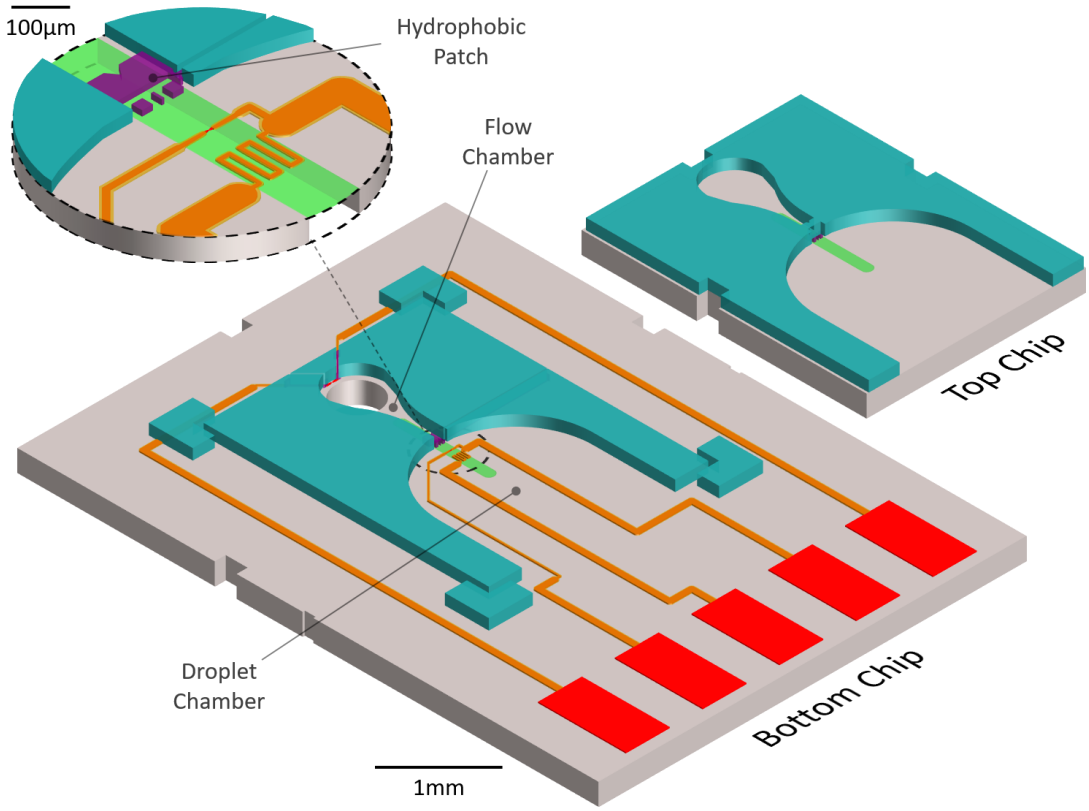

Figure 3.21: Schematic of hybrid liquid cell device. Note the channel featuring the flow chamber and larger droplet chamber separated by a hydrophobic patch. Inlay: magnified view of experimental region.

Figure 3.22 shows a schematic process flow for these two potential experimental techniques. The dried particle method can be potentially used to view particle aggregates as they are rehydrated with a second sample from the flow chamber, while the undried sample method can potentially be used to view liquid mixing events, though this has yet to be achieved experimentally. Figure 3.23 shows a fabricated device and detail of the functional region of the bottom chip surface. As mentioned above, this device features electrodes for *in situ* sample biasing, an insulated heater electrode for temperature control, and pump electrodes to initiate flow from the upper flow chamber down into the lower droplet chamber. The locations of these active components are shown schematically in Figure 3.24.

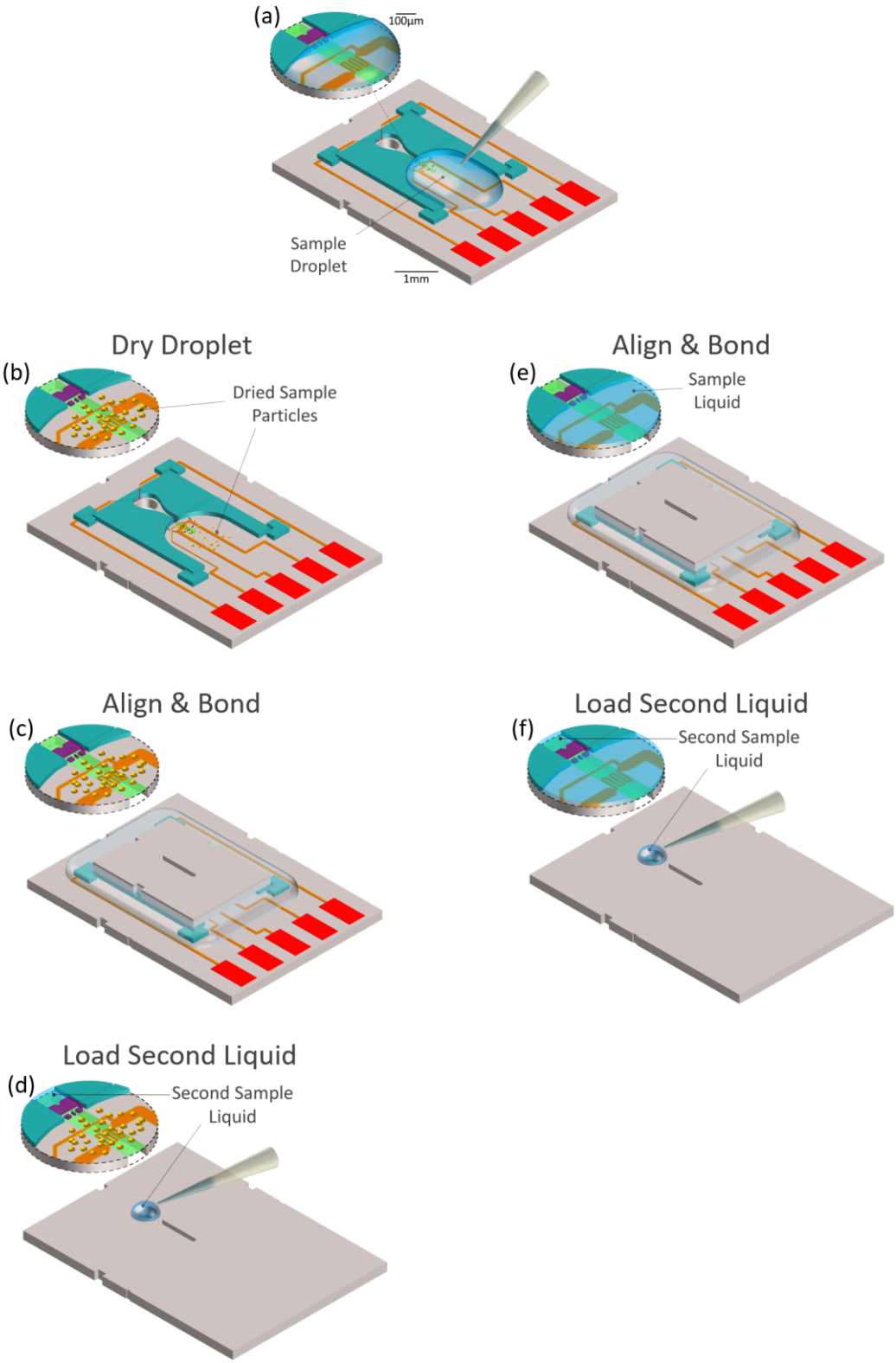

Figure 3.22: Schematic process flow for hybrid device preparation. (a) shows the initial placement of a sample droplet in the droplet chamber of the chip. It is held in place by the hydrophobic spacer and hydrophobic patch. (b)-(d) shows the process for viewing initially dried particles while (e)-(f) shows the process for loading two sample liquids which are kept initially separated by the hydrophobic patch

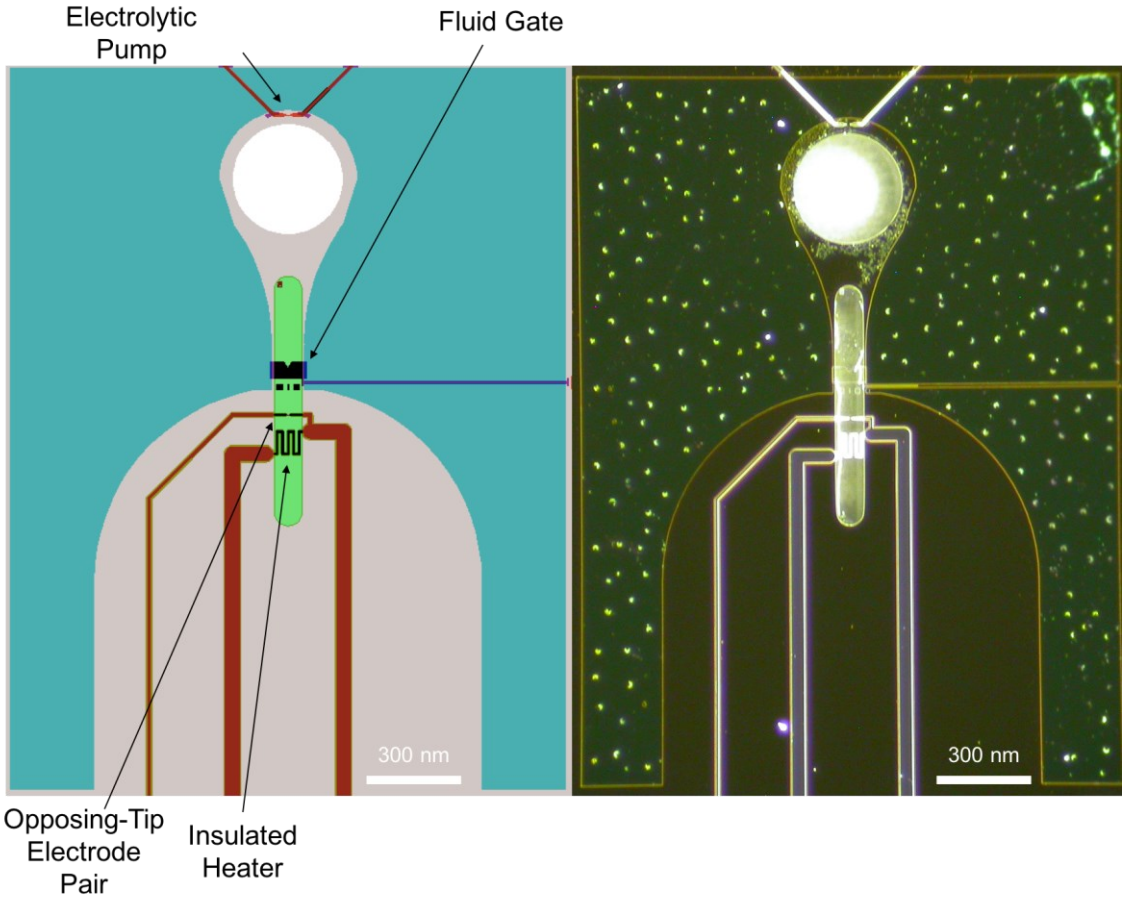

Figure 3.23: Fully-integrated combined liquid cell with biasing, heating, and flow capabilities.

As with previous devices, the droplet and flow chambers are separated by a hydrophobic patch. In this device, additional hydrophobic patterns are applied to serve as a barrier to prevent the droplet from flowing upward during application with a micropipette. The inlet to the flow chamber is flanked by a pair of pump electrodes that can be used to drive fluid down into the droplet chamber during STEM observation. Within the droplet chamber, a pair of electrodes is present on the observation membrane and also features an insulating layer to prevent extraneous electrical fields being applied to the device inhibiting the precise observation bubble nucleation events. Finally, a heater electrode insulated by 100 nm of sputtered SiO_2 is also present to enable temperature control capability.

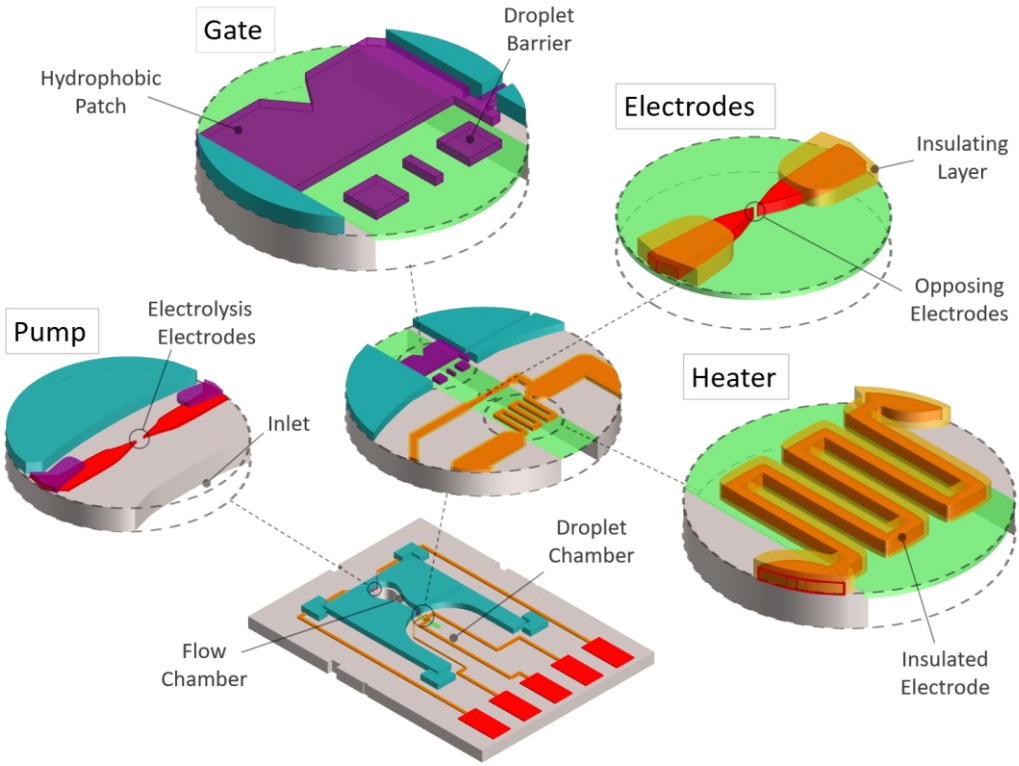

Figure 3.24: Active MEMS components of the hybrid liquid cell device.

This hybrid liquid cell prototype has been fabricated and tested for static STEM observations of liquid samples, but the active MEMS features have not yet been tested. However, the design integrates the three sample interaction methods being pursued in this study on a single device. The ability to electrically bias, heat, and initiate flow within a single liquid cell device that is compatible with generic electrical TEM holders represents a significant increase in the sophistication of standalone liquid cell designs.

3.5. Summary

In this chapter, the liquid cell platforms introduced in Chapter 2 were each augmented with various active MEMS components to enable interaction with samples under being observed in TEM. The two-chip device was equipped with basic electrodes for use in electrochemical studies as well as electrolysis experiments, a heating structure to enable temperature control within the observational region of the membrane, as well

as a novel flow control feature to separate and introduce liquid into one or both of the chambers on the device. The nanochannel was improved with a heating electrode structure, and possibilities for the incorporation of flow capabilities were also discussed. A brief summary of the various device and capabilities tested and achieved is shown in Table 9. In the next chapter, the use of the functionalities developed here for a range of scientific studies will be discussed for the purposes of providing examples of the applicability of liquid cell *in situ* TEM experimentation.

	Parameter	**Variations/Value**
Electrodes	Location	On-membrane, behind inlets
	Shape	Sharp, round, wide
	Devices tested	9
	Achieved in nanochannel	Prototype fabricated
Heater	Resistance (Ω)	20-1000
	Insulation	None, 100 nm SiO_2
	Temperature range (ºC)	20-80(+)
	Response time (s)	<4
	Devices tested	>20
	Achieved in nanochannel	Yes, no relevant sample test
Flow	Hydrophobic patch width (μm)	50, 100
	Devices tested	>20
	Achieved in nanochannel	No

Table 9: MEMS component variations and capabilities

Chapter 4: Scientific Demonstrations and Applications

The active sample interaction techniques described in Chapter 3 represent a step forward in terms of making the advanced experimentation capabilities achievable through the use of specialized TEM holders accessible to those without such equipment. By lowering the barrier to entry for *in situ* experimentation with liquid-phase TEM observation, these techniques can be brought to bear on new scientific challenges and provide insight into systems previously incompatible with TEM in general and liquid-phase TEM specifically. In this chapter, three particular examples of scientifically significant biochemical systems will be introduced, and the ongoing work to analyze them using the liquid cell techniques detailed in this report will be described.

4.1. Sample Investigation Strategy

To investigate a new sample or system using the devices that have been developed as a part of this research, a general experimental strategy was implemented in order to determine both the observability of the sample and the viability of that observation in both nanochannel and two-chip devices. When presented with a potential new sample to be investigated, the nanochannel was first used to verify that the sample was capable of generating a sufficient TEM contrast so as to be resolvable in the STEM setup. With a smaller liquid column and thinner membranes as compared to the two-chip devices used here, the nanochannel devices are capable of achieving somewhat higher resolutions and sample contrast. The nanochannel, therefore, represents the best potential imaging quality that can be achieved with the devices developed in this study and as such was used primarily for this type of initial sample investigation.

If sample observability could be established using the nanochannel, the sample could then be loaded into any particular two-chip device to verify that the marginal loss of resolution was insignificant enough to enable proper particle visibility in the two-chip liquid cell. If two-chip observation was determined to be feasible, the sample could then be tested using the MEMS components integrated onto the device that correspond to the activity desired in the experimental system.

Due to the narrower geometry of the nanochannel, there are cases where samples can be visualized in two-chip structure and not the nanochannel. As discussed in Section 2.3.2, the narrow gap between the upper and lower membranes of the nanochannel, as well as the two-chip device to a lesser degree, can sometimes serve to filter out particles dispersed in a sample fluid that would otherwise be visible. In such situations, while the nanochannel should theoretically be capable of resolving the particles in question, in practical terms those particles are filtered out and prevented from reaching the observable region of the device. The two-chip device, with its larger membrane gap as defined by the thickness of the spacer layer, fares better with these samples, and the "hybrid" device as described in Section 3.4.1 is specifically designed to mitigate this issue. As such the two-chip device can potentially still be viable for sample observation even if initial tests with the nanochannel show no observable particles.

Using the overall strategy discussed here as summarized below in Figure 4.1, samples were tested first for their TEM visibility and compatibility before moving on to more in-depth TEM experiments. In the rest of this section, three distinct scientific samples are introduced and their investigation using the liquid cell devices developed as a part of this study is detailed.

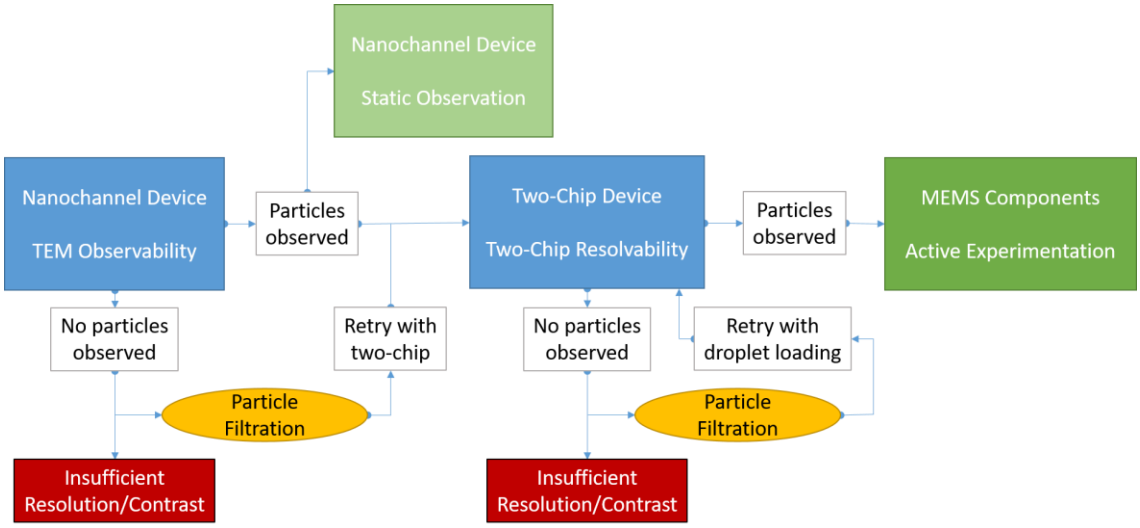

Figure 4.1: Sample observability verification strategic flow. The use of the active MEMS components of the two-chip device on specimens is the ultimate goal of the study, but static observation of samples using the relatively high-resolution nanochannel is also beneficial.

4.2. Silver Nanoparticles, Calix[n]arenes, and Proteins

Due to their high density, high atomic weight, and varied applications, metallic nanoparticles are a very common and versatile target for TEM studies. With properties arising from their nanometer-scaled dimensions, metallic nanoparticles have been studied for use in drug-delivery, enzyme interaction, material synthesis, and beyond. In this section, the use of silver nanoparticles (AgNP) in conjunction with synthetic molecules known as calixarenes as a means of interacting with biologically relevant proteins is explored.

4.2.1. Calix[n]arenes as Synthetic Biomolecules

Calix[n]arenes are a class of chemical structure that has attracted the attention of researchers due to their extensive customizability [97] and capacity for enzymatic and ionic interactions [98] [99]. In this study, the interaction of *para*-suphonato-calix[8]arene

with proteins associated with the formation of clotting tissue is explored using the nanochannel liquid cell device.

Calix[n]arenes in general and calix[8]arene specifically exhibit the ability to interfere with thrombosis, or the formation of biological aggregates or clots through the activation of various other specific anti-thrombotic biomolecules [100]. The presence of certain calix[n]arenes can delay the formation of polymer-like structures that contribute to the clotting cascade in the body [101]. In this experiment, silver nanoparticles (AgNP) coated with *para*-sulphonato-calix[8]arene (sc8) are mixed with a clotting protein, and the duration and degree of subsequent aggregation is observed.

4.2.2. Direct Observation of Protein-Induced Aggregation

First, *para*-sulphonato-calix[8]arene-coated AgNP were observed directly in solution using the static nanochannel structure to establish a baseline for the aggregation properties of the system. Very few aggregates could be found, with the largest measuring only around 40 nm in diameter as seen in Figure 4.2.

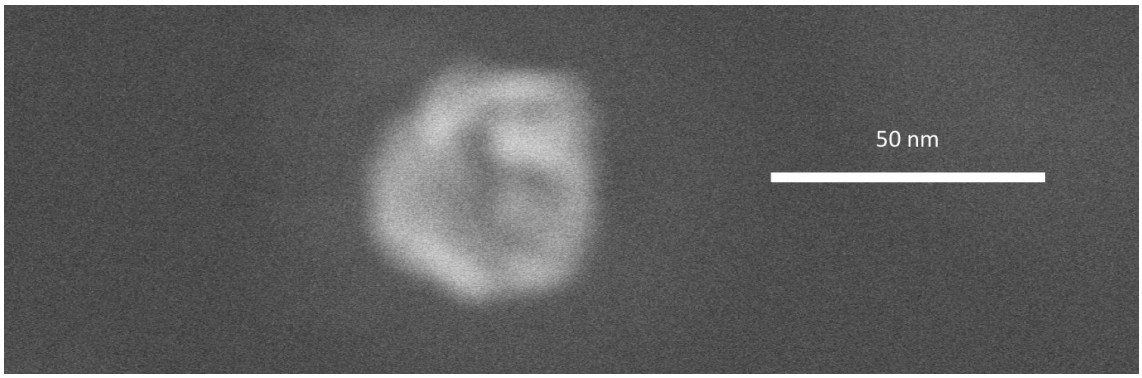

Figure 4.2: Largest aggregate observed during bare Ag/sc8 imaging

Next, the AgNP/sc8 solution was mixed with the thrombosis protein and loaded into the nanochannel for observation. Figure 4.3 shows the progression of aggregate growth for this system starting at 1.75 hours after initial mixing of the sample.

After 1 hour and 45 minutes of incubation, the cluster size of AgNP/sc8+ protein particles in the solution was quite similar to that of the pure AgNP/sc8 suspension at around 40-50 nm per visible cluster. However, at 1 hour and 50 minutes after mixing, larger aggregates began to form, tripling in size over the course of 10 minutes and proceeding to form large fiber-like structures that collected more particles as they drifted about the solution. Cluster size seemed to saturate at around 700 nm in length and 100 nm in width, with additional particles being subsumed and increasing the apparent density of the cluster rather than the overall size.

As stated above, it is known that this system of *para*-sulphonato-calix[8]arene-coated AgNP will undergo aggregation when exposed to the particular protein used in this experiment. The characteristic aggregation time for this system has previously been demonstrated to be on the scale of hours which correlated with the observed behavior. Additionally, the specific formation of intermediate crescent-shaped clusters and large-scale drifting mechanism for aggregate growth observed here has not yet been verified, and could not otherwise be identified without the use of liquid-phase TEM investigation.

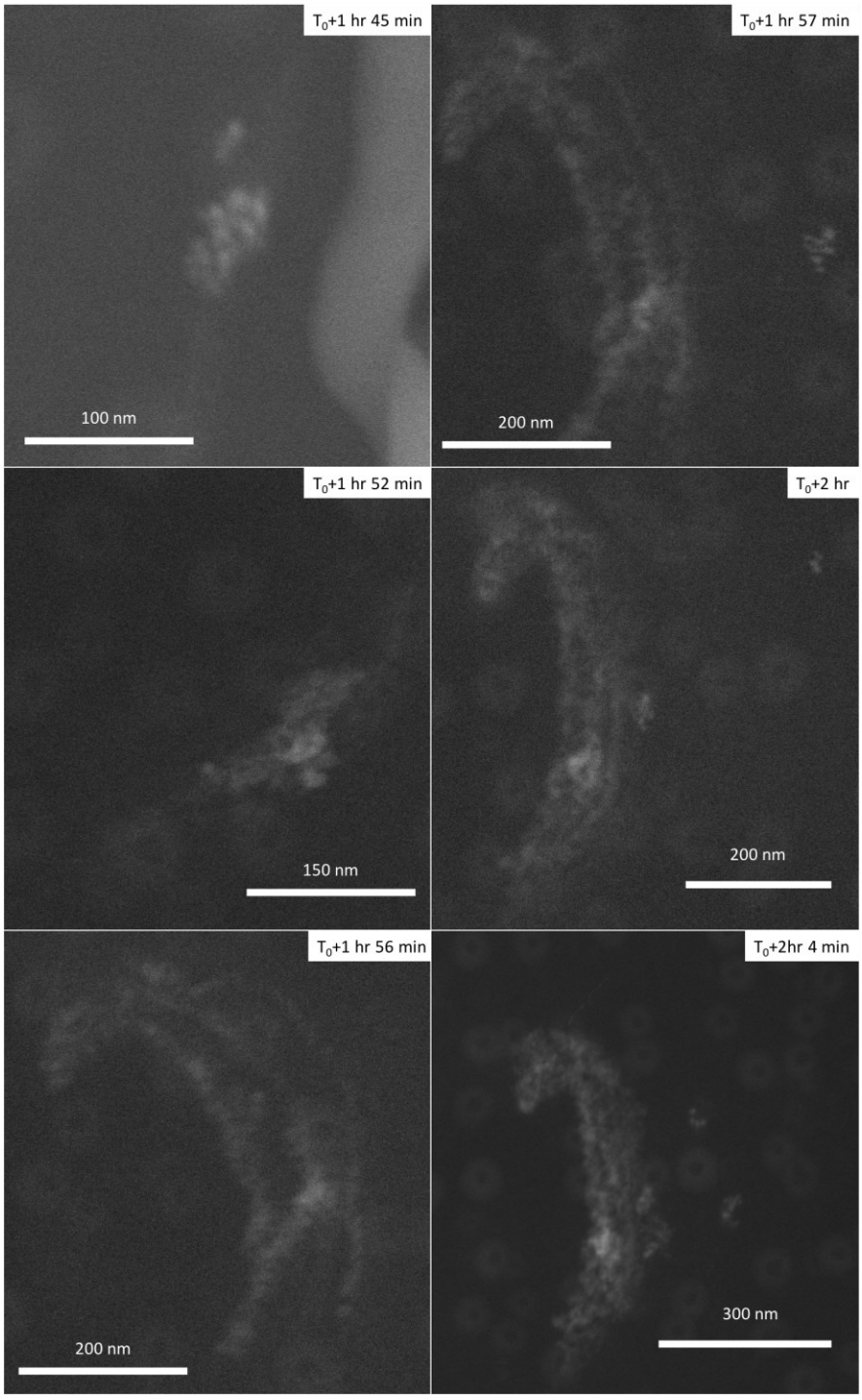

Figure 4.3: Rapid growth of characteristic cluster size after 1.5 h incubation of sc8 and thrombosis protein.

4.2.3. Flow-Control for Improved Kinetic Analysis

This experiment represents a good first step for the investigation of this system, and the active sample interaction features that have been incorporated into the two-chip

liquid cell could serve to produce a more quantitative and informative analysis of the structure. In this work, the protein sample was mixed with the AgNP/sc8 solution before loading into the liquid cell, so while it is known that this system has relatively slow kinetics, there was no way to verify that no activity occurs at the first instant of mixing. Furthermore, there is no concentration gradient of the aggregating protein that can be used to quantify and identify threshold concentrations for triggering the clustering response. The use of flow control to introduce the protein solution to the AgNP/sc8 solution from only one end of the chamber could serve to achieve both of these objectives simultaneously, allowing the observation of the first moments of mixing as well as the development of a concentration gradient as the protein diffuses through the channel from end to end.

4.3. Zeolite Ion Exchange

Zeolite structures are lattice-based materials with nanometer-and-below sized pores that have many applications for use in applications involving, filtration, ion transport, and beyond. In these experiments, the use of zeolites as ionic contrasting agents in Magnetic Resonance Imaging (MRI) is investigated. The flow control of the two-chip device was used to immerse a zeolite structure in an ionic solution in an attempt to observe the uptake of heavier ionic constituents.

4.3.1. Zeolites for Drug Delivery and *in-vivo* Staining

The porous nature of zeolites makes them highly appropriate for the transport of materials within various media. The cage-like structure and surface activity can be used to selectively protect or exchange ions or molecules depending on the specific zeolite used. In this case, X-type faujasite zeolites immersed in a sodium ion solution will take

up the Na^+ ions and exhibit a baseline level of brightness in Z-contrast STEM imaging. The ability for faujasite structures to exchange Na^+ ions for Gd^{3+} ions is being investigated for use in supplying concentrations of gadolinium ions in tissue in order to increase the imaging contrast during MRI analysis [102] [103]. Due to the relative difference in atomic weight between sodium and gadolinium, Z-contrast STEM could potentially be able register the uptake of Gd^{3+} ions as an increase in brightness. Figure 4.4 shows a schematic representation of the zeolite structure replacing sodium with gadolinium ions.

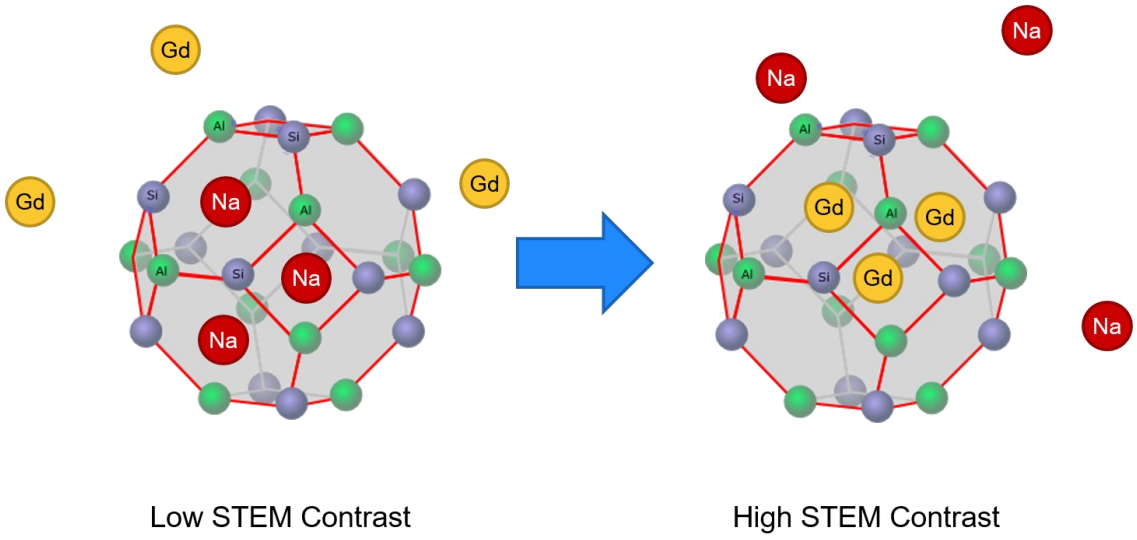

Figure 4.4: Schematic illustration of zeolite STEM contrast with internalized sodium ions (left) and gadolinium ions (right).

4.3.2. Dynamic Flow-Induced Ion Exchange

Because zeolite structures are very low-density and porous, they do not naturally generate a large contrast in TEM. As described in Section 2.3.1, while the nanochannel is capable of imaging collections of the faujasite zeolite structure, the two-chip device is really only capable of doing so in the dry state. However, with the advent of the flow control device, a dry faujasite structure can be deposited on the membrane for initial

baseline imaging with its original adsorbed ion. The zeolite can then be flooded with another ionic solution and incubated for a time to allow for any potential ion exchange. The flow can then be reversed to dry the sample and image it again to detect a change in the sample brightness, indicating ion exchange had taken place.

This experiment was performed by depositing Na^+-laden faujasite (FAU-X Na) onto the membrane of a flow-control two-chip device. The flow chamber was then loaded with a solution of $Gd(NO_3)_3$. The FAU-X Na was imaged in its original state after which the gadolinium nitrate solution was flowed onto it and allowed to incubate for 1.5 hours. The flow was then reversed to remove the liquid from the zeolite area and the sample was imaged again. The results of this experiment can be seen in Figure 4.5.

As can be seen, a distinct increase in sample brightness occurred, most likely explained by the uptake of heavy Gd^{3+} ions into the faujasite lattice replacing Na^+ as predicted by the literature. In the future, these results can be confirmed using EDX analysis of the same sample after drying, and the incorporation of flow control capabilities into the nanochannel liquid cell would allow for the direct monitoring of the ion exchange in real time in the liquid state.

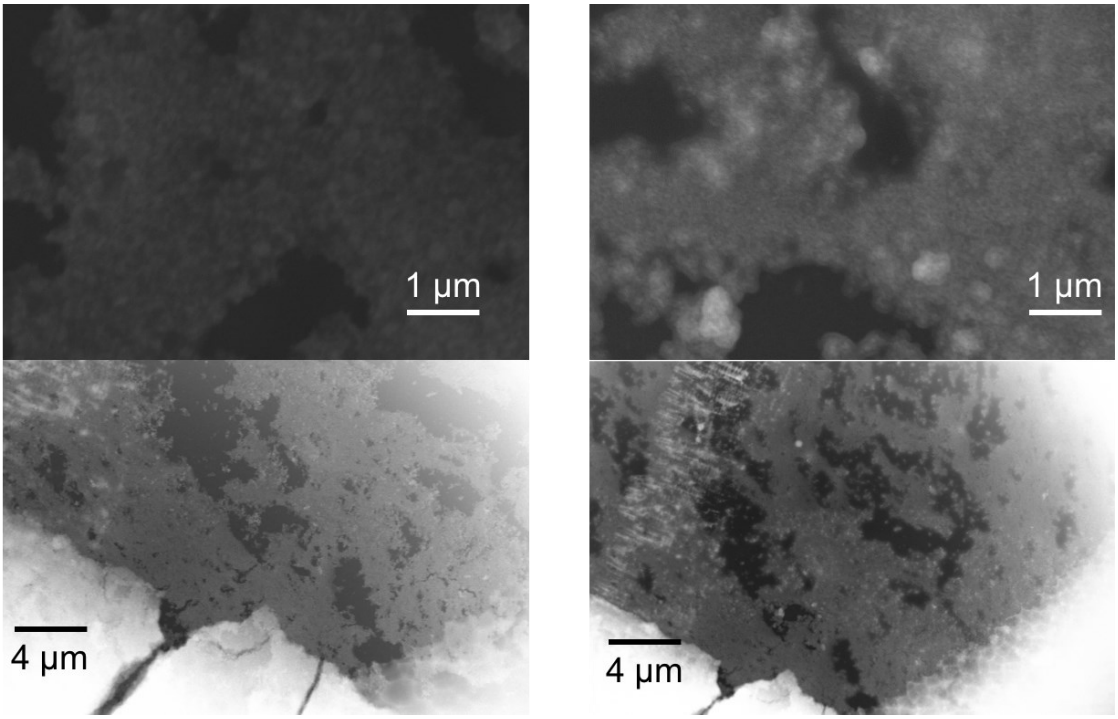

Figure 4.5: Dry FAU-X Na before gadolinium nitrate incubation (left) and after 1.5 hours (right)

4.4. DNA-Linked Gold Nanoparticles

As discussed previously, metallic nanoparticles are attractive for study in TEM systems due to their large contrast and flexible surface chemistry. Gold nanoparticles are of particular interest due to their unique properties outside of TEM, including exhibiting Surface Plasmon Resonance (SPR) which gives colloidal gold its characteristic color based on the size and spacing of the individual nanoparticles. One unique application of gold nanoparticles (AuNP) is their functionalization with strands of DNA. By coating the surface of AuNPs with specific DNA sequences, the selective hybridization of DNA strands can be used to manipulate the spacing AuNP, and thereby change the color absorbance of the solution. Such techniques have been used to develop novel biological assays to detect DNA mutations without the use of specialized fluorescent assays [104] as well as a new means of generating directed crystalline structures [105]. The directed aggregation of DNA can be controlled and reversed by manipulating both the temperature

of the solution as well as the concentration of complementary DNA. As such, the use of the temperature-control liquid cell to observe DNA/AuNP hybridization events as well as the flow-control device to introduce linker solutions to un-aggregated DNA/AuNPs could yield new insights into the functionality of this unique biochemical system.

4.4.1. Temperature-Reversible Hybridization

When elevated above a certain threshold temperature usually below 80º C, the ambient thermal energy is sufficient to break the approximately 0.5 eV bond per base pair and double stranded DNA separates into individual strands. However, the same DNA will recombine or "hybridize" with complementary DNA when the temperature is reduced below the threshold. This reversible separation has unique consequences when combined with the properties of colloidal gold nanoparticles. Because the SPR of AuNP solutions is very dependent on the inter-particle spacing of the colloid, complementary DNA strands can be used to directly control that particle spacing when AuNP have been functionalized with DNA. Figure 4.6 illustrates this concept schematically. At the macro-scale, this transition manifests itself as a change in color, but at the nanoscale, the inter-particle spacing is being changed, and this can theoretically be observed directly in real time using liquid-phase TEM techniques.

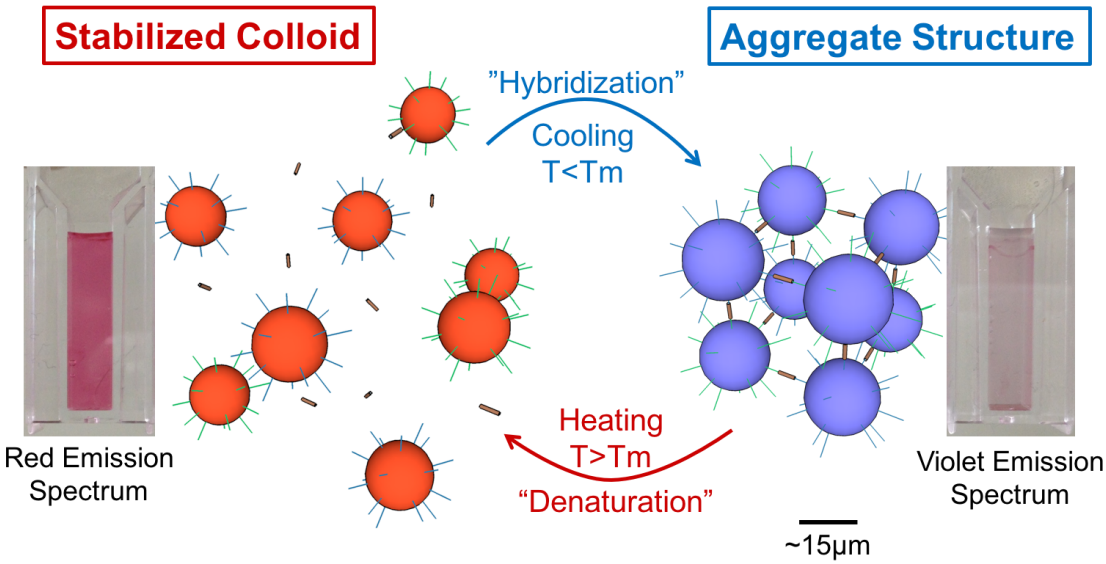

Figure 4.6: Schematic representation of the reversibility of DNA-induced gold nanoparticle aggregation. DNA-functionalized gold nanoparticles will become tightly packed when complementary linker DNA (brown rods) binds the particles together, resulting in a colorimetric shift. If the solution is heated past a threshold temperature, the process can be reversed *ad infinitum*.

4.4.2. Heating of DNA/AuNP Aggregates

In order to attempt to directly view the dynamism of DNA/AuNP solutions as driven by temperature, suspension of 50 nm diameter gold nanoparticles was prepared with a surface treatment of complementary DNA. In the presence of a solution of linker DNA, the suspension undergoes a color change, indicating the aggregation of AuNP as directed by DNA has occurred. This sample was loaded into a heater-equipped two-chip liquid cell and observed in TEM. Once a cluster of gold nanoparticles was found, the temperature of the cell was raised from room temperature up to 81.6º C, 20º C beyond the transition temperature for this DNA/AuNP solution, over the course of four minutes. In macroscale experiments, this is more than enough time for even microliter volumes of solution to begin to shift color. The results of this particular experiment are shown in Figure 4.7.

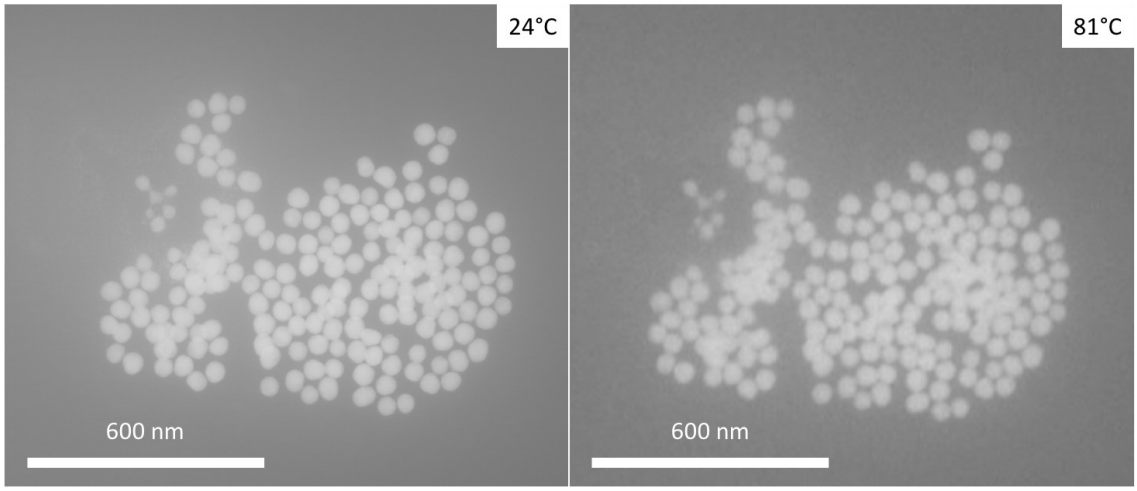

Figure 4.7: Heating of DNA-linked gold nanoparticles. Almost no motion is observed, likely due to membrane stiction.

As can be seen, despite the elevated temperature, little more than a slight shift of the particles was observed. This is most likely due to the membranes of this particular liquid cell sticking to each other upon loading this sample, and essentially trapping larger aggregates in place on the membrane surface, preventing their normal motion in an open fluid. Effectively this would mean that even if the DNA-DNA bonds undergo dehybridization at elevated temperature as expected, surface stiction can serve to inhibit the normal Brownian motion that would cause the nanoparticles to physically separate. Subsequent experiments with more recent versions of the liquid cell with a more stable device membrane will help to ensure that particles have enough room to move about. Additionally, given that these 50 nm particles are much larger than the imaging resolution of the LCTEM setup, future experiments can be performed using DNA-linked 15 nm or 5 nm gold nanoparticles whose aggregates would potentially be less likely to stick to the membrane surface and become immobilized. In this way the real-time mechanism for the reversible formation of DNA-induced crystallization can be explored.

4.4.3. Linker-Flow Aggregation

In addition to reversing aggregation by heating the sample, DNA/AuNP systems could be triggered to aggregate dynamically by introducing a solution of linker DNA to a solution of particles without complementary DNA strands. This way the initial state of the system is a stable colloid, and the gradual aggregation of the solution as the linker DNA spreads through the chamber could potentially be observed. With the development of the flow control liquid cell, this experiment is now possible.

4.5. Summary

In this chapter, three preliminary scientific experiments were discussed to demonstrate the ability of the liquid cell devices to both image relevant samples as well as meaningfully interact with them. Each experiment represents a first step proof-of concept, and with the development of active MEMS liquid cells in this report, more advanced experimentation can be performed at larger scales to achieve scientifically and statistically significant quantitative data regarding the reaction kinetics of thrombosis and clotting, the transport and exchange of various aqueous ions in zeolite structures, as well as the nanoscale dynamics involved with the reversible hybridization of DNA-linked gold nanoparticle structures.

Chapter 5: Summary, Perspectives, and Conclusions

In this chapter the achievements of this study are outlined as well as the limitations involved with the devices developed here and liquid-phase TEM in general. Finally, prospective experiments to be carried out in the future if this research continues to be pursued are proposed.

5.1. Primary Achievements and Novelty

At the start of this study, the two-chip liquid cell was relatively unreliable both in terms of fabrication and operation, and by the end not only are the basic liquid cell structures functioning effectively, but true sample interactivity has also been achieved in the form of electrical biasing, heating, and flow control all using only a generic electrical TEM holder without any sealing or flow components.

5.1.1. Development of Adaptable Two-Chip Platform

The further optimization of the two-chip liquid cell structure allowed it to be used as a prototyping test bed for the development of new liquid-phase experimental techniques. The stabilization of the membrane release process, the spacer layer, and overall device fabrication and handling has served to both increase device yield and functionality. The fabrication of previous versions of the device was somewhat unreliable and inhibited the consistent performance necessary for the development of more advanced and scientifically relevant functionality. The basic fabrication improvements achieved in this study resulted in cleaner devices with more repeatable and reliable performance which in turn enabled the development of more advanced sample interaction capabilities in the standalone liquid cell device.

While the changes made to the liquid cell fabrication process improved the durability and useability of the devices, this was not done at the cost of their performance as an observational tool for TEM. Specifically, as discussed in Section 2.1.1, while the resolving capabilities of the TEM system used are dependent on the equipment available and the particle/medium contrast is determined by the sample being observed, the achievable resolution for a particular liquid cell device is primarily dependent on the thickness of the encapsulated fluid layer and the thickness and atomic density of the encapsulating membrane. The latest active two-chip liquid cell device used in this study features 50-nm-thick silicon nitride membranes with a fluid thickness defined by the spacer pattern of approximately 1 μm which are both typical values for active liquid cell devices. While the primary goal of this study was the achievement of novel functionality, improvements in TEM resolution can also be pursued in subsequent devices through the use of thinner membrane and spacer. While thinning the membrane should have minimal effect on device functionality, the use of a thinner spacer will exacerbate the filtration issue discussed in Section 2.3.2 and increase reliance on loading samples via droplets deposited directly on the membrane rather than through device inlets. As long as proper consideration is given to the particle size of the sample to be investigated, however, both of these avenues represent viable means toward improving the resolution of the device.

5.1.2. Integration of MEMS-Based Active Functionality

Whereas previous devices were only capable of reliably applying a biasing voltage to the liquid cell, now a single device is capable of biasing, heating, and flowing of sample liquids, all without the use of a customized TEM holder. Previous devices have demonstrated biasing and heating capabilities on fully-sealed chips as well as flow control using specialized LCTEM holders and auxiliary equipment, but to-date no other devices

could be found that have achieved directed fluid motion in a standalone liquid cell device without the use of external pumps and fluid interconnects. Combining all of these capabilities onto a single device that can be used with a generic TEM holder with simple electrical interconnects represents a step towards making sample interaction during LCTEM observation an investigative technique with less of an initial barrier to entry. In this way, making liquid-phase TEM experimentation more accessible may help make the technique more appealing to general researchers who could benefit from its capabilities and advantages but might have otherwise shied away from the practice due to its current cost and somewhat niche nature.

5.1.3. Demonstration of *in situ* Experimentation

In addition to the development and characterization of standalone active liquid cells, the potential utility of the devices was also demonstrated with initial proof-of concept experiments. As discussed throughout Chapter 4, various samples with biological relevance were investigated using the devices developed here to explore their activity and reactivity at the nanoscale. While comprehensive, statistical studies have not yet been conducted, the initial experiments to observe protein-induced silver nanoparticle aggregation as well as ion-exchange within zeolite nanostructures both yielded promising results that merit further investigation. As discussed in Section 2.3.5, a researcher with no MEMS experience is capable of taking the fabricated liquid cell chips, aligning and sealing them with the help of a simple chuck, filling the device via its inlets, and loading it to be viewed in TEM all without the use of a specialized TEM holder or other auxiliary equipment. Now that the development of the device capabilities is more or less complete, subsequent research can focus fully on the use of the devices as experimental tools to perform thorough scientific investigations of a wide variety of relevant samples.

5.1.4. Primary Novelty

Within the greater scientific and engineering context, the most significant novel capability demonstrated here is the ability to transfer a sample liquid from one chamber to another during STEM observation without the use of external pumps or fluidic interconnects. The ability to immerse a specimen in a given liquid during TEM observation can be beneficial when studying various biological and chemical systems. As discussed earlier, previous commercial and custom devices rely on specialized external plumbing to flow fluid through a dedicated liquid cell TEM holder to the device which limits their accessibility to researchers who are hesitant to invest in such specialized equipment. In this way, achieving comparable functionality without the use of a dedicated holder or other auxiliary equipment represents an important step forward in making active LCTEM experimentation available to researchers who do not already have expertise and access to the technique.

The mechanism through which on-chip flow initiation has been achieved has further potential benefits beyond its ability to be used without a specialized holder. As discussed previously commercially available flow-capable LCTEM holders usually suffer from a lack of direct fluid flow over the observable membrane due to designs that allow much of the flow to bypass the membrane and flow around the chips within the TEM holder. This can lead to analytical complexity as the resulting concentration of reactants during experimentation depends on a combination of both driven flow and diffusion [76] [69]. The design introduced in this study injects a contained volume of fluid directly into the downstream chamber, meaning the resulting concentration will be the same as that of the initially loaded sample. In an as-yet undemonstrated experiment involving the merging of liquids in two adjacent chambers, once the two liquid fronts

meet mixing is achieved solely through the diffusion between two confined volumes yielding a resulting reactant concentration over time that is much more easily predictable.

Finally, while devices have been fabricated but not yet demonstrated in a scientifically novel experiment, the development of a single sealed device capable of electrical biasing, temperature control, and flow initiation using only electrical interconnects on a generic TEM holder has also never before been achieved. As with the flow initiation device, while these individual functions can be achieved with specialized commercial TEM holders and chips, integrating all these functions onto a single chip that can be used with a simple TEM holder can serve to democratize the technique of active LCTEM experimentation.

5.2. Limitations and Constraints

While liquid phase TEM in general and these devices specifically have many advantages, there are a variety of drawbacks and limitations that must be considered when applying these techniques. These can arise from the TEM system, the sample being viewed, and from the device itself.

5.2.1. Beam-Induced Effects

One of the most common concerns raised with the use of the TEM investigation of liquids is the effect of the electron beam on the liquid itself. Previous studies have shown that for typical conditions for liquid-phase TEM are only capable of locally heating the sample by a few degrees; not enough to significantly interfere with most observation targets [106] [107]. The main effect is the radiolytic splitting of water into hydrogenated and oxygenated ions that can locally cause pH gradients in the solution. Care must be taken when observing systems that are very sensitive to those particular ionic species.

Beam effects for samples viewed in liquid cells can largely be broken down into "electronic" effects and thermal effects [108] [109]. Electronic effects here refer to the electrical and chemical consequences of incident electron radiation while thermal effects, while also caused by the incident electron, are largely independent of the particle charge. The most significant effect that must be considered for liquid cell observation is the generation of new chemical species within the observed liquid due to radiolysis of the medium from the ionizing electron beam [107]. Electrons accelerated at 200kV serve to react with liquid water through the formation of ionized water (H_2O^+), excited water molecules, and free electrons within the medium. These resulting particles break down within femtoseconds, reacting with the surrounding water and each other. The ultimate result of this cascade is a distribution of 35% aqueous electrons, 35% hydroxide radicals ($^{\bullet}OH$), 10% H_2O_2 8% hydrogen radicals $H^{\bullet}$, 6% H_2, and hydroperoxyl radicals 1% $HO_2^{\bullet}$ at a rate of approximately 0.7 μmol per input Joule and a slight reduction of the local pH [110] [70]. These species, especially the electron and various radicals, are quite reactive and must be accounted for when observing chemically sensitive solutions at high electron dosages. Many studies have used the incident electron beam to generate reactive species which can cause the precipitation of metallic and inorganic nanoparticles out of liquid precursor solutions [30] [44] [61] [52] [73] [111] [112] [113] [114]. This effect was observed when visualizing highly concentrated solutions of $Gd(NO_3)_3$ in the nanochannel device. Leaving the electron beam exposing a region of the channel for several minutes resulted in an appreciable growth of Gd nanoparticles, represented by a brightening and growing of particles initially visible in the region. The results of this experiment can be seen in Figure 5.1. In order to mitigate this effect when observing solutions that can be potentially affected by the species resulting from the radiolysis of water, overall exposure

dose should be kept limited by only imaging the sample when necessary and avoiding extended high-magnification imaging of the same location. Of course, the chemical effect of radiolysis can be accounted for in quantitative analysis of observed chemical species, and the sample solution itself can be augmented with scavenging species that reduce the overall amount of reactive radiolytic present in the sample [70].

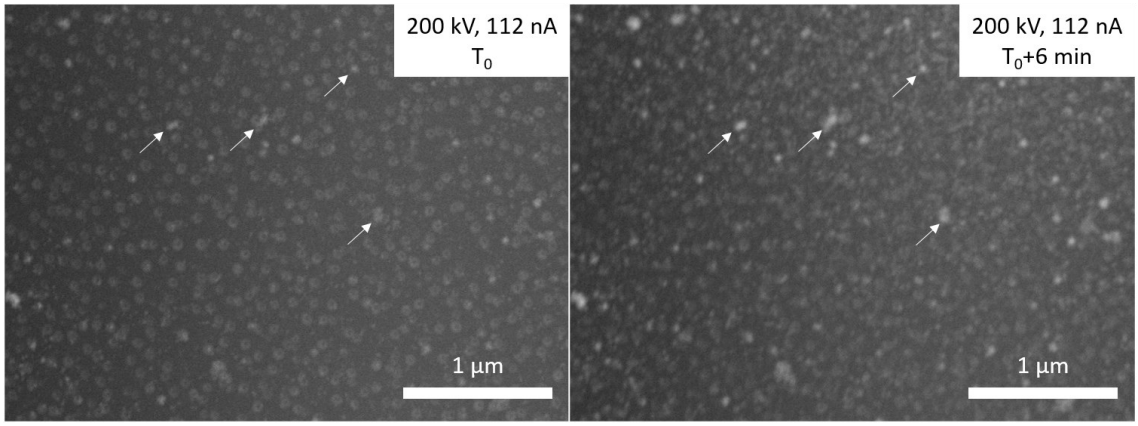

Figure 5.1: Beam-driven growth of Gd nanoparticles from highly concentrated $Gd(NO_3)_3$ solution. Arrows indicate certain particles present in the initial image (left) that grew appreciably in both size and contrast after 6 minutes of exposure (right).

One other electronic effect of the incident beam is its potential to alter the surface ζ potential of particles due to a local drop in solution pH [107]. Many studies have demonstrated beam-induced nanoparticle aggregation, and while the mechanism for this phenomenon is not fully clear, one potential explanation is a reduction of individual particle ζ potential due to extended high-magnification imaging beam exposure [115].

Another significant beam effect is heating caused by incident electron bombardment. For very thin dry samples, TEM heating can be a quite powerful, and some studies have used the beam at very high doses and magnifications to melt metallic particles [116] [117]. However, in liquid cells, due to the presence of a surrounding structure as well as the fluid medium spreading the energy of the electron beam along its thickness, under normal observational conditions even at high magnification, the local

beam-induced heating is estimated to never exceed a few degrees Celsius [106]. The most significant consequence of this phenomenon during normal liquid cell operation is the induction of increased particle motion at high magnification due to highly-localized heating of particles relative to the surrounding solution [118]. To mitigate this issue, observation of small, mobile nanoparticles should be done at relatively low magnification where any localized heating effects, however small, are distributed evenly over a wide area and therefore do not significantly alter any local particle-particle interactions.

5.2.2. Imaging Time

Another limitation of TEM and microscopy techniques in general is the imaging time. In STEM, the electron beam must raster over the entire viewing area every time the image is updated, with the system used in this study capable of achieving up to 30 frames per second. This means that if the observational target moves or acts on timescales below 33 milliseconds, it would be impossible to observe clearly with this setup. Given that LCTEM enables the observation of liquid-phase samples which are by nature dynamic, a slow imaging time can potentially limit the detailed information that could be gleaned from a particular specimen. As such, limiting beam-induced particle motion through the use of lower magnifications and electron doses can be advantageous to mitigate the effects of a limited framerate. For specimens featuring rapidly-evolving activity of interest, using "spotlight-style" conventional TEM illumination with a high electron dose in conjunction with a high-speed TEM detector can achieve higher framerate observation [72]. When micro to femtosecond time resolutions are necessary, a technique known as Dynamic Transmission Electron Microscopy (DTEM) can be applied in which short electron pulses are generated through photoemission triggered by a laser pulse hitting a

metallic cathode [119] [120]. DTEM with its snapshot-like imaging duration, has been used to image rapid laser-induced activity within liquid cells [52] [121].

5.2.3. Analyte Contrast

STEM Z-contrast imaging tends to provide the best imaging results in liquid cell microscopy due to the generation of contrast based on the atomic number of the material being viewed rather than on the material thickness and density alone. However, this means that it can be difficult to resolve similarly-weighted elements using this technique. This can be a significant challenge when trying to view aqueous biological samples, as carbon-based materials tend to exhibit very similar contrast properties as the oxygen-based medium of water in which they reside. In these cases, labeling with nanoparticles or other high-contrast materials is appropriate and often necessary.

5.2.4. Sample Size

As discussed in Chapter 2, there is a direct tradeoff between the thickness of the fluid medium being observed in STEM and the smallest achievable resolution. Nanoparticles that are excessively small may not be observable in devices with larger fluid columns, so care must be taken to choose the appropriate observational device when attempting to view a new sample. Similarly, some samples may simply be too big to fit within the liquid cell structure or even the TEM holder itself.

5.3. Further Experimentation and Development

In this study, the main objective was the development of a self-contained liquid cell structure capable of interacting with the enclosed sample in multiple ways. Having achieved that, the door is now open to the proper application of these techniques to thoroughly investigate scientific phenomena. Of course, that is not to say that the devices

developed here cannot be improved further to achieve better performance or additional functionalities. Here a few next research steps are described if the devices introduced in this report are to continue development.

5.3.1. Refinement of Membrane and Chamber Design

Currently one of the main challenges associated with using the liquid cell devices is their tendency to filter out particles of interest as discussed in Section 2.3.2. This can be mitigated by loading the sample directly on the membrane and sandwiching the devices together with the liquid already present, but doing so is often messy and inhibits the use of precise flow control features. New membrane and chamber designs that can funnel particles to the membrane surface while maintaining proper alignment and liquid confinement would be necessary to achieve a proper balance between functionality and sample compatibility.

5.3.2. Nanochannel Development and Coupled Devices

The main limitation to the development of the nanochannel device is its stringent fabrication requirements that restrict the ability to easily incorporate active components on the device. This could potentially be mitigated by adopting a coupled device design in which the nanochannel structure is bonded to another micromachined silicon wafer that has been specifically designed to include devices for sample interactivity without needing to encapsulate the fluid. Essentially, the job of encapsulation could be performed by one half of the device while the activity would be housed on the other, potentially increasing the ability to customize the nanochannel structure.

5.3.3. Active Liquid Cell Experiments

As this research focused on the development standalone liquid cells with sample interaction capabilities, the natural next step is the use of these devices for the investigation of scientifically relevant samples. Various initial proof of concept tests have already been performed including those outlined in Chapter 4, and pursuing those studies further would likely yield interesting results. The protein-driven aggregation introduced in Section 4.2 could be studied in more detail using the active MEMS features of the two-chip liquid cell to control the reaction temperature and to initiate aggregation through the *in situ* injection of the protein solution during observation rather than doing so beforehand. Similarly, if the resolution of the two-chip device were improved by thinning the spacer layer and encapsulating membranes, the observation of zeolite structures discussed in Section 4.3 could be performed in both the dry and liquid state. This would allow for real-time observation of the ion exchange process as it occurs in solution. Furthermore, the development of the flow-initiation MEMS component could help to mitigate the aggregate-membrane adhesion issues described in Section 4.4 for the observation of DNA-linked gold nanoparticles. If AuNP are initially loaded in the observation chamber in the non-aggregated stable state, they should remain more mobile within the encapsulated structure. If the electrolytic pump is then used to introduce a solution of the linker DNA to the unaggregated AuNP, it should be possible to observe the DNA-driven aggregation of the initially stabilized nanoparticles. Furthermore, the onboard heater could then be used to attempt to observe the reversal of that aggregation at elevated temperatures.

In addition to the systems initially explored here, the two-chip liquid cell developed in this research represents an adaptable experimental platform that can

potentially be used to explore a variety of samples and specimens including those that have been used in previous liquid cell studies. Nanoparticle synthesis, biological interactions, material degradation and more can all potentially be studied as driven by the electron beam, direct electrical biasing, chemical concentrations, and temperature manipulation. In particular, the use of a patterned hydrophobic layer to pin a liquid front in repeatable location within the observable region of the liquid cell could be useful in the study of activity and reactivity at liquid-gas or even solid-liquid-gas interfaces. Similar to ETEM systems that have been used to study chemical vapor deposition using a specialized TEM differential pumping setup, the two-chip device developed in this research is capable of preserving an environment within the TEM chamber in which solids, liquids, and gasses can interact. The ability to create such an environment using only a pair of microchips and a generic TEM holder rather than a dedicated environmental TEM setup is surely a step toward the increased accessibility for the experimental technique.

5.4. Conclusions

In this report, the refinement and development of two existing liquid cell devices was discussed. From the optimization of the basic liquid observational capabilities to the integration of sample interactivity, this research has focused on the engineering challenge of designing standalone liquid cell devices that feature the functionality of more complex and specialized systems. The devices developed here have the potential to help make liquid-phase TEM experimentation a more ubiquitous and accessible investigative technique that is available to anyone interested in observing dynamic phenomena at the nanoscale.

Acknowledgements

I would like to acknowledge the support given to me by both Professor Fujita, who started me on this project during my time as a Master's student, and Professor Toshiyoshi who accepted me into his lab and allowed me to continue my work. The support and guidance they have provided has been invaluable to me, and the patience they have afforded me despite my many failings has allowed me to continue to try to live up to the atmosphere of excellence they engender.

I would also like to thank my direct collaborators on this liquid cell project, Matthieu Denoual and Edin Sarajlic, for offering their time and expertise. I truly value the dedication enthusiasm with which you approach your work.

To everyone in the Fujita and Toshiyoshi laboratories and environs with whom I have worked and been supported by I offer my humblest appreciation. I hope that we can continue to work together in some form in the future.

Publications and Presentations

(Conference) Vivek Menon, Laurent Jalabert, Momoko Kumemura and Hiroyuki Fujita, "Toward Real Time Visualization of DNA and Gold Nanoparticle Hybridization Events using Heater-Integrated Liquid Cells in TEM," presented at 32nd Annual Sensor Symposium on Sensors, Micromachines, and Applied Systems, Niigata, Japan, 2015, p. 29pm3-PS-123.

(Conference) Matthieu Denoual, Vivek Menon, Takaaki Sato and Hiroyuki Fujita, "On-Chip Fluidic Actuation for TEM Liquid Cell" in Proceedings of the 21st International Conference on Miniaturized Systems for Chemistry and Life Sciences (MicroTAS 2017), Savannah, United States of America, 2017, pp. 1573-1574.

(Conference) Vivek Menon, Matthieu Denoual, Sato Takaaki and Hiroyuki Fujita, "Pressure-Driven Liquid Actuation for *in situ* TEM Observation of Fluid Mixing", presented at 34th Annual Sensor Symposium on Sensors, Micromachines, and Applied Systems, Hiroshima, Japan, 2017, p. 31pm3-PS-32.

(Journal) Vivek Menon, Matthieu Denoual, Hiroshi Toshiyoshi and Hiroyuki Fujita, "Self-contained on-chip fluid actuation for flow initiation in liquid cell transmission electron microscopy", *Japanese Journal of Applied Physics*, vol. 58, no. 9, p. 090909, 2019.

Related Work

(Journal) Matthieu Denoual, Vivek Menon, Takaaki Sato, Olivier de Sagazan, Anthony William Coleman and Hiroyuki Fujita, "Liquid cell with temperature control for in-situ TEM chemical studies", *Measurement Science and Technology*, vol. 30, no. 1, p. 017001, 2018.

Works Cited

[1] S. W. Hell and J. Wichmann, "Breaking the diffraction resolution limit by stimulated emission: stimulated-emission-depletion fluorescence microscopy," *Optics Letters,* vol. 19, no. 22, pp. 780-782, 1994.

[2] T. Müller, C. Schumann and A. Kraegeloh, "STED Microscopy and its Applications: New Insights into Cellular Processes on the Nanoscale," *ChemPhysChem,* vol. 13, no. 8, pp. 1986-2000, 2012.

[3] R. E. Thompson, D. R. Larson and W. W. Webb, "Precise Nanometer Localization Analysis for Individual Fluorescent Probes," *Biophysical Journal,* vol. 82, no. 5, pp. 2775-2783, 2002.

[4] E. Betzig, G. H. Patterson, R. Sougrat, O. W. Lindwasser, S. Olenych, J. S. Bonifacino, M. W. Davidson, J. Lippincott-Schwartz and H. F. Hess, "Imaging Intracellular Fluorescent Proteins at Nanometer Resolution," *Science,* vol. 313, no. 5793, pp. 1642-1645, 2006.

[5] G. Patterson, M. Davidson, S. Manley and J. L. Lippincott-Schwartz, "Superresolution Imaging using Single-Molecule Localization," *Annual Review of Physical Chemistry,* vol. 61, no. 1, pp. 345-367, 2010.

[6] M. Yamanaka, N. I. Smith and K. Fujita, "Introduction to super-resolution microscopy Masahito," *Microscopy,* vol. 63, no. 3, pp. 177-192, 2014.

[7] B. Turkowyd, D. Virant and U. Endesfelder, "From single molecules to life: microscopy at the nanoscale," *Analytical and Bioanalytical Chemistry,* vol. 408, no. 25, pp. 6885-6911, 2016.

[8] C. A. Combs and H. Shroff, "Fluorescence Microscopy: A Concise Guide to Current Imaging Methods," *Current Protocols in Neuroscience,* vol. 79, no. 1, pp. 2.1.1-2.1.25, 2017.

[9] R. F. Egerton, Physical Principles of Electron Microscopy, New York: Springer Science+Business Media, 2005.

[10] D. B. Williams and C. B. Carter, Transmission Electron Microscopy: A Textbook for Materials Science, New York: Springer Science+Business Media, 2009.

[11] M. De Graef, Introduction to Conventional Transmission Electron Microscopy, Cambridge: Cambridge University Press, 2003.

[12] N. Tanaka, Scanning Transmission Electron Microscopy of Nanomaterials: Basics of Imaging and Analysis, London: Imperial College Press, 2015.

[13] S. J. Pennycook and P. D. Nellist, Scanning Transmission Electron Microscopy: Imaging and Analysis, New York: Springer Science+Business Media, 2011.

[14] R. Erni, M. D. Rossel, C. Kisielowski and U. Dahmen, "Atomic-Resolution Imaging with a Sub-50-pm Electron Probe," *Physical Review Letters,* vol. 12, p. 096101, 2009.

[15] D. E. Jesson and S. J. Pennycook, "Incoherent Imaging of Crystals Using Thermally Scattered Electrons," *Proceedings: Mathematical and Physical Sciences,* vol. 449, no. 1936, pp. 273-293, 1955.

[16] T. W. Hansen, J. B. Wagner and R. E. Dunin-Borkowski, "Aberration corrected and monochromated environmental transmission electron microscopy: challenges and prospects for materials science," *Materials Science and Technology,* vol. 26, no. 11, pp. 1338-1344, 2010.

[17] J. B. Wagner, F. Cavalca, C. D. Damsgaard, L. D. L. Duchstein and T. W. Hansen, "Exploring the environmental transmission electron microscope," *Micron,* vol. 43, no. 11, pp. 1169-1175, 2012.

[18] T. W. Hansen and J. B. Wagner, "Catalysts under Controlled Atmospheres in the Transmission Electron Microscope," *ACS Catalysis,* vol. 4, no. 6, pp. 1673-1685, 2014.

[19] P. L. Hansen, J. B. Wagner, S. Helveg, J. R. Rostrup-Nielsen, B. S. Clausen and H. Topsøe, "Atom-Resolved Imaging of Dynamic Shape Changes in Supported Copper Nanocrystals," *Science,* vol. 295, no. 5562, pp. 2053-2055, 2002.

[20] J. B. Wagner, P. L. Hansen, A. M. Molenbroek, H. Topsøe, B. S. Clausen and S. Helveg, "In Situ Electron Energy Loss Spectroscopy Studies of Gas-Dependent Metal−Support Interactions in Cu/ZnO Catalysts," *The Journal of Physical Chemistry B,* vol. 107, no. 31, pp. 7753-7758, 2003.

[21] H. Yoshida, Y. Kuwauchi, J. R. Jinschek, K. Sun, S. Tanaka, M. Kohyama, S. Shimada, M. Haruta and S. Takeda, "Visualizing Gas Molecules Interacting with Supported Nanoparticulate Catalysts at Reaction Conditions," *Science,* vol. 335, no. 6066, pp. 317-319, 2012.

[22] T. W. Hansen, J. B. Wagner, P. L. Hansen, S. Dahl, H. Topsøe and C. J. H. Jacobsen, "Atomic-Resolution in Situ Transmission Electron Microscopy of a Promoter of a Heterogeneous Catalyst," *Science,* vol. 294, no. 5546, pp. 1508-1510, 2001.

[23] H. Yoshida, S. Takeda, T. Uchiyama, H. Kohno and Y. Homma, "Atomic-Scale In-situ Observation of Carbon Nanotube Growth from Solid State Iron Carbide Nanoparticles," *Nano Letters,* vol. 8, no. 7, pp. 2082-2086, 2008.

[24] S. Helveg, C. López-Cartes, J. Sehested, P. L. Hansen, B. S. Clausen, J. R. Rostrup-Nielsen, F. Abild-Pedersen and J. K. Nørskov, "Atomic-scale imaging of carbon nanofibre growth," *Nature,* vol. 427, no. 6973, pp. 426-429, 2004.

[25] A. D. Gamalski, J. Tersoff and E. A. Stach, "Atomic Resolution in Situ Imaging of a Double-Bilayer Multistep Growth Mode in Gallium Nitride Nanowires," *Nano Letters,* vol. 16, no. 4, pp. 2283-2288, 2016.

[26] D. Jacobsson, F. Panciera, J. Tersoff, M. C. Reuter, S. Lehmann, S. Hofmann, K. A. Dick and F. M. Ross, "Interface dynamics and crystal phase switching in GaAs nanowires," *Nature,* vol. 531, no. 7594, pp. 317-322, 2016.

[27] N. de Jonge, W. C. Bigelow and G. M. Veith, "Atmospheric Pressure Scanning Transmission Electron Microscopy," *Nano Letters,* vol. 10, no. 3, pp. 1028-1031, 2010.

[28] N. de Jonge and F. M. Ross, "Electron microscopy of specimens in liquid," *Nature Nanotechnology,* vol. 6, no. 11, pp. 695-704, 2011.

[29] J. M. Grogan and H. H. Bau, "The Nanoaquarium: A Platform for In Situ Transmission Electron Microscopy in Liquid Media," *Journal of Microelectromechanical Systems,* vol. 19, no. 4, pp. 885-894, 2010.

[30] J. M. Yuk, J. Park, P. Ercius, K. Kim, D. J. Hellebusch, M. F. Crommie, J. Y. Lee, A. Zettl and A. P. Alivisatos, "High-Resolution EM of Colloidal Nanocrystal Growth Using Graphene Liquid Cells," *Science,* vol. 336, no. 6077, pp. 61-64, 2012.

[31] J. M. Yuk, H. K. Seo, J. W. Choi and J. Y. Lee, "Anisotropic Lithiation Onset in Silicon Nanoparticle Anode Revealed by in Situ Graphene Liquid Cell Electron Microscopy," *ACS Nano,* vol. 8, no. 7, pp. 7478-7485, 2014.

[32] M. Textor and N. de Jonge, "Strategies for Preparing Graphene Liquid Cells for Transmission Electron Microscopy," *Nano Letters,* vol. 18, no. 6, pp. 3313-3321, 2018.

[33] L. Reimer and H. Kohl, Transmission Electron Microscopy: Physics of Image Formation, New York: Springer, 2008.

[34] N. de Jonge, D. B. Peckys, G. J. Kremers and D. W. Piston, "Electron microscopy of whole cells in liquid with nanometer resolution," *Proceedings of the National*

Academy of Sciences of the United States of America, vol. 106, no. 7, pp. 2159-2164, 2009.

[35] N. de Jonge, N. Poirier-Demers, H. Demers, D. B. Peckys and D. Drouin, "Nanometer-resolution electron microscopy through micrometers-thick water layers," *Ultramicroscopy,* vol. 110, no. 9, pp. 1114-1119, 2010.

[36] D. C. Joy and C. S. Joy, "Scanning electron microscope imaging in liquids – some data on electron interactions in water," *Journal of Microscopy,* vol. 221, no. 2, pp. 84-88, 2006.

[37] "Protochips Fusion," Protochips, [Online]. Available: https://www.protochips.com/products/fusion/. [Accessed 30 11 2018].

[38] "Hummingbird Scientific Furnace Heating," Hummingbird Scientific, [Online]. Available: http://hummingbirdscientific.com/products/bulk-sample-heating/. [Accessed 30 11 2018].

[39] "DENSsolutions Wildfire," DENSsolutions, [Online]. Available: https://denssolutions.com/products/wildfire/. [Accessed 30 11 2018].

[40] "Gatan TEM Specimen Holders," Gatan, [Online]. Available: http://www.gatan.com/products/tem-specimen-holders. [Accessed 30 11 2018].

[41] "Protochips Poseidon Select," Protochips, [Online]. Available: https://www.protochips.com/products/poseidon-select/. [Accessed 30 November 2018].

[42] "Hummingbird Scientific Liquid Flow," Hummingbird Scientific, [Online]. Available: http://hummingbirdscientific.com/products/liquid/. [Accessed 30 November 2018].

[43] M. J. Williamson, R. M. Tromp, P. M. Vereecken, R. Hull and F. M. Ross, "Dynamic microscopy of nanoscale cluster growth at the solid–liquid interface," *Nature Materials,* vol. 2, no. 8, pp. 532-536, 2003.

[44] H. Zheng, R. K. Smith, Y.-W. Jun, C. Kisielowski, U. Dahmen and A. P. Alivisatos, "Observation of Single Colloidal Platinum Nanocrystal Growth Trajectories," *Science,* vol. 325, no. 5932, pp. 1309-1312, 2009.

[45] A. J. Leenheer, J. P. Sullivan, M. J. Shaw and C. T. Harris, "A Sealed Liquid Cell for In Situ Transmission Electron Microscopy of Controlled Electrochemical Processes," *Journal of Microelectromechanical Systems,* vol. 24, no. 4, pp. 1061-1068, 2015.

[46] F. M. Ross, "Opportunities and challenges in liquid cell electron microscopy," *Science,* vol. 350, no. 6267, p. aaa9886, 2015.

[47] H.-G. Liao and H. Zheng, "Liquid Cell Transmission Electron Microscopy," *Annual Review of Physical Chemistry,* vol. 67, no. 1, pp. 719-747, 2016.

[48] N. de Jonge, L. Houben, R. E. Dunin-Borkowski and F. M. Ross, "Resolution and aberration correction in liquid cell transmission electron microscopy," *Nature Review Materials,* vol. 4, no. 1, pp. 61-78, 2019.

[49] S. Pu, C. Gong and A. W. Robertson, "Liquid cell transmission electron microscopy and its applications," *Royal Society Open Science,* vol. 7, no. 1, p. 191204, 2020.

[50] A. Radisic, P. M. Vereecken, P. C. Searson and F. M. Ross, "The morphology and nucleation kinetics of copper islands during electrodeposition," *Surface Science,* vol. 600, no. 9, pp. 1817-1826, 2006.

[51] A. Radisic, F. M. Ross and P. C. Searson, "In Situ Study of the Growth Kinetics of Individual Island Electrodeposition of Copper," *The Journal of Physical Chemistry B,* vol. 110, no. 15, pp. 7862-7868, 2006.

[52] J. E. Evans, K. L. Jungjohann, N. D. Browning and I. Arslan, "Controlled Growth of Nanoparticles from Solution with In Situ Liquid Transmission Electron Microscopy," *Nano Letters,* vol. 11, no. 7, pp. 2809-2813, 2011.

[53] K. Liu, C. Wu, Y. Huang, H. Peng, H. Chang, P. Chang, L. Hsu and T. Yew, "Novel microchip for in situ TEM imaging of living organisms and bio-reactions in aqueous conditions," *Lab on a CHip,* vol. 8, no. 11, pp. 1915-1921, 2008.

[54] D. B. Peckys and N. de Jonge, "Visualizing Gold Nanoparticle Uptake in Live Cells with Liquid Scanning Transmission Electron Microscopy," *Nano Letters,* vol. 11, no. 4, pp. 1733-1738, 2011.

[55] D. B. Peckys and N. de Jonge, "Liquid Scanning Transmission Electron Microscopy: Imaging Protein Complexes in their Native Environment in Whole Eukaryotic Cells," *Microscopy and Microanalysis,* vol. 20, no. 2, pp. 346-365, 2014.

[56] E. S. Pohlmann, K. Patel, S. Guo, M. J. Dukes, Z. Sheng and D. F. Kelly, "Real-Time Visualization of Nanoparticles Interacting with Glioblastoma Stem Cells," *Nano Letters,* vol. 15, no. 4, pp. 2329-2335, 2015.

[57] E. R. White, S. B. Singer, V. Augustyn, W. A. Hubbard, M. Mecklenburg, B. Dunn and R. B. C., "In Situ Transmission Electron Microscopy of Lead Dendrites and Lead Ions in Aqueous Solution," *ACS Nano,* vol. 6, no. 7, pp. 6308-6317, 2012.

[58] M. Egawa, T. Ishida, L. Jalabert and H. Fujita, "In-situ realtime monitoring of nanoscale gold electroplating using micro-electro-mechanical systems liquid cell operating in transmission electron microscopy," *Applied Physics Letters,* vol. 108, no. 2, p. 023104, 2016.

[59] X. Chen, K. W. Noh, J. G. Wen and S. J. Dillon, "In situ electrochemical wet cell transmission electron microscopy characterization of solid–liquid interactions between Ni and aqueous NiCl2," *Acta Materialia,* vol. 60, no. 1, pp. 192-198, 2012.

[60] H. L. Xin and H. Zheng, "In Situ Observation of Oscillatory Growth of Bismuth Nanoparticles," *Nano Letters,* vol. 12, no. 3, pp. 1470-1474, 2012.

[61] Y. Liu, K. Tai and S. J. Dillon, "Growth Kinetics and Morphological Evolution of ZnO Precipitated from Solution," *Chemistry of Materials,* vol. 25, no. 15, pp. 2927-2933, 2013.

[62] E. R. White, M. Mecklenburg, S. B. Singer, S. Aloni and B. C. Regan, "Imaging Nanobubbles in Water with Scanning Transmission Electron Microscopy," *Applied Physics Express,* vol. 4, no. 5, p. 055201, 2011.

[63] K. Tai, Y. Liu and S. J. Dillon, "In Situ Cryogenic Transmission Electron Microscopy for Characterizing the Evolution of Solidifying Water Ice in Colloidal Systems," *Microscopy and Microanalysis,* vol. 20, no. 2, pp. 330-337, 2014.

[64] "DENSsolutions Stream," DENSsolutions, [Online]. Available: https://denssolutions.com/products/stream/. [Accessed 30 11 2018].

[65] E. A. Ring and N. de Jonge, "Microfluidic System for Transmission Electron Microscopy," *Microscopy and MIcroanalysis,* vol. 16, no. 5, pp. 622-629, 2010.

[66] K. Klein and I. d. J. N. Anderson, "Transmission electron microscopy with a liquid flow cell," *Journal of Microscopy,* vol. 242, no. 2, pp. 117-123, 2011.

[67] H. H. Pérez Garza, D. Morsink, J. Xu, J. Hermannsdörfer, M. Sholkina, M. Pen, S. van Weperen and N. de Jonge, "The “Ocean” System: Microfluidic based system for in-situ analysis of liquid processes inside the TEM," in *European Microscopy Congress 2016: Proceedings*, Weinheim, Germany, 2016.

[68] C. Mueller, M. Harb, J. R. Dwyer and R. J. D. Miler, "Nanofluidic Cells with Controlled Pathlength and Liquid Flow for Rapid, High-Resolution In Situ Imaging with Electrons," *Journal of Physical Chemistry Letters,* vol. 4, no. 14, pp. 2339-2347, 2013.

[69] J. T. van Omme, H. Wu, H. Sun, A. F. Beker, M. Lemang, R. G. Spruit, S. P. Maddala, A. Rakowski, H. Friedrich, J. P. Patterson and H. H. Pérez Garza,

"Liquid phase transmission electron microscopy with flow and temperature control," *Journal of Materials Chemistry C,* vol. 8, no. 31, pp. 10781-10790, 2020.

[70] T. J. Woehl, K. L. Jungjohann, J. E. Evans, I. Arslan, W. D. Ristenpart and N. D. Browning, "Experimental procedures to mitigate electron beam induced artifacts during in situ fluid imaging of nanomaterials," *Ultramicroscopy,* vol. 127, pp. 53-63, 2013.

[71] M. H. Nielsen, S. Aloni and J. J. De Yoreo, "In situ TEM imaging ofCaCO3 nucleation reveals coexistence of direct and indirect pathways," *Science,* vol. 345, no. 6201, pp. 1158-1162, 2014.

[72] J. R. Vance and S. J. Dillon, "Thermally driven bubble evolution at a heater wire in water characterized by high-speed transmission electron microscopy," *Chemical Communications,* vol. 53, no. 36, pp. 4930-4933, 2017.

[73] K. Niu, J. Park, H. Zheng and A. P. Alivisatos, "Revealing Bismuth Oxide Hollow Nanoparticle Formation by the Kirkendall Effect," *Nano Letters,* vol. 13, no. 11, pp. 5715-5719, 2013.

[74] V. Menon, M. Denoual, H. Toshiyoshi and H. Fujita, "Self-contained on-chip fluid actuation for flow initiation in liquid cell transmission electron microscopy," *Japanese Journal of Applied Physics,* vol. 58, no. 9, p. 090909, 2019.

[75] F. M. Ross, Liquid Cell Electron Microscopy, New York: Cambridge University Press, 2017.

[76] A. Ianiro, W. H., M. M. J. van Rijt, M. Paula Vena, A. D. A. Keizer, A. C. C. Esteves, R. Tuinier, H. Friedrich, N. A. J. M. Sommerdijk and J. P. Patterson, "Liquid–liquid phase separation during amphiphilic self-assembly," *Nature Chemistry,* vol. 11, no. 4, pp. 320-328, 2019.

[77] V. Menon, L. Jalabert, M. Kumemura and H. Fujita, "Toward Real Time Visualization of DNA and Gold Nanoparticle Hybridization Events using Heater-Integrated Liquid Cells in TEM," in *Proceedings of the 32nd Annual Sensor Symposium on Sensors, Micromachines and Applied Systems*, Niigata, 2015.

[78] N. de Jonge, "Theory of the spatial resolution of (scanning) transmission electron microscopy in liquid water or ice layers," *Ultramicroscopy,* vol. 187, pp. 113-125, 2018.

[79] T. L. Daulton, B. J. Little, K. Lowe and J. Jones-Meehan, "In Situ Environmental Cell–Transmission Electron Microscopy Study of Microbial Reduction of Chromium(VI) Using Electron Energy Loss Spectroscopy," *Microscopy and Microanalysis,* vol. 7, no. 6, pp. 470-485, 2001.

[80] K. Nishijima, J. Yamasaki, H. Orihara and N. Tanaka, "Development of microcapsules for electron microscopy and their application to dynamical observation of liquid crystals in transmission electron microscopy," *Nanotechnology,* vol. 15, no. 6, 2004.

[81] M. Krueger, S. Berg, D. Stone, E. Strelcov, D. A. Dikin, J. Kim, L. J. Cote, J. Huang and A. Kolmakov, "Drop-Casted Self-Assembling Graphene Oxide Membranes for Scanning Electron Microscopy on Wet and Dense Gaseous Samples," *ACS Nano,* vol. 5, no. 12, pp. 10047-10054, 2011.

[82] R. Matsui, Y. Takayama, L. Jalabert, T. Sato and H. Fujita, "水中生体分子の高分解能アクティブ観察に向けたグラフェン隔壁を持つ TEM 用 MEMS リキッドセル," in *Proceedings of the 32nd Annual Sensor Symposium on Sensors, Micromachines and Appied Systems*, Niigata, 2015.

[83] Y. B. Arik, R. Matsui, E. Sarajlic, Y. Takayama, B. Boom, E. Berenschot, S. Le Gac, N. R. Tas and H. Fujita, "Ultra-thin nanochannel-based liquid TEM cell for EELS analysis and high resolution imaging," in *2016 IEEE 29th International Conference on Micro Electro Mechanical Systems (MEMS)*, Shanghai, 2016.

[84] R. F. Egerton, "Electron energy-loss spectroscopy in the TEM," *Reports on Progress in Physics,* vol. 72, no. 1, 2009.

[85] H. Gabrisch, L. Kjelgdaard, E. Johnson and U. Dahmen, "Equilibrium shape and interface roughening of small liquid Pb inclusions in solid Al," *Acta Materialia,* vol. 49, no. 20, pp. 4259-4269, 2001.

[86] J. Wu, W. Gao, H. Yang and J. M. Zuo, "Imaging Shape-Dependent Corrosion Behavior of Pt Nanoparticles over Extended Time Using a Liquid Flow Cell and TEM," in *Proceedings of Microscopy and Microanalysis 2014*, Hartford, 2014.

[87] W. L. Tsai, P. C. Hsu, C. H. Chen, L. W. Chang, J. H. Je, H. M. Lin, A. Groso and G. Margaritondo, "Building on bubbles in metal electrodeposition," *Nature,* vol. 417, no. 6885, p. 139, 2002.

[88] L. Saraf, D. R. Baer, Z. Wang, J. Young, M. H. Engelhard and S. Thevuthasan, "Hydrogen bubbles and formation of nanoporous silicon during electrochemical etching," *Surface and Interface Analysis,* vol. 37, no. 6, 2005.

[89] L. Zhang, Y. Zhang, X. Zhang, Z. Li, G. Shen, M. Ye, C. Fan, H. Fang and J. Hu, "Electrochemically Controlled Formation and Growth of Hydrogen Nanobubbles," *Langmuir,* vol. 22, no. 19, pp. 8109-8113, 2006.

[90] S. Yang, P. Tsai, E. S. Kooij, A. Prosperetti, H. J. W. Zandvliet and D. Lohse, "Electrolytically Generated Nanobubbles on Highly Orientated Pyrolytic Graphite Surfaces," *Langmuir,* vol. 25, no. 3, pp. 1466-1474, 2009.

[91] Q. Chen, L. Luo, H. Faraji, S. W. Feldberg and H. S. White, "Electrochemical Measurements of Single H2 Nanobubble Nucleation and Stability at Pt Nanoelectrodes," *Journal of Physical Chemistry Letters,* vol. 5, no. 20, pp. 3539-3544, 2014.

[92] Y. Liu and S. J. Dillon, "In situ observation of electrolytic H2 evolution adjacent to gold cathodes," *Chemical Communications,* vol. 50, no. 14, pp. 1761-1763, 2014.

[93] G. Valet, M. Kumemura, L. Jalabert, Takayama Y., T. Sato and H. Fujita, "A new TEM liquid-cell with integrated MEMS microfluidic valve," in *Proceedings of the 31st Annual Sensor Symposium on Sensors, Micromachines and Applied Systems*, Matsue, 2014.

[94] M. Denoual, V. Menon, T. Sato, O. de Sagazan, A. W. Coleman and H. Fujita, "Liquid cell with temperature control for in situ TEM chemical studies," *Measurement Science and Technology,* vol. 30, no. 1, p. 017001, 2018.

[95] K. Handique, B. P. Gogoi, D. T. Burke, C. H. Mastrangelo and M. A. Burns, "Microfluidic flow control using selective hydrophobic patterning," in *Proceedings of Micromachining and Microfabrication III*, Austin, 1997.

[96] H. Andersson, W. van der Wijngaart, P. Griss, F. Niklaus and G. Stemme, "Hydrophobic valves of plasma deposited octafluorocyclobutane in DRIE channels," *Sensors and Actuators B: Chemical,* vol. 75, no. 1-2, pp. 136-141, 2001.

[97] S. Jebors, F. Fache, S. Balme, F. Devoge, M. Monachino, S. Cecillon and A. W. Coleman, "Designer amphiphiles based on para-acyl-calix[8]arenes," *Organic and Biomolecular Chemistry,* vol. 6, pp. 319-329, 2008.

[98] K. Suwinska, E. Janneau, Y. Tauran and A. W. Coleman, "The solid-state structures of the ethanol solvated complexes of para-sulphonato-calix[4]arene with magnesium and calcium ions," *Journal of Inclusion Phenomena and Macrocyclic Chemistry,* vol. 79, 2013.

[99] S. Rekkab, M. Lahouel, T. B. Hadda, C. Félix and Z. Kabouche, "Design, synthesis and anticoagulant activity of new flexible calix[8]arene sulfonic acids," *Comptes Rendus Chimie,* vol. 16, no. 7, pp. 672-678, 2013.

[100] E. D. Silva, D. Ficheux and A. W. Coleman, "Anti-thrombotic Activity of Water-soluble Calix[n]arenes," *Journal of Inclusion Phenomena and Macrocyclic Chemistry,* vol. 52, no. 3-4, pp. 201-206, 2005.

[101] E. V. Lugovskoy, P. G. Gritsenko, T. A. Koshel, I. O. Koliesnik, S. O. Cherenok, O. I. Kalchenko, V. I. Kalchenko and S. V. Komisarenko, "Calix[4]arene methylenebisphosphonic acids as inhibitors of fibrin polymerization," *The FEBS Journal,* vol. 278, no. 8, pp. 1244-1251, 2011.

[102] I. Bresinska and K. J. Balkus, "Studies of Gd(III)-Exchanged Y-Type Zeolites Relevant to Magnetic Resonance Imaging," *Journal of Physical Chemistry,* vol. 98, pp. 12989-12994, 1994.

[103] É. Csajbók, I. Bányai, L. V. Elst, R. N. Muller, W. Zhou and J. A. Peters, "Gadolinium(III)-Loaded Nanoparticulate Zeolites as Potential High-Field MRI Contrast Agents: Relationship Between Structure and Relaxivity," *Chemistry,* vol. 11, no. 16, 2005.

[104] J.-H. Oh and J.-S. Lee, "Designed Hybridization Properties of DNA–Gold Nanoparticle Conjugates for the Ultraselective Detection of a Single-Base Mutation in the Breast Cancer Gene BRCA1," *Analytical Chemistry,* vol. 83, no. 19, pp. 136-713, 2011.

[105] E. Auyeung, T. I. N. G. Li, A. J. Senesi, A. L. Schmucker, B. C. Pals, M. O. de la Cruz and C. A. Mirkin, "DNA-mediated nanoparticle crystallization into Wulff polyhedra," *Nature,* vol. 505, pp. 73-77, 2013.

[106] J. M. Grogan, N. M. Schneider, F. M. Ross and H. H. Bau, "Bubble and Pattern Formation in Liquid Induced by an Electron Beam," *Nano Letters,* vol. 14, no. 1, pp. 359-364, 2014.

[107] N. M. Schneider, M. M. Norton, B. J. Mendel, J. M. Grogan, F. M. Ross and H. H. Bau, "Electron–Water Interactions and Implications for Liquid Cell Electron Microscopy," *Journal of Physical Chemistry,* vol. 118, no. 38, pp. 22373-22382, 2014.

[108] R. F. Egerton, P. Li and M. Malac, "Radiation damage in the TEM and SEM," *Micron,* vol. 35, no. 6, pp. 399-409, 2004.

[109] P. Abellan, T. J. Woehl, L. R. Parent, N. D. Browning, J. E. Evans and I. Arslan, "Factors influencing quantitative liquid (scanning) transmission electron microscopy," *Chemical Communications,* vol. 50, no. 38, pp. 4873-4880, 2014.

[110] S. Le Caër, "Water Radiolysis: Influence of Oxide Surfaces on H2 Production under Ionizing Radiation," *Water,* vol. 3, no. 1, pp. 235-253, 2011.

[111] Y. Liu, X. Chen, K. W. Noh and S. J. Dillon, "Electron beam induced deposition of silicon nanostructures from a liquid phase precursor," *Nanotechnology,* vol. 23, no. 38, p. 385302, 2012.

[112] H.-G. Liao, D. Zherebetskyy, H. Xin, C. Czarnik, P. Ercius, H. Elmlund, M. Pan, L.-W. Wang and H. Zheng, "Facet development during platinum nanocube growth," *Science,* vol. 345, no. 6199, pp. 916-919, 2014.

[113] C. Zhu, S. Liang, E. Song, Y. Zhou, W. Wang, F. Shan, Y. Shi, C. Hao, K. Yin, T. Zhang, J. Liu, H. Zheng and L. Sun, "In-situ liquid cell transmission electron microscopy investigation on oriented attachment of gold nanoparticles," vol. 9, no. 1, p. 421, 2018.

[114] T. J. Woehl, J. E. Evans, I. Arslan, W. D. Ristenpart and N. D. Browning, "Direct in Situ Determination of the Mechanisms Controlling Nanoparticle Nucleation and Growth," *ACS Nano,* vol. 6, no. 10, pp. 8599-8610, 2012.

[115] J. M. Grogan, L. Rotkina and H. H. Bau, "In situ liquid-cell electron microscopy of colloid aggregation and growth dynamics Joseph," *Physical Review E,* vol. 83, no. 6, p. 061405, 2011.

[116] T. Yokota, M. Murayama and J. M. Howe, "In situ Transmission-Electron-Microscopy Investigation of Melting," *Physical Review Letters,* vol. 91, no. 26, p. 265504, 2003.

[117] J. M. Howe, T. Yokota, M. Murayama and W. A. Jesser, "Effects of heat and electron irradiation on the melting behavior of Al–Si alloy particles and motion of the Al nanosphere within," *Journal of Electron Microscopy,* vol. 53, no. 2, pp. 107-114, 2004.

[118] H. Zheng, S. A. Claridge, A. M. Minor, A. P. Alivisatos and U. Dahmen, "Nanocrystal Diffusion in a Liquid Thin Film Observed by in Situ Transmission Electron Microscopy," *Nano Letters,* vol. 9, no. 6, pp. 2460-2465, 2009.

[119] H. Dömer and O. Bostanjoglo, "High-speed transmission electron microscope," *Review of Scientific Instruments,* vol. 74, no. 10, pp. 4369-4372, 2003.

[120] T. LaGrange, M. R. Armstrong, K. Boyden, G. G. Brown, G. H. Campbell, J. D. Colvin, W. J. DeHope, A. M. Frank, D. J. Gibson, F. V. Hartemann, J. S. Kim, W. E. King, B. J. Pyke, B. W. Reed, M. D. Shirk, R. M. Shuttlesworth, B. C. Stuart, B. R. Torralva and N. D. Browning, "Single-shot dynamic transmission electron microscopy," *Applied Physics Letters,* vol. 89, no. 4, p. 044105, 2006.

[121] N. D. Browning, M. A. Bonds, G. H. Campbell, J. E. Evans, T. LaGrange, K. L. Jungjohann, D. J. Masiel, J. McKeown, S. Mehraeen, B. W. Reed and M. Santala,

"Recent developments in dynamic transmission electron microscopy," *Current Opinion in Solid State and Materials Science,* vol. 16, no. 1, pp. 23-30, 2012.